Technical Report

TR-10-36

Fault Rock Zones Characterisation – Final report

TRUE-1 Continuation Project

Anders Winberg (editor), Conterra AB

November 2010

Svensk Kärnbränslehantering AB
Swedish Nuclear Fuel
and Waste Management Co

Box 250, SE-101 24 Stockholm
Phone +46 8 459 84 00

ISSN 1404-0344
SKB TR-10-36

Fault Rock Zones Characterisation – Final report

TRUE-1 Continuation Project

Anders Winberg (editor), Conterra AB

November 2010

Keywords: Epoxy, fault rock, fracture, image analysis, pore space.

Foreword

This report accounts for the multi-disciplinary work performed as part of the Fault Rock Zones Characterisation project, a subproject within the TRUE-1 Continuation project.

Important contributions to the current report have been provided by;

- Eva Hakami, Itasca Geomekanik AB (image analysis and interpretation) – Chapter 7.
- Weixing Wang, Itasca Geomekanik AB (image analysis) – Chapter 7.
- Eva-Lena Tullborg, Terralogica AB and Henrik Drake, Isochron Geoconsulting (mineralogy, fracture mineralogy) – Section 6.2.
- Lars Maersk-Hansen, Golder Associates AB (on-site geology and documentation) – Chapters 3 and 5.
- Katarina Malaga, SP (petrophysical analyses and documentation) – Section 6.1.

The project is also indebted to the following individuals for their contributions at various stages of the project:

- Lars Andersson, SKB (on-site coordination).
- Lars Birgersson, Kemakta Consultants (resin injection premises and techniques, continuity).
- Martin Stigsson, SKB (geometrical modelling using the RVS system).
- Isabelle Olofsson (nee Staub), SKB (geometrical modelling using the RVS system, core sectioning plan)
- Joakim Stoor, GEOSIGMA (resin injection equipment and *in situ* resin impregnation).
- Sven Snäll, Geological Survey of Sweden (XRD analyses).
- Mauriusz Kalinowski, CBI (laboratory investigation of resin behaviour relative to site-specific material).

Anders Winberg

Project leader, editor

Abstract

At the conclusion of the TRUE-1 and TRUE Block Scale experimental programmes at the Äspö Hard Rock Laboratory one remaining identified uncertainty was the *in situ* internal structure of conductive structures, and in particular the *in situ* material properties of unconsolidated fault gouge of such conductive structures. With the aim of reducing these uncertainties an experimental program has been conducted at depth in the Äspö Hard Rock Laboratory.

Four conductive structures in the immediate vicinity of the Äspö tunnel were identified for further study. Following basic geometrical and geological modelling based on tunnel observations, geological/mineralogical and hydrogeological investigations in four boreholes at each site, epoxy resin was injected in selected packed off borehole sections containing the structure. Following a sufficient time for curing of the epoxy, the injected borehole 72 mm sections were overcored with a 300 mm core barrel. Customised techniques were employed to section the core in the borehole and for its retrieval out of the borehole.

Following basic geological mapping, selected overcores were sectioned and were subject to image analysis to assess the pore structure using a variety of different descriptive geometrical attributes. In addition, an attempt was made to infer the porosity of the fault rock (including fault gouge) using binary images. Since analysis has been made on multiple slices of impregnated rock it is also possible to crudely map the 3D variability of a given entity. It was furthermore identified that porosity estimates, which range from some 10–70% are, apart from being dependent on the penetration of the epoxy, dependent on the resolution of the given image, the size of the averaging window, and the porosity components contained therein. The obtained quantifications of porosity can therefore only be regarded as ball-park relative porosities of a complete fault rock zones. It does not, however, provide firm quantification of the porosity of the fault gouge as such.

It was noted that the information obtained from the current study, descriptive geometrical and quantitative, is not in conflict with conceptual microstructural models devised on a metre scale for conductive structures at Äspö. However, the ambition to produce firm and unambiguous quantification of the *in situ* porosity of fault rock and fault gouge has not worked out. One reason being the said dependency of porosities derived from image analysis on the underlying resolution in imagery. However, it was noted that the produced imagery provides additional supporting information which may be used to properly inform and sustain developed conceptual models

Sammanfattning

Efter slutförandet av de inledande experimentella programmen inom ramen för TRUE-experimenten på Äspölaboratoriet identifierades den interna *in situ* strukturen hos konduktiva strukturer, och specifikt *in situ* egenskaper hos okonsoliderade sprickfyllnader (fault gouge), som kvarstående osäkerheter. För att reducera dessa osäkerheter har ett experimentellt program genomförts under jord i Äspölaboratoriet.

Fyra konduktiva och tunnelnära strukturer identifierades för fortsatta undersökningar. Efter en inledande geometrisk och geologisk modellering av varje struktur baserad på tunnelinformation, geologiska, mineralogiska och hydrogeologiska undersökningar i fyra borrhål på varje plats, injicerades epoxy i utvalda avmanschetterade borrhålssektioner som innehåller strukturerna. Efter en tidperiod för att säkerställa nödvändig härdning överborrades det injicerade borrhålet (72 mm) med ett kärnrör med en diameter av 300 mm. Specialanpassade metoder utnyttjades för att bryta borrkärnan i hålet, och för dess transport ut ur borrhålet.

Efter grundläggande strukturgeologisk kartering delades grovkärnorna och utnyttjades för bildanalys för att bestämma porstrukturen med utnyttjande av ett antal beskrivande attribut. Vidare gjordes ett försök att bestämma porositeten hos strukturen (inklusive sprickfyllnader) med utnyttjande av binära bilder. Givet att dessa analyser har genomförts på ett flertal skivor av impregnerat berg finns det en möjligt att grovt beskriva den tredimensionella variationen i en given parameter. Det identifierades vidare att porositetsbestämningar från bildanalys, som varierar mellan c. 10–70% är, förutom av epoxyns inträngning, beroende av upplösningen i bilden, storleken på det analyserade området/volymen, och porositetskomponenterna i denna. Den erhållna kvantifieringen av porositet kan därför endast betraktas som en ungefärlig relativ porositet av ett typiskt tvärsnitt av en konduktiv zon. Analysen ger dock inte en klar kvantitativ bestämning av porositeten av sprickfyllanderna som sådana.

Det noterades att informationen som erhållits från denna studien, beskrivande geometrisk såväl som kvantitativ, inte står i konflikt med de konceptuella mikrostrukturella modeller som tagits fram i meterskala för konduktiva strukturer på Äspö. Däremot har den ursprungliga ambitionen, att generera relevanta indirekta mått på sprickfyllanders *in situ* porositet, inte lyckats fullt ut. En bidragande orsak är den redan nämnda beroendet hos porositetsbestämningen av den underliggande upplösningen i bilden. Det kan dock konstateras att de producerade bildmaterialet ger tillkommande understödjande information som kan användas för att informera och understödja redan framtagna konceptuella modeller.

Contents

1 Introduction

1.1 Background and rationale

Over the time frames of contaminant transport experiments conducted at the Äspö Hard Rock Laboratory (Äspö HRL) the transported solutes are interacting with geological materials distributed along the along parts of the fractures making up the investigated flow paths (Winberg et al. 2000, Andersson et al. 2002a, 2007, Poteri et al. 2002). Only sparse geological, geochemical and mineralogical information on fault rock zones at Äspö exist through e.g. the FCC project (Mazurek et al. 1996) and investigations run within the TRUE Block Scale project (Andersson et al. 2002a). No Äspö-related data on *in situ* measured porosity of the fine-grained fault gouge component of the fault rock exist. The latter, with high clay content, is interpreted to contribute significantly to radionuclide retention over experimental time scales. Typically, based on experiences from the investigations at the Grimsel test site (Bossart et al. 1991) and from the Fracture Classification and Characterisation project (FCC) at the Äspö HRL (Mazurek et al. 1996) attributed typical fault gouge at Äspö HRL a porosity of 10–20%.

In the conclusions related to the TRUE Block Scale experiment (Winberg et al. 2003) it was noted that there existed a need to 1) assess the pore space and porosity of fault gouge materials of fault rock zones and 2) to verify experimentally the solute distributions coefficients (K_d) of fault gouge and fracture rim zone materials. The latter entity had so far only been estimated on the basis of mineralogy, CEC, selectivity coefficients and groundwater composition but is currently the focus of a comprehensive laboratory programme (Byegård and Tullborg 2012) focused on rim zone and fault gouge materials collected within the scope of various experiments at Äspö HRL.

The backbone of the experimental approach employed in this work is the usage of *in situ* resin injection in fault rock to provide the means to assess the geometry of the *in situ* pore space of the fault rock zone and possibly also provide quantification of *in situ* porosity of the fine-grained fault gouge, the latter indirectly through image analysis. The involvement of resin injection to assess pore structure and *in situ* porosity constitutes a new entity, potentially associated with experimental and analytical difficulties. The other components of the characterisation (hydrogeology and mineralogy/geochemistry) are of complementary and/or supporting nature, placing the analysed fault rock zones into a context of other conductive structures investigated at the Äspö HRL.

The planned injection at Äspö HRL will be into a fault rock zone structures consisting of various types of fault rock, cf. Section 1.2. The aim will be to achieve a radial resin spread of about 0.1–0.2 m outward from the injection borehole section and sample the impregnated rock volume with large diameter cored boreholes in order to collect intact rock samples that could be used in the study of geometry and composition of the structure. A potential problem, which has to be circumvented, is the possible destruction/disturbance of the *senso stricto* pore structure of the fault rock zone sample and the fine-grained fault gouge in particular. Too high injection pressures during epoxy injection may mobilise the gouge material and cause disturbance to the original structure.

The methodology developed as part of the current work (or variants thereof) is intended to be applied in the *in situ* assessment of the pore structure of Feature A as part of the TRUE-1 Completion at the Äspö HRL. Feature A at the TRUE-1 site has previously been investigated *in situ* using sorbing tracers (Winberg et al. 2000).

1.2 Context and defintions of terms used

The definitions discussed here mainly relate to structural elements. The term "*fault rock zone*" introduced in the title of this project relates a typical deformation zone found in the rock at the Äspö HRL, characterised for the most part by initial ductile deformation followed by brittle deformation, the latter of which has formed the main hydraulic feature associated with the zone. The zones are in most cases associated with mylonite and cataclasite. The fault rock zones are usually characterised by hydrothermal alteration and red staining of the wall rock, brecciated rock (centimetre sized *pieces*

and millimetre sized *fragments* (1–3 mm)). This assembly of rocks are in the following collectively denoted "*fault rock*". A comprehensive *in situ* study and compilation of fractures and faults in the Äspö HRL access tunnel has been made by Mazurek et al. (1996) which also includes conceptualisations at various scales, the latter partly based on epoxy resin impregnations of rock samples in the laboratory. Work in the TRUE Project (Winberg et al. 2000, Andersson et al. 2002a, Dershowitz et al. 2003) have provided conceptualisations of fault fractures based on available characterisation and laboratory data, the latter in part based on laboratory impregnations of poly-methylmethaacrylate (PMMA), (cf. Hellmuth et al. 1994) of core samples. The fault rock fractures at Äspö HRL are, unlike the non-fault joints, typically characterised by *fault gouge* (clayey, mostly non-cohesive and highly porous, but in places showing up as well cemented and less porous) and the development of a fracture rim zone with properties different from the intact rock away from the fracture. The fracture *rim zone*, which largely coincides with the red-stained zone, extending some centimetres to a decimetre from the conductive fracture, is characterised by a successively reduced porosity over a distance of some centimetres away from the fracture. The basis for these inferences are PMMA injections of laboratory samples (Kelsokaski et al. 2001, Byegård et al. 2001, Andersson et al. 2002a), subsequently introduced in conceptual modelling (Dershowitz et al. 2003) and in modelling of transport experiments, see e.g. Poteri et al. (2002) and Andersson et al. (2007). However, the conceptual models lacked firm *in situ* quantification of the porosity of fault gouge material.

1.3 Objectives

The overall objective of this work is to improve the description of fault rock zones and properties related to fault rock. The characterisation and analysis is planned to provide an improved description of fault rock zones of variable dignity (thickness) related to;

- Geology.
- Mineralogy and geochemistry.
- Porosity of fine-grained fault gouge.
- Detailed description of resin-filled pore spaces.

The proposed work will serve to fill gaps in the databases related to the findings of the TRUE experiments at the Äspö HRL. The generic nature in the search for suitable candidate repository sites, and also the variability in nature of fault rock zones along the Äspö access tunnel, implies that general knowledge will be assembled which can be used to improve conceptual models of fault rocks, not only applicable and valid for Äspö HRL and its experiments specifically, but also in a more general sense. The latter aspect implies that the collected information should be complementary to the results of the site investigations and site-descriptive modelling programmes performed at the Forsmark (SKB 2008) and Laxemar (SKB 2009) sites in Sweden.

The planned resin injections in Feature A at the TRUE-1 site and subsequent excavation/analysis, cf. Section 1.1, aim to give further input about pore spaces, transport path geometry and relative fixation of radionuclides on the geological materials of the fracture walls of Feature A and its fracture infillings.

1.4 Previous experience and important problem areas

1.4.1 The pilot resin experiment

Although new in the context of assessing the internal *in situ* structure of fault rock zones, a Pilot Resin Experiment was carried out at Äspö HRL as part of the First TRUE Stage. The main results are accounted for by Birgersson et al. (2000a). Background information and detailed results from hydraulic tests, tracer tests, core loggings and aperture measurements are found in a separate report (Birgersson et al. 2000b). The ensuing pore space analysis is described by Hakami and Gale (1999). The Pilot Resin Experiment provided development and testing of techniques for characterisation of the connected pore space of a selected target volume using resin injection and subsequent excavation (overcoring), sample preparation and analysis. The experience gained from this experiment in part constitutes the foundation on which the current work rests.

The technique that developed in the Pilot Resin Experiment enabled:

- Continuous mixing and injection of resin over time periods up to about 10 h.
- Injection of resin over distances of metre(-s) into a low transmissive structure.
- Sampling of the impregnated structures by large diameter cored holes.
- Analysis and evaluation of pore space data in quantitative and statistical terms.

The methodology applied in Pilot Resin Experiment was in turn to a large extent based on experiences from similar experiments carried out in by Nagra at the underground Grimsel laboratory, cf. the excavation project (EP), cf. Alexander et al. (2003) and the connected porosity project (CP), cf. Frieg et al. (1998), Möri et al. (2003).

1.4.2 Choice of resin

The two-component epoxy resin, EpoTek 301 used in the Pilot Resin Experiment worked satisfactory for its intended application. The injection system was based on a continuous in-line mixing of resin and hardener. It was possible to continuously mix and inject resin for time periods up to about 10 h with injected volumes ranging from a few 100´s ml´s to more than 1,000 ml.

Consequently, at the onset the main alternative was to use EpoTek 301 for the resin injections in fault rock zones and in Feature A. However, the viscosity of EpoTek 301 is about 100 times higher compared to water and the resin starts to cure a few hours after start of injection. It was therefore necessary to consider also other resins, for example the resins used by Nagra at Grimsel. The following resins have been used at Äspö and Grimsel:

- Äspö HRL, Pilot Resin Experiment. Epoxy resin, EpoTek 301. Viscosity about 100 cps (0.1 Pas).
- Grimsel laboratory, Excavation Project (EP). Epoxy resin, Sika INJ 26. Viscosity about 0.1 Pas.
- Grimsel laboratory, Connected Porosity (CP). Acrylic resin, Sika NHC-9. Viscosity about 0.03 Pas at 5°C, < 0.01 Pas at 20°C.

The EP-project at Grimsel included injection of an epoxy resin into a high porosity fault breccia with fault gouge. The investigated structure probably resembles the foreseen fault rock zones at Äspö from a mineralogical and chemical standpoint, although the latter may be less transmissive that the one investigated at Grimsel. A one-component acrylic resin was used in the Connected Porosity, CP, project.

A general finding of Nagra is that it is easier to use an epoxy resin at a new site (different water chemistry and mineralogy etc). An acrylic resin requires more development, primarily regarding its overall chemical composition. Furthermore, the viscosity and the curing time (or “pot time”) of an epoxy resin can be controlled well by adjusting e.g. the resin composition, resin base and hardener mixing ratios and temperature.

1.4.3 Equipment for resin injection

The equipment SKB designed for the Pilot Resin Experiment employed constant flow rate (Q) and variable pressure (P). It was considered possible to use the SKB equipment at other localities since the flow rate can be adjusted and the equipment can be used with high pressures. The equipment is designed for a mixing ratio of 4:1 (resin:hardener) but has to be partly rebuilt if other resins (and mixing ratios) are to be employed.

The equipment that Nagra used in Grimsel for injection of acrylic resin employed either variable pressure (P) or variable flow rate (Q).

When injecting resin into the fault rock zones at Äspö HRL it is important to restrict the applied pressure. It is therefore better to use constant P and variable Q. The same is probably true for the planned injections in Feature A at the TRUE-1 site.

1.4.4 Retrieval of large diamater overcore

The principal problem when overcoring and retrieving the large diameter overcores is to maintain the integrity of the cores. During the TRUE-1 Pilot Resin Experiment a technique to reinforce the overcore using a steel bolt anchored in the central injection borehole. For the current application plans are to use the plastic dummy body, introduced in the small diameter injection boreholes, as the necessary reinforcement in the near horizontal boreholes. The retrieval of large portions of overcore from the inclined boreholes during a future application to Feature A at the TRUE-1 site introduces an added challenge.

1.5 Project components

The basic project components comprise:

- Identification of basic output parameters and information required from site characterisation.
- Review of available resin injection methodology and adaptation to site-specific needs, including laboratory tests of selected epoxy resins on site-specific rock material.
- Review, screening and selection of suitable experimental sites along the Äspö access tunnel.
- Laboratory test evaluating resin behaviour in relation to site-specific geological material from one of the sites.
- Drilling of a total of 10–20 short core-drilled boreholes distributed evenly at four sites along the tunnel. Basic characterisation includes core logging, measurements of pressure and inflow and quantification of hydraulic properties.
- Development of a customised mechanical packer for resin injection.
- Resin injection and subsequent overcoring.
- Analyses of pore space and assessment of porosity of resin impregnated samples using analysis of binary images.
- Assessment of mineralogy and geochemistry of select geological materials.
- Petrophysical analyses of select geological material.

Regarding quantification of retention properties of the fault rock materials, insufficient amounts of fault gouge material from the target structures in the pilot boreholes were recovered to allow batch sorption measurements in the laboratory. However, it should be mentioned that batch sorption and leaching experiments have been carried out on fault gouge and fracture rim zone materials from other localities, including structures investigated as part of the TRUE Block Scale and TRUE Block Scale Continuation projects (Byegård and Tullborg 2012). The rationale behind the latter tests is to confirm the sorption coefficients estimated for fault gouge and rim zone materials determined using mineralogy, CEC, selectivity coefficients and site-specific hydrogeochemistry, cf. Andersson et al. (2002a).

1.6 Identification of experimental sites

The process of selecting suitable candidates for this experiment started out from the FCC compilation and detailed characterisation of water-bearing faults along the Äspö HRL access tunnel (Mazurek et al. 1996). This data set is the most appropriate and comprehensive one for finding suitable features since it includes detailed descriptions of the geological character of conductive fractures. However, it was identified that there may be other relevant structures in the laboratory as the database compiled by Mazurek et al. (1996) only concentrates on features that intersect the whole tunnel periphery and the fact that additional tunnels have been made available (as of early 2003) compared to in 1995 when the survey by Mazurek et al. was conducted.

The requirements defined for a suitable candidate geological structure include:

- Intersection with the tunnel.
- Water-conducting.
- Not grouted or covered by shotcrete.
- Should be a potential candidate for sampling fault gouge.

The experimental requirements include that the chosen structure should be possible to intercept by new short cored boreholes in close vicinity to the immediate tunnel in order to sample fault gouge and to enable injection of epoxy resin for pore space analysis. The projected borehole intercept should, if possible, be minimised to a distance in the order of 5 to 15 m radially away from the tunnel. Also, the chosen target structure should be at such a location so that it is feasible to place a drilling rig nearby without blocking the tunnel.

The scan of the Mazurek et al. (1996) database produced a series of potential candidates, cf. Table 1-1.

These potential candidate structures were examined in the field and a "Comments column" was added describing the noted *in situ* specifics of each candidate. Finally, it was decided to construct local structural models in the Rock Visualisation System (RVS) for the four most promising candidates, cf. Table 1-2. These models would serve to guide the planning of the exploration drilling to be performed.

The respective locations of these local RVS models are illustrated in Figure 1-1.

Table 1-1. Compilation of potential suitable candidates for the Fault Rock Zones Characterisation programme (based on the Mazurek et al. (1996) database).

Tunnel length (m)	Geological characteristics	Geometry	Width	Water inflow to the tunnel	Comments
1,600 NE-2	1–2 master faults with some // fractures and splays, 1–2 clayish and mica-rich fault breccia zones 5–20 cm	N30E/70S	<1.5 m	0.8 and 0.5 l/min	Accessible. Dry in places. Very rich in chlorite and probably clay minerals. Sample collected.
1,905	Several subparallel fractures, 5–10 cm	N20W/steep		0.66 l/min	Relatively small structure. Possibly too close to niche.
1,990	1–2 master fault, fault crush grading to fault breccia 2–10 cm	N70W/steep	0.2–1 m	2 l/min	Accessible. Grout in upper part? Corresponds to 1,985 m sampled for REX experiments.
2,163	1 master fault with few splays, small lenses <10 cm, and fault crush <1 cm	N50W/steep	0.1–0.2 m	0.12 and 6.24 l/min	Accessible. Close to Microbe laboratory at –450 m.
2,351	1 master fault, fault breccia 1.5 cm wide	N40W/steep	0.1–0.4 m	0.3 and 2.9 l/min	Accessible. One intersecting fracture may complicate things.
2,369	1 master fault, fault crush to fault breccia lenses 3–20 cm wide	N50W/steep	0.3–0.8 m	3.5 l/min	Accessible. Pre-grouting.
2,430	1 master fault, some splays, fault breccia with thin clayish zones 2–10 cm wide	N15W/steep	0.3–0.8 m	Drop	Accessible. Similar to TRUE Block Scale Structure #19. Sample collected.
2,545	1–3 slightly curved master faults, intense small scale fracturing and crush, 1–20 cm	N50W/70S	1–2 m	0.05 l/min	Accessible. Possibly grouted. Complex structure.

Table 1-2. Compilation of the most suitable potential candidates. Subsequently subject to construction of local RVS models.

Model	Tunnel length	Characteristics	Geometry	Width	Water inflow to the tunnel	Comments
A	2/545 m	1–3 slightly curved master faults, intense small scale fracturing and crush, 1–20 cm.	N50W/70S	1–2 m	0.05 l/min	Readily accessible. Partially grouted? Complex structure.
B	2/430 m	1 master fault, some splays. Fault breccia with thin clayish zones 2–10 cm wide.	N15W/steep	0.3–0.8 m	Drop	Readily accessible. Similar to TRUE Block Scale Structure #19. Sample collected. for mineralogical and geochemical analyses.
C	2/163 m	1 master fault with few splays, small lenses <10 cm, and fault crush <1 cm.	N50W/steep	0.1–0.2 m	0.12 and 6.24 l/min	Readily accessible. Close to Microbe Laboratory at –450 m.
D	1/596 m	1–2 master faults with some parallel fractures and splays, 1–2 clayish and mica-rich fault breccia zones 5–20 cm.	N30E/70S	<1.5 m	0.8 and 0.5 l/min	Fracture zone NE-2. Readily accessible. Dry in places. Very rich in chlorite and probably clay minerals. Sample collected for mineralogical and geochemical analyses.

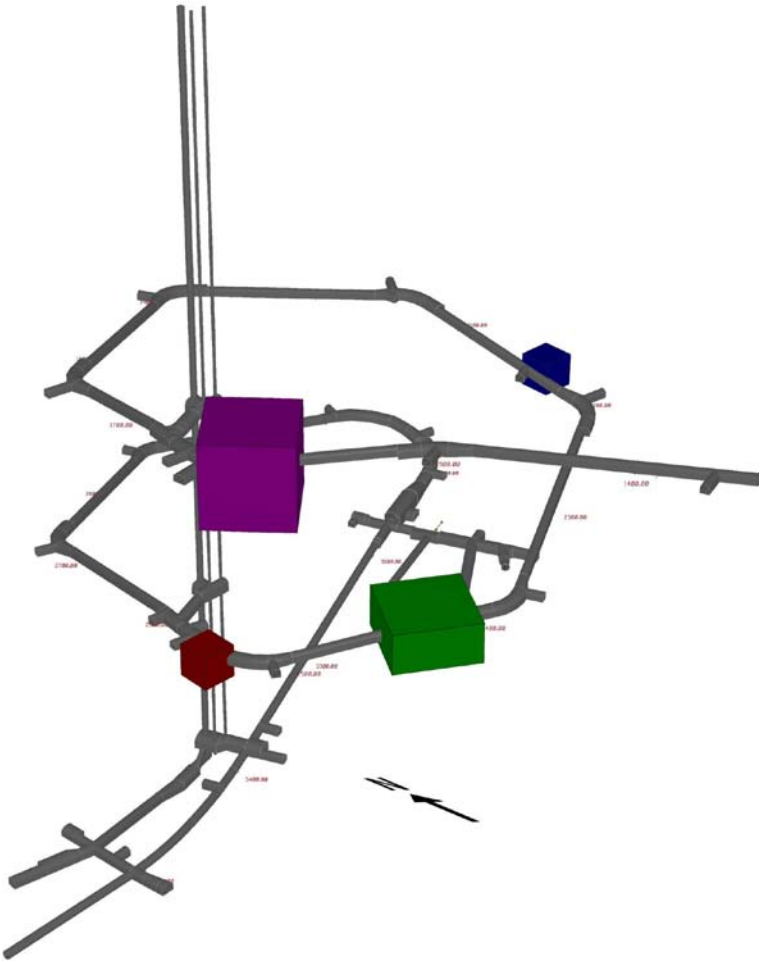

Figure 1-1. *Overview of the Äspö HRL spiral tunnel and location of tentative experimental sites for the Fault Rock Zones Characterisation programme. The boxes show the locations and sizes of the four structural RVS models constructed. The colouring of the models being A (red, 2/545 m), B (green, 2/430 m), C (blue, 2/163 m) and D (purple, 1/596 m), respectively.*

2 Laboratory tests

Laboratory tests were carried out to test various combinations of resins, selection of dye and its concentration. The results were expected to provide a basis for judging resin penetration, suitable dye concentration and image quality for subsequent image analysis. The experiments were carried out using fault rock zone and wall rock material associated with zone '1/600', also denoted zone NE-2 in the Äspö HRL site descriptive structural model (Rhén et al. 1997). Extraction of material was made using two 200 mm slightly downward inclined (5°) c. 1.5 m long single core barrel boreholes drilled using a conventional cement coring machine, see Figure 2-1. Stabilisation of the material on site was achieved using a supporting fixation using Serifix resin (rapidly hardening). Subsequently cube-shaped samples of dimension c. 0.05 m were produced for use in the laboratory.

Two resins were employed in the experiment, Epo-Tek 301 (Epoxy Technology), used in the Pilot bresin experiment and Barrikade (Hesselberg Bygg), being the standard resin used by the Swedish Cement and Concrete Research Institute (CBI). The rationale being that if Epo-Tek 301 behaves equally good, or better than Barrikade, the former can be used *in situ*. In the reversed case the risk of using a new resin not tested *in situ* has to be considered.

Figure 2-1. *Left : Coring with 200 mm barrel in zone NE-2 (zone '1/600'), Right : Example of resulting core.*

2.1 Procedure

The basic procedure for the tests have been:

A) Preparation (sawing) and stabilisation (supporting epoxy) of samples. Sawing of sample in two halves, cuts orthogonal to foliation. Cleansing of test surface of sample. Glass plate mounted on opposite sample face using Plastic padding, which prevents epoxy to penetrate sample from this face during step (D).

B) Saturation of test surfaces in ethanol. Drying of sample in the oven (at 35°C).

C) Inundation of sample with dye. A concentration of 14 grammes of EpoDye (Struers) per kg of resin is used by CBI as a standard. No alternative dyes were used.

D) Impregnation of resin at vacuum (110–130 mbar) and at temperatures of 35°C (standard temperature used by CBI) and at 12°C (assumed to reflect *in situ* conditions at c. 400m). Temperatures measured with a calibrated digital thermometer. Impregnation time was 30 minutes.

E) Surface grinding in order to remove excess of hardened epoxy. Sawing of samples orthogonal to foliation and test surface. Cleansing and polishing of surfaces.

F) Digital photography at ordinary and UV light. Camera used is a Olympus Camedia C-3030 with a resolution of 118 pixels/cm. Postprocessing of images taken via microscope using MS Photo Editor was employed to make them light enough for analysis.

G) Apparent fracture apertures were measured in the microscope using a magnification of 50x using a ruler with a resolution of 0.01 m.

Summary of analysed samples

First run: ”Sample I – Right” and ”Sample I – Left”.

”Sample I – R” impregnated with epoxy Barrikade, at 35°C.

”Sample I – L” impregnated with epoxy EPO-TEK 301, at 35°C.

Second run : ”Sample II – Right” and ”Sample II – Left”.

Sample II – R impregnated with epoxy EPO-TEK 301, at 12°C.

Sample II – L impregnated with epoxy Barrikade, at 12°C.

Summary of basic properties of resins employed

Viscosity

Epo-Tek 301 : 100–200 cps (0.1–0.2 Pa·s) at 23°C according to the manufacturer’s product sheet. Elevation of temperature to 40–50°C results in a 50% reduction of viscosity according to the manufacturer.

Barrikade EP (Concrete injection) : 380 cps at 10°C, 150 cps at 20°C, 55 cps at 30°C according to the manufacturer’s product sheet.

Hardening time

Epo-Tek 301 : Some 14 days at 10°C according to the Swedish supplier.

Barrikade EP (Concrete injection) : Some 16 days at 10°C according to the manufacturer’s product sheet.

2.2 Results

2.2.1 Hardening times

The Epo-Tek resin had hardening times of c.30 min and > 3 h, < 15 h t at 35°C and 12°C, respectively. Correspondingly, the Barrikade resin had hardening times of c. 40 minutes and >3h, < 15 h at 35°C and 12°C, respectively. In conclusion both resins showed approximately the same hardening times, although it can be effectively regulated by adjusting the amount of hardener. Also the total volume of epoxy (base + hardener) affects the speed of reaction, the smaller the volume the shorter the hardening time.

2.2.2 Penetration depth

In all four samples the epoxy has penetrated fractures throughout the cross-section, cf. examples under UV light in Figure 2-2, however restricted to those fractures, networks of fractures, with entry points on the test surface of the sample. Given the fact that fractures are extending in their full length of the cross section it is not possible to assess the maximum penetration depths. Consequently the penetration depths of Sample I L/R of 59 mm and Sample II L/R of 49 mm, reflect the sample thickness. Based on the conducted investigations it can be concluded that there are no differences between the two resins, or the two injection temperatures, 35 and 12°C, respectively.

2.2.3 Minimum apparent apertures of epoxy-filled fractures

The minimum apparent aperture of fractures extending over the complete cross section of the sample was 20 µm. These fractures exhibit complete epoxy fill along their complete extent and show lengths in the order of centimetres. Correspondingly, the minimum apparent aperture of fractures which do not extend over the full length of the sample, typically showing extents in the order of millimetres, are in the order of 10 µm. No differences in apparent minimum aperture between the four samples can be noted.

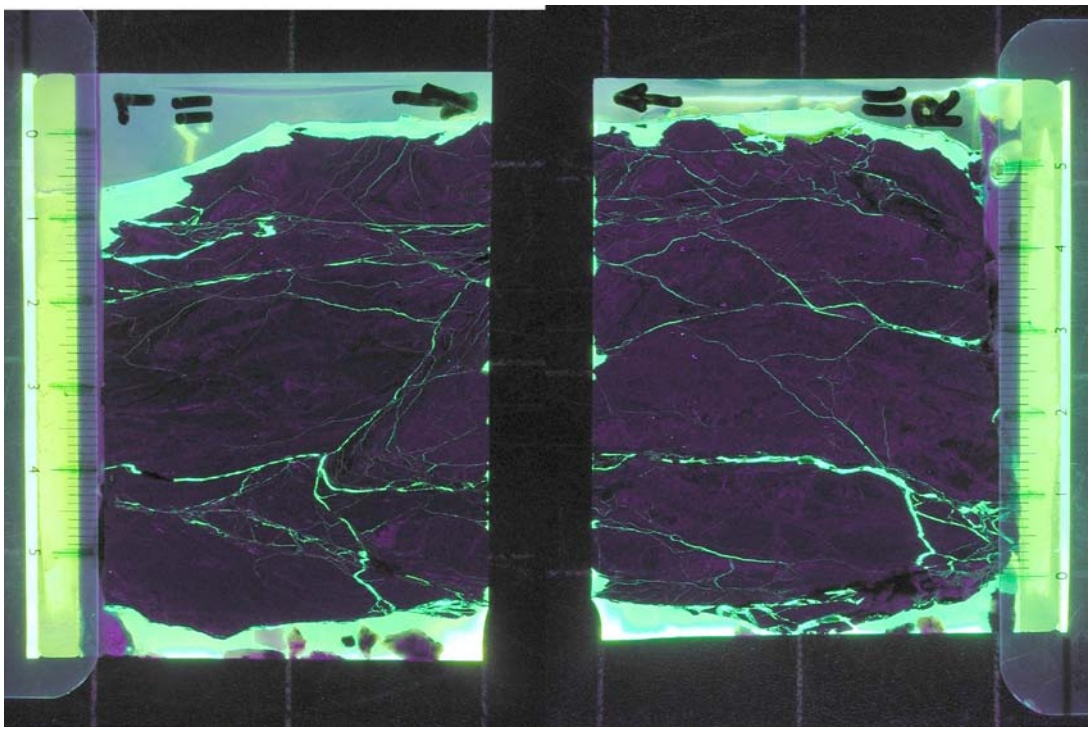

Figure 2-2. *Example of sample crossections at UV light. Sample II at 12°C. Left: Barrikade, Right : Epo-tek. At hardening time of 30 minutes..Test surce of both samples is towards the centre of the combined image.*

2.2.4 Penetration of epoxy in matrix pores

The term matrix pores in this context correspond to systems of micro fractures which show up submicroscopically at a magnification level of 50x, including the pore spaces constituting boundaries between individual mineral grains. The samples show no readily visible penetration front in the matrix pores. Heavily fractured parts of the samples (micro breccia) however show a good penetration. In many locations in all fours samples impregnated subzones centred on fractures occur, mainly associated with fractures with apparent apertures of > 10 μm. These subzones may occur evenly distributed along the fracture, or may vary in width (< 20 μm) and occur in a more patchy manner. The subzones occur across the full cross section, but are most prominent closer to the test surface. The subzones are generally wider in samples impregnated at 35°C than at 12°C.

2.3 Conclusions

No significant differences were noted between the Barrikade and Epo-Tek resins with regards to penetrability and hardening behaviour. Given the restrictions regarding resin properties and usage posed in Section 1.4, previous experience of *in situ* use of Epo-Tek at Äspö HRL and the results of the laboratory experiments presented in the preceding sections it was decided to proceed with plans to use Epo-Tek in the planned *in situ* application.

3 Site characterisation

3.1 General

Core drilling campaigns were carried out through four interpreted fault and fracture zones, in the access tunnel at chainages 1/596, 2/163, 2/430 and 2/545m, respectively, cf. Figure 1-1. Four short holes (from 2.93 to 5.94 meters in length) were drilled at each site representing, in all 72.1 meters of drilled core. 76-mm coring using a triple-tube core barrel was employed, the innermost tube being divided in two half-tubes in order to ascertain good samples (quality and volume) of fault gouge, breccia, and/or crushed materials. Photographs of zone exposures in the tunnel and drill cores were taken: whole box, half box, and zone details, as required. The cores were logged tentatively with respect to rock type, fractures and fracture angles relative to the core axis, and rock quality designation (RQD) index. Zone intersections in cores were mapped in detail, usually at 1:2 scale. At each site the zone was mapped in detail with respect to master faults, fault material, lithology, and adjacent fractures such as splay cracks, as described by Mazurek et al. (1996). Each borehole was also logged using the BIPS borehole imaging system, enabling orientation of structures such as mylonites, faults and fractures. Each borehole was surveyed in order to obtain the accurate location, bearing and plunge of the hole. The pre-existing mapping of the tunnel walls and roof was judged to have an accuracy in position within 1 to 2 metres which was not considered sufficient for the current project. Therefore the evidences of geological structures in the tunnel have been surveyed with an accuracy better than 0.02 m using a total station (electronic/optical theodolite used in modern surveying) in order to obtain improved input to the RVS modelling. The four site models previously constructed in RVS were updated on the basis of new more accurate tunnel survey and borehole observations, cf. Section 3.2. The north arrow in the figures of Section 3.2 refers to the north of the Äspö96 coordinate system which has a bearing of 348° from magnetic north. Strike and dip of structures are given in relation to magnetic north.

3.2 Results of exploratory drilling

3.2.1 Site 1/596 m

This zone intersects the tunnel crest line at chainage 1/596 m. The structure, as interpreted prior to drilling, has a geometry of 44°/85° (Stigsson et al. 2003) and corresponds to deformation zone NE-2 of the Äspö HRL site-descriptive model (Rhén et al. 1997).

The accurate survey made in conjunction with the preparation for the experiment showed discrepancies in the position of zone occurrences in the tunnel. The ‘zone 1596’ therefore has been remodeled. The points used for reinterpretation are illustrated in Figure 3-1. The remodeled structure geometry is 28°/75°.

Four boreholes; KA1596A01, KA1596A02, KA1596A03 and KA1596A04 were drilled from the tunnel in the vicinity of the interpreted structure (Figure 3-1). The bedrock encountered in the boreholes is Äspö Diorite, which has, in conjunction with the Laxemar site investigations, been renamed quartz monzodiorite to granodiorite (porphyritic), cf. Wahlgren et al. (2008), with subordinate chloritic phyllonite, fine-grained, red protocataclastic granite, and minor occurrences of pegmatite, RQD varies between 75 (where the zone occurs) and 100 (Mærsk Hansen et al. 2003).

The structure occurs in all four boreholes, at L=5.55 m in KA1596A01, at L=4.7 m in KA1596A02, at L=3.3 m and L=4.2 m in KA1596A03, and at L=2.55 m in KA1596A04 (Figure 3-2). The thickness of the zone varies from 10 cm to 40 cm and the zone is divided into two branches in borehole KA1596A03.

The occurrences of ’zone 1596’ in the drill cores fit fairly well with tunnel observations and with orientations indicated by BIPS logging, see Figure 3-2. The fault gouge contains clay minerals (mainly chlorite) and rock fragments.

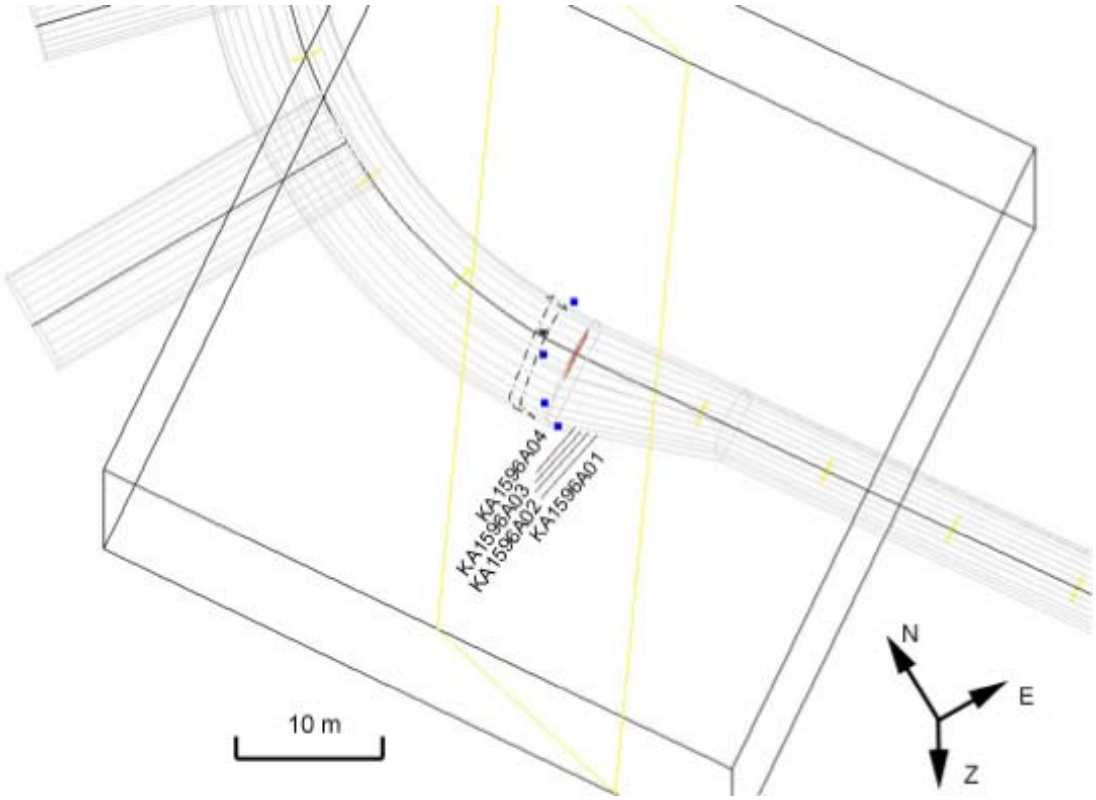

Figure 3-1. *Visualization of the points (blue) based on tunnel survey and used for the remodeling of the plane of 'zone 1596', cf. yellow frame, and positions of the boreholes (Mærsk Hansen et al. 2003).*

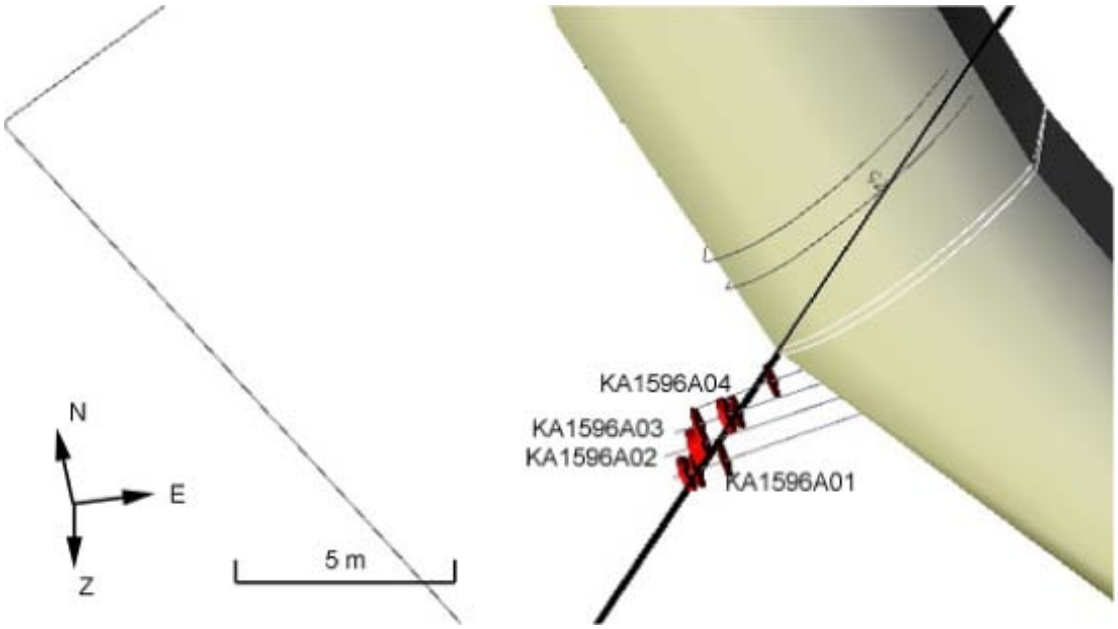

Figure 3-2. *Location of zone occurrences in the boreholes associated with 'zone 1596' (black) as modeled from tunnel observations (Mærsk Hansen et al. 2003).*

No water flow was observed during drilling in boreholes KA1596A02 through KA1596A04. Some water flow was however measured in the last metre of drilling in borehole KA1596A01. Water flow after the completion of drilling shows significant variability between the boreholes: 600 mL/min was measured in KA1596A01, 4 mL/min in KA1596A03, and no flow in KA1596A02 and KA1596A04, suggesting significant heterogeneity.

The structure occurs in various rock types, such as chloritic phyllonite, pegmatite and granite. When sheared, these rocks have been deformed in different ways. Chloritic phyllite has undergone ductile (plastic) deformation (to a phyllonite) and is practically hydraulically tight, as can be seen on tunnel wall A (outer wall) and in boreholes KA1596A02-A04 (Mærsk Hansen et al. 2003). The brittle granite and pegmatite have been crushed and are highly water bearing, as can be seen on tunnel wall B (inner wall) and in borehole KA1596A01.

The zone shows almost the same appearance in all four boreholes although some variations can be noticed. The structure can be characterised as a normal fault, considering how some splay cracks are bent, but no magnitude of displacement can be determined. The structure consists of extremely chlorite/clay mineral rich material on both sides of a quartz pegmatite (0.1–0.2 m wide). The structure is partly water bearing, especially where fault gouge is encountered in borehole KA1596A01. The zone is not one single zone and diverges and converges in width, with a total thickness varying between 0.4 to 0.5 metres. It contains 0.05–0.10 m wide sub-zones of chloritic fault gouge with some rock fragments (Mærsk Hansen et al. 2003). In borehole KA1596A01 the fault gouge is coarser and this borehole carried water (after drilling through the structure, while the other holes were almost entirely dry, 0–4 mL/min. The former part seems to be crushed portions of pegmatite and wall rock, while in the other boreholes the zone is in an amphibolite, which is altered and mechanically deformed to chlorite phyllonite.

The zone was regarded as being suitable for resin injection experiments.

The part of the structure at chainage 1/596 m being of interest for the resin injection experiment is the c. 0.2 m wide chlorite/clay-rich section found in the inner part of the boreholes (beyond the quartz-pegmatite). From macroscopical observations of sieved material from this zone it is obvious that the larger fragments (0.5 to 2 mm) are also very rich in chlorite/clay minerals although some grains containing quartz and K-feldspar were also observed. Complete sieving was not possible due to the clay-rich material in this zone. XRD identification of the clay minerals suggests that mixed layer clays (probably chlorite/smectite-vermiculite or smecitite/illlite) are important constituents of the fine-grained fraction.

3.2.2 Site 2/169 m

The zone identified at this site intersects the tunnel ceiling at chainage 2/163 m. The structure interpreted prior to drilling has the geometry 139°/79° (Stigsson et al. 2003). Based on tunnel observations the zone can be characterised as a single fracture rather than a fault, with some added local sections of crushed rock. There are no brittle splay structures, and no signs of displacement, see Mærsk Hansen et al. (2003) for a detailed geological map of the tunnel wall.

Four holes, KA2169A01, KA2169A02, KA2169A03 and KA2169A04, were drilled from the tunnel in the proximity of the identified structure (Figure 3-3). The rock identified in the boreholes is granodiorite (Äspö Diorite), in conjunction with the Laxemar site investigations reclassified as quartz monzodiorite, cf. Wahlgren et al. (2008), with occasional aplite and granite, see Mærsk Hansen et al. (2003). The RQD varies between 81 and 99.

Crushed rock and subordinate breccia occur with widths of 1–5 cm in the four holes, at L=2.5 m in KA2169A01, at L=3 m in KA2169A02, at L=3.95 m in KA2169A03, and at L=2.87 m in KA2169A04, see Figure 3-3. Flakey sub-zones are less than 0.01 m wide. Minerals in the zone appear to be minerals of the wall rock. The sub-zones occur in good quality rock and do not influence the RQD. The structures identified in KA2169A01 through KA2169A03 appear aligned and their orientations determined from BIPS logging fit well with the interpreted orientation of the zone in the tunnel. They are found somewhat deeper in the boreholes than expected from the previously modeled structure. The intercept identified in KA2169A04 is much closer to the face of the tunnel than the depth of intersection predicted from the modeled structure. Furthermore, the orientation of the intercept

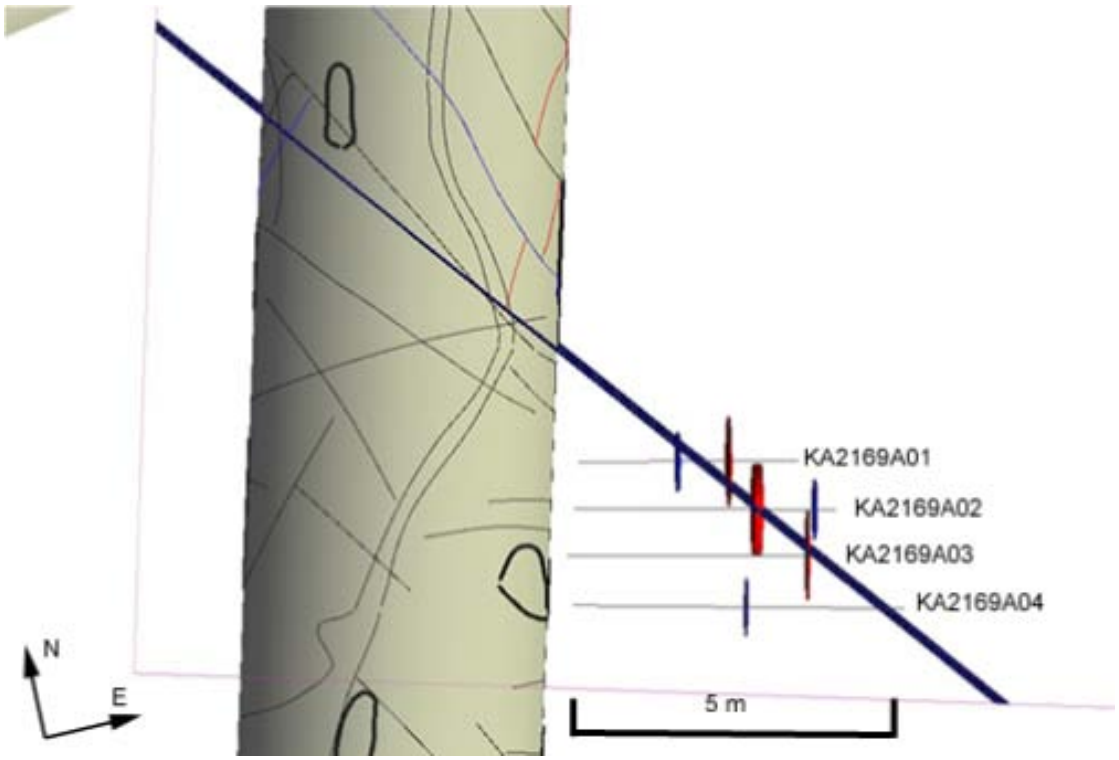

Figure 3-3. *RVS model C with borehole and fault geometry. The red discs are indications of 'zone 2163'. The smaller blue discs are indications of zones not associated with the main structure (Mærsk Hansen et al. 2003).*

identified in KA2169A04 does not fit very well with 'zone 2163' in the tunnel. Hence this structure is considered to be essentially dominated by a single fracture (red in Figure 3-3). Two other single fractures (blue in Figure 3-3) are identified in KA2169A01 and KA2169A02.

No water flow was observed in any of the boreholes during drilling. Water flows between 235 and 250 mL/min were measured after completion of boreholes KA2169A01 to KA2169A03. Similar water flows in these three holes indicate that these intercepts belong to the same water-bearing structure. The borehole KA2169A04 was found dry both during and after drilling.

The structure has been remodeled on the basis of the tunnel survey and the mapped occurrences in the boreholes (Figure 3-4). The deviation of the geometry of the updated structure compared to the one based on the original model is minor and the updated orientation is 309/85°.

The structure is identified as a NW trending structure in quartz monzodiorite running parallel with a set of thin epidote sealed fractures (possibly very thin mylonites?), cf. Mærsk Hansen et al. (2003). The structure contains fault crush as well as fault gouge, at least in boreholes KA2169A02 and KA2169A03, and to some extent in KA2169A01. The crush may be due to tensile cracking in response to a two- dimensional stress in the fracture plane, rather than to shear. The zone is widest in borehole KA2169A02 (c. 0.15 m of crush and fault gouge). The absence of water flow in KA2169A04 confirms the judgment that the structure is more or less a single fracture. The absence of 'zone 2163' in this borehole might be an indication that the zone gradually bends to the east, or that it peters out.

The structure was regarded suitable for resin injection in boreholes KA2169A01 to KA2169A03.

Macroscopical observations of the 1–2 mm fraction show the presence of grains of altered quartz monzodiorite and epidote-rich fine-grained (mylonitic?) grains. A few grains containing idiomorphic calcite crystals in the order of 50–100 μm indicate growth of these crystals in open pore spaces. Weights of sieved samples are presented in Section 6.2.

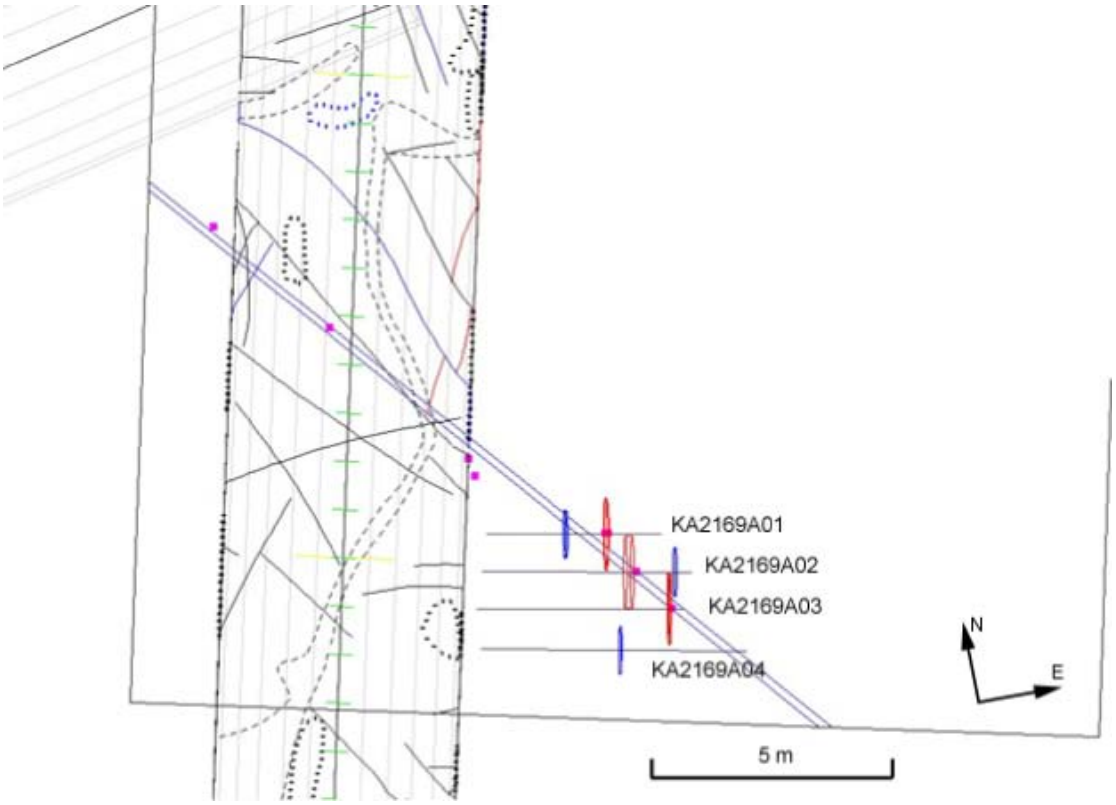

Figure 3-4. *Illustration of the points (purple) in the tunnel and in the boreholes used for remodeling the 'zone 2163' (Mærsk Hansen et al. 2003).*

3.2.3 Site 2/430 m

The zone identified at this site intersects the centre line of the tunnel crest at chainage 2/430 m. The structure interpreted from existing tunnel data has a geometry of 341/87° (Stigsson et al. 2003). Its width varies from zero to 0.25 m, and the material can be characterised as a cataclasic or mylonitic, see Mærsk Hansen et al. (2003) for a detailed geological map of the tunnel wall.

More accurate measurements of the zone indications in the tunnel prior to drilling showed a slight discrepancy with the data used in the preceding modeling. The remodeled 'zone 2430' was attributed a geometry of 338.4/ 85°.

Four holes, KA2423A01, KA2423A02, KA2423A03 and KA2423A04 were drilled from the tunnel in the proximity of the target structure (Figure 3-5). The rock identified in the holes is mainly Småland Granite (Ävrö granite, ie. granite to quartz monzodiorite, generally porphyritic) and granodiorite (Äspö Diorite, in conjunction with the Laxemar site investigations reclassified as quartz monzodiorite to granodiorite, (porphyritic), cf. Wahlgren et al. (2008)), cf. Mærsk Hansen et al. (2003). RQD varied between 85 and 96 in the four exploration boreholes.

All four holes intercept fault breccia and crushed material in zones about 0.01–0.03 m wide. The zone occurs in borehole KA2423A01 at 4.25 m, in borehole KA2423A02 at 2.75 m, in borehole KA2423A03 at c. 3.3 m, and in borehole KA2423A04 at c. 1.9 m (Figure 3-6). In the drillcores the zone is located in protocataclasite and includes thin mylonites. It is characterised by repeated 0–01 to 0.02 m thick sub-zones of fault breccia and subordinate fault crush. The material is flaky with green, hard, unidentified minerals. There are also a number of subhorizontal fractures interpreted as splay cracks.

The sub-zones are thin, usually located in rock of good quality and therefore only marginally influence the general quality of the rock mass as expressed by RQD. They may however constitute a discontinuity which can influence adversely the local stability of an engineered structure, if such structure forms the footwall.

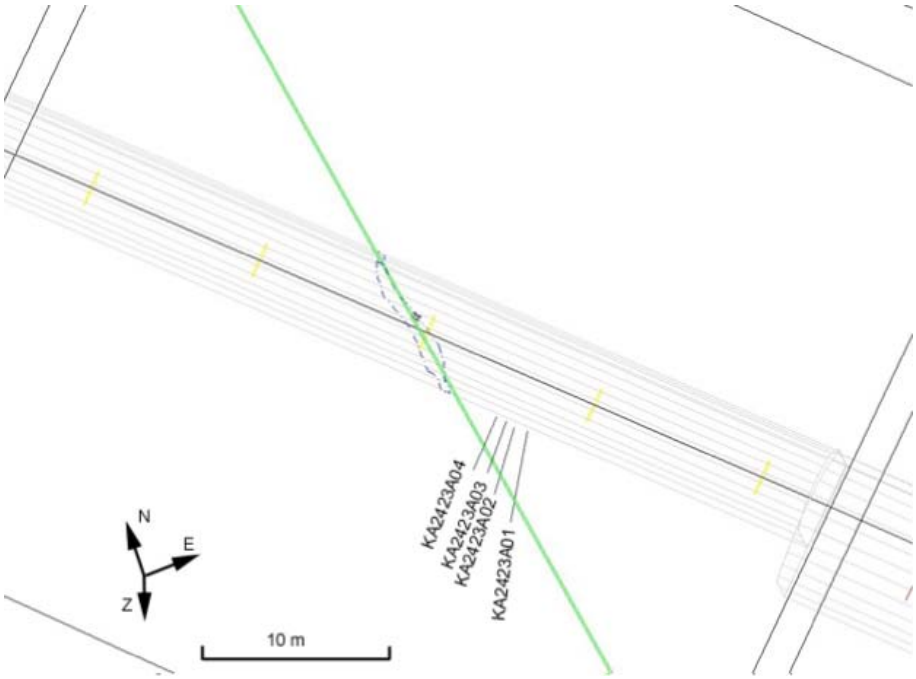

Figure 3-5. *Illustration of the zone occurrence in the tunnel (stippled area) including discrete points used for modelling the geometry of 'zone 2430' before drilling, and localisation of the boreholes (Mærsk Hansen et al. 2003).*

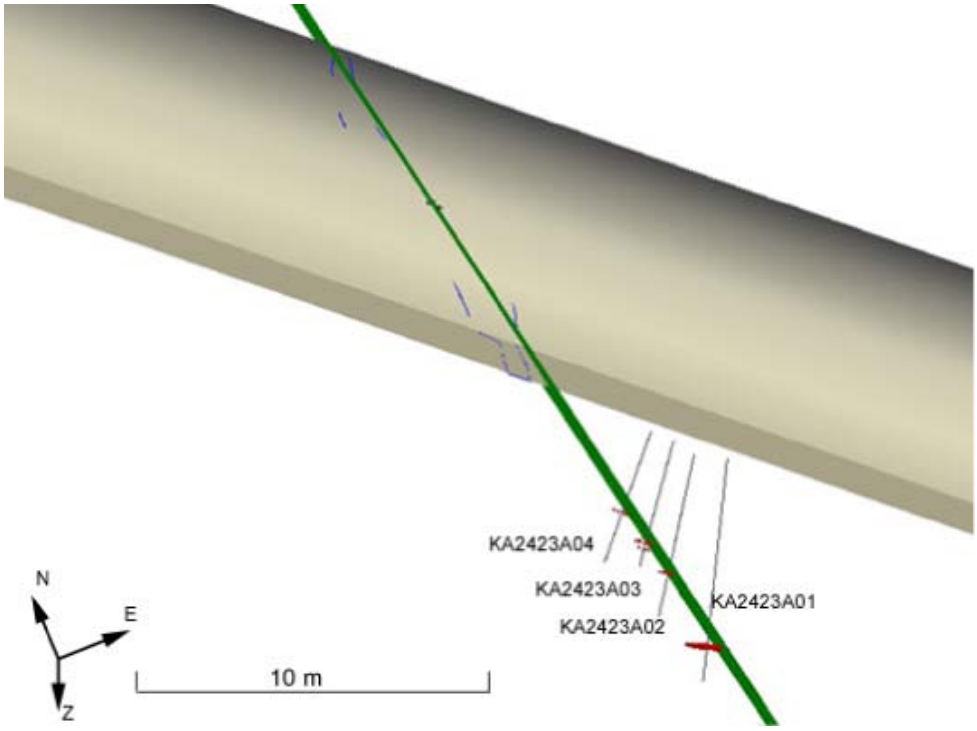

Figure 3-6. *RVS model B with visualisation of the zone occurrence in the tunnel (stippled area) boreholes (shown as discs) used to model the fault geometry. The zone intersects the tunnel crest at chainage 2/430 m.*

The zone appears to be a normal fault, considering the arrangement and bending of the splay cracks, but there are no marker structures by which to quantify the magnitude of displacement.

The depths of occurrence in the boreholes and the orientation of the individual intercepts in the boreholes (as determined from BIPS logging) fit very well with the expected depths projected from the modeled structure, see Figure 3-6. The ‘zone 2430’ has therefore not required remodelling after drilling.

This zone constitutes a reactivated epidote-rich mylonite hosted in red-stained and hydrothermally altered granite/granodiorite. The zone varies in width from 0.04 m (KA2423A04) to 0.1m (KA2423A01). The structure is characterised at all four borehole intercepts by open pore spaces and fault crush. The amount of clay in this structure is quite low compared with the other zones (‘zone 2163’ and ‘zone 1596’). An explanation might be that the cementation of the grains has been slightly more intense in this zone. An argument for this hypothesis is the observation of particles that look like clay- cemented grains in the 1 to 2 mm fraction. Grains of altered granite and mylonite were also identified in this size fraction. Grains of quartz, fluorite and sulphides precipitated as a result of hydrothermal circulation are frequent. Idiomorphic crystal growth indicates open pore spaces. Weights of sieved samples are presented in Section 6.2.

No water flow was observed in any borehole during drilling. Low water flows were measured after completion of drilling in boreholes KA2423A01 and KA2423A03, amounting to 23 and 13 mL/min, respectively. The fact that two boreholes are totally dry does not necessarily mean that the zone is partially non-conductive, but can be due to the vicinity of the drained zone close to the tunnel. In any case, ‘zone 2430’ gives an opportunity to study the variations in porosity and hydraulic conductivity within a few metres in the same structure. The structure is considered suitable for resin injection experiments for this type of fault rock material, cf. Mærsk Hansen et al. (2003).

3.2.4 Site 2/545 m

The identified structure at this site occurs in the ceiling of the tunnel at chainage 2/545 m. The structure, as interpreted before drilling and referred to as ‘zone 2545’, has an interpreted geometry of 307/65° (Stigsson et al. 2003). See Mærsk Hansen et al. (2003) for a detailed geological map of the tunnel wall.

The detailed surveying of the tunnel in conjunction to the drilling campaign highlighted the inaccuracy of the measurements of zone locations on the tunnel wall. Therefore the zone was remodeled prior to drilling based on new survey data. The remodeled structure geometry is 303°/89.6°, see (Figure 3-7).

NW-striking features are often encountered in the Äspö tunnels and they are often water conductors. Some of them are characterised by crushed rock and breccia.

Four boreholes, KA2548A01, KA2548A02, KA2548A03 and KA2549A01 were drilled from the tunnel at the location of the interpreted target structure (Figure 3-7).

The rock identified in the boreholes is mainly granodiorite to diorite (Äspö diorite in conjunction with the Laxemar site investigations relabeled as quartz monzodiorite, cf. Wahlgren et al. (2008)), with subordinate red, fine-grained granite and occasional cataclasite, pegmatite and aplite, see Mærsk Hansen et al. (2003). RQD varied between 81 and 98.

In the tunnel the structure appears to terminate against a steeply dipping fracture striking NNE, which is crossing the tunnel ceiling at 2/550 m, see Figure 3-8. This was confirmed during drilling of KA2549A01 where a shear plane, featuring narrow breccias (235/65–70°) was identified at a depth of c. 2.1 meters (Figure 3-9). Beyond that shear zone other NW striking fractures were identified by BIPS logging, but none of them at a depth extrapolated from to the target fracture exposed in the tunnel. Thus, these fractures were not deemed suitable for the experiment as epoxy resin would be injected into different fractures. As illustrated in Figure 3-9 indications of the shear zone are not found in KA2548A01 (no modeled purple disc) which may indicate that the zone changes direction to a more northerly orientation beyond KA2549A01, or alternatively, that the zone has a limited extent.

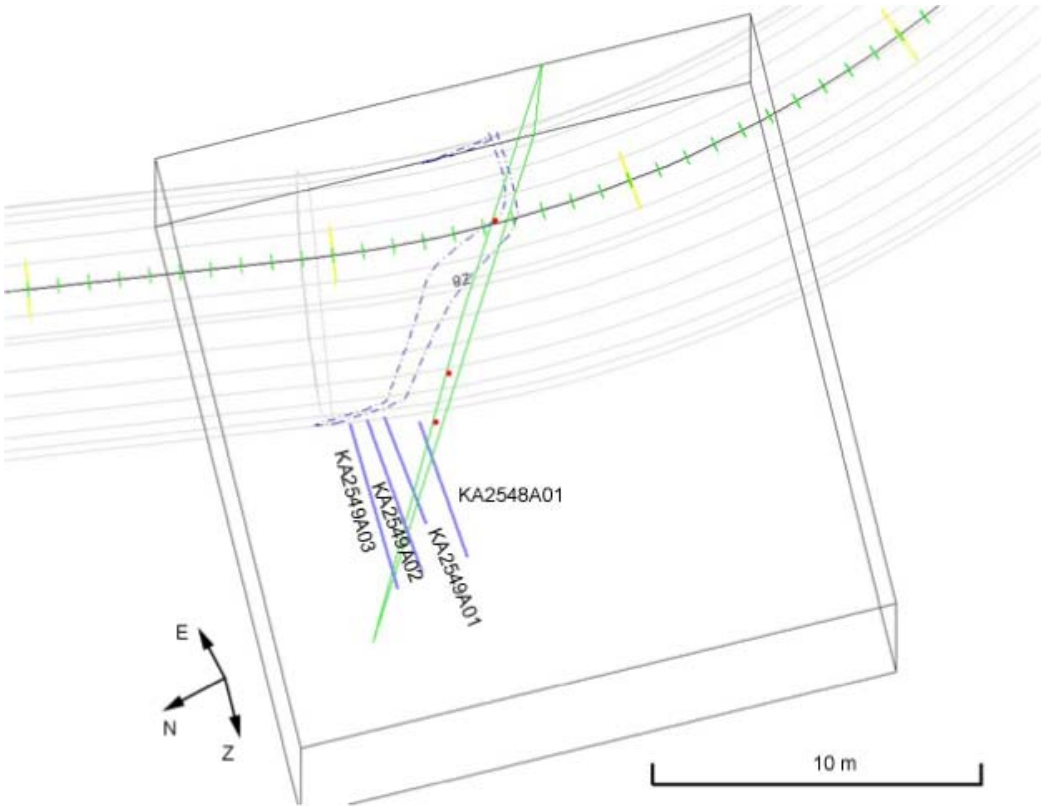

Figure 3-7. *The model of 'zone 2545' as interpreted before drilling but using data from the new tunnel survey. The red points illustrate the tunnel intercepts of the zone used for the modelling and the green frame indicates the modeled fault plane. Blue lines indicate the four boreholes (Mærsk Hansen et al. 2003).*

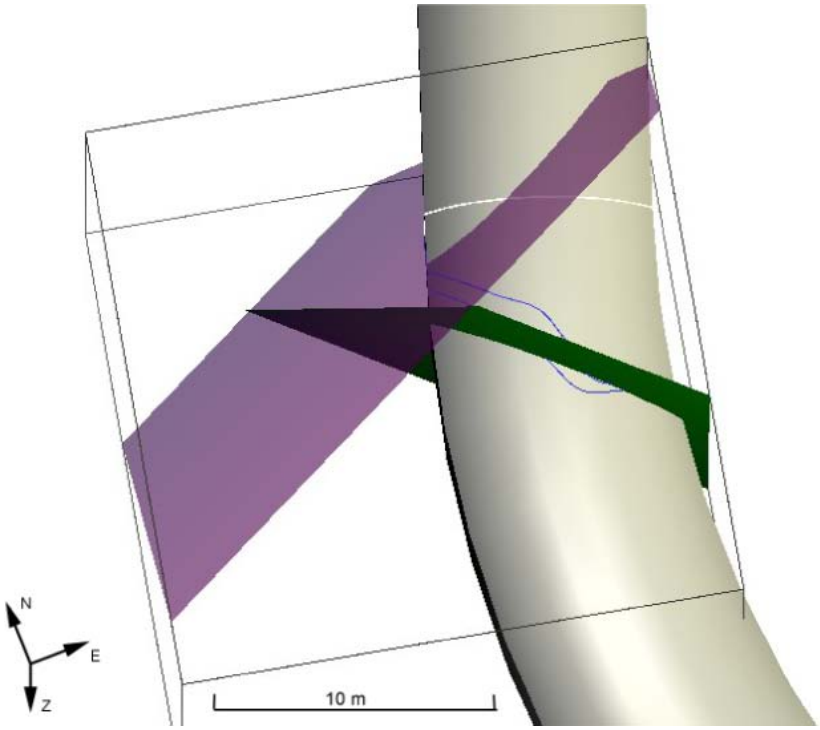

Figure 3-8. *Overview of the RVS model A. The target zone 'zone 2545' (green) terminates onto a narrow shear plane (transparent purple) (Mærsk Hansen et al. 2003).*

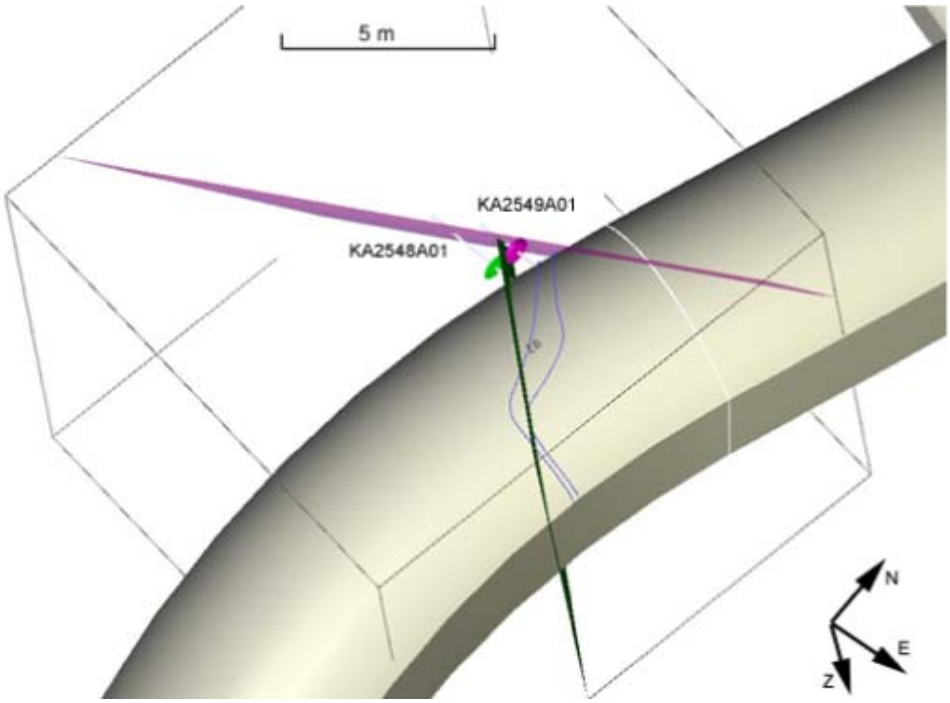

Figure 3-9. *RVS model A with borehole and fault geometry. View along 'zone 2545' intersection axis (crest of the tunnel, chainage 2/545 m). The purple disc shows an indication of the NNE shear zone, the green disc is an indication of a NW-striking feature.*

In boreholes KA2548A01, KA2549A01, and KA2548A03, no water flow was observed during or after drilling. In borehole KA2548A02 water could be observed after the last uptake, 3.88–5.21 m, and a flow of 950 mL/min was measured after completion of the drilling.

Neither breccia nor fault gouge occur in the selected structure. As 'zone 2545' does not contain any loose material, and as the original target fracture does not extend beyond a crossing structure, as shown in Figure 3-8 and Figure 3-9, its character is regarded as not being suitable within the scope of the present project, and was thus not recommended for resin injection experiments. The injection boreholes may however be suitable for study of the "porosity" of a fracture zone or of very coarse (10–20 cm blocks) "crushed zone" rather than of what is usually regarded as fault material, such as fault crush, fault breccia or fault gouge.

3.3 Measurements of groundwater flow and hydraulic head

Measurements of groundwater inflow to the tunnel from the 16 boreholes of 76 mm diameter were made immediately after completion of the boreholes. Subsequently all boreholes were equipped with front valves and pressure gauges. The resulting inflows and pressures are presented in Table 3-1.

On the basis of the results presented in Table 3-1 it was deemed meaningful to instrument 13 of the boreholes with mechanical packers, of the design presented in Section 2.4, to facilitate subsequent epoxy resin injection. The boreholes excluded from further consideration for resin injection on the basis of geological and hydrogeological constraints were KA2169A04, KA2548A03 and KA2548A03. A compilation of geometrical data related to zone location and packer position in the remaining 13 boreholes is provided in Table 3-2.

Table 3-1. Compilation of borehole data including recordings of outflow and pressure in the boreholes at different times.

Borehole specs		Flow (L/min)		Pressure (bar)			
Borehole id	L [m]	Drilling	Valve *)	030424	030428	030429	030506
KA 2169 A01	3.62	0.25	0.17 (0.18)	2.5	2	2.5	2.5
KA 2169 A02	4.32	0.235	0.25 (0.275)	2.7	2.5	2.5	3
KA 2169 A03	4.28	0.145	0.21 (0.21)	7	7	7	6
KA 2169 A04	5.47	0	5 drops/min (0.005)	5	5	5	5
KA 2548 A01	4.64	0	0.007 (1 drop/min)	14.5	15	15.5	16
KA 2549 A01	3.69	0.09	0.11 (0.12)	11.5	12	13.5	14.5
KA 2549 A02	5.21	0.82	0.84 (0.9)	20	20	20.5	20.5
KA 2549 A03	5.57	0	0.008 (0.087)	19.5	19.5	19.5	19.5
KA 1596 A01	5.94	0.7	0.7 (1.7)	9.5	10	10	10
KA 1596 A02	5.62	0	0.68 (0.6)	9.5	9.5	19 **)	9.5
KA 1596 A03	4.80	0.004	0.31 (0.52)	10.5	10.5	10.5	10.5
KA 1596 A04	4.10	0	0.073 (0.084)	8.5	9	9.5	9
KA 2423 A01	5.04	0	22 drops/min	19.5	20	20	20
KA 2423 A02	3.72	0	20 drops/min	12.5	12.5	12.5	13
KA 2423 A03	2.93	0	0.021 (0.066)	8.5	9	9	9
KA 2423 A04	3.11	0	0.023 (0.097)	8	8	8	8

*) Flow after some 4 hours. Initial flow is shown within parentheses.

**) Most likely an error in reading the pressure gauge.

Table 3-2. Compilation of coordinates of target zone, packer and resulting test section length.

Injection borehole	Length [m]	Zone location [m]	Packer position [m]		Test section length [m]
			Secup	Seclow	
KA 2169 A01	3.62	2.47–2.49	1.9	2.08	1.54
KA 2169 A02	4.32	2.96–3.10	2.6	2.78	1.54
KA 2169 A03	4.28	3.95–3.98	3.5	3.68	0.6
KA 2548 A01	4.64	1.58–1.62	1.17	1.35	3.29
KA 2549 A01	3.69	2.02–2.15	1.35	1.53	2.16
KA 1596 A01	5.94	5.48–5.62	5	5.18	0.76
KA 1596 A02	5.62	4.5–4.84	3.45	3.63	1.99
KA 1596 A03	4.8	3.14–3.52;4.15–4.22	2.65	2.83	1.97
KA 1596 A04	4.1	2.32–2.80	1.1	1.28	2.82
KA 2423 A01	5.04	4.22–4.26	3.5	3.68	1.36
KA 2423 A02	3.72	2.72–2.75	2.2	2.38	1.34
KA 2423 A03	2.93	2.36–2.53	1.8	1.98	0.95
KA 2423 A04	3.11	1.92–1.94	1.3	1.48	1.63

3.4 Mechnical packer design

The mechanical packer of diameter 76 mm is made up of a 0.18 m long mechanical packer which is operated from the surface using a swivel bolt, cf. Figure 3-10. Two hydraulic lines connect the test section with the borehole collar (at the tunnel wall), one line at the bottom and one at the top of the section, in order to facilitate efficient circulation of epoxy resin. In order to reduce the volume of the test section, it is filled with a 74 mm polyethene cylinder (dummy) in which the circulation lines are embedded.

3.5 Mechanical packer postions in boreholes

Mechanical packers were manufactured for the 13 boreholes identified in Section 2.3. The geometrical data related to the instrumented boreholes are indicated in Table 3-2 in terms of borehole length, zone location, packer position (packer length is 0.18 m) and the resulting test section length for the respective holes is given in Table 3-2.

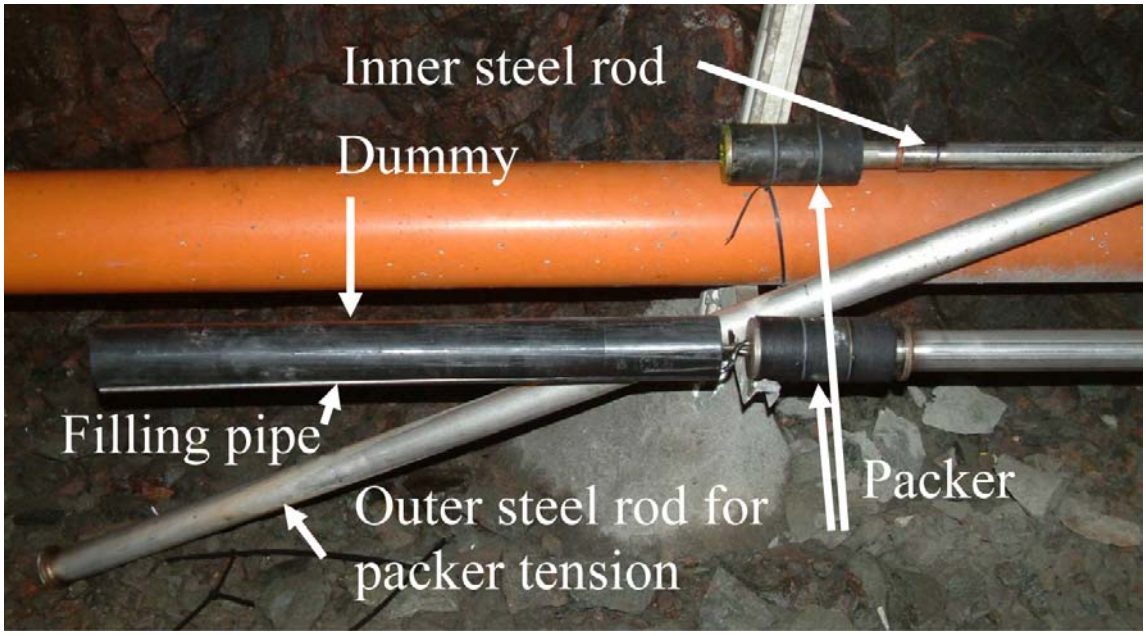

Figure 3-10. *Mechanical packer with plastic dummy and associated equipment.*

3.6 Flow tests after emplacement of injection packers

Following installation of the injection packers at the selected positions in the boreholes, a series of flow tests using water were conducted to assess the likelihood of successful injection of epoxy. The applied excess pressures are not expected to have damaged the internal structure of the fault zones. Similar experience is available from the Nagra resin work at Grimsel (Alexander W R, personal communication). The tests were generally conducted in a sequence whereby the ambient formation pressure (P_o) in the packed-off section and the corresponding sustained yield (Q_{Po}) when opening the connection valve at atmospheric pressure were established. Subsequently the corresponding yield at excess pressure increments of 2 bars was generally established. In the case of the boreholes at chainage 1/596 m attempts were also made to optimise the packer position to maximize epoxy take.

Table 3-3 accounts for the measured pressures and yield, jointly with the respective section length and the (average) transmissivity evaluated using Moye's formula. Notable are the no-flows, or very low transmissivities established for the tested borehole sections in KA1596A01 and KA1596A03 (corresponding to deformation zone NE-2 in the Äspö HRL site-descriptive model). This led to exclusion of these boreholes from epoxy injection, cf. Section 3.6. The remainder of the proposed sections to be used for epoxy injection show transmissivities ranging from $6 \cdot 10^{-10}$ to $1.1 \cdot 10^{-7}$ m^2/s. The transmissivities, which are attributed to the identified target structures in the packed-off sections, show variability, but are, with one exception ('zone 1596'), contained within one order of magnitude, in terms of local transmissivity.

Table 3-3. Compilation of steady state pressure (Po) and associated flow, resulting flow due to an applied excess pressure (P1 and P2) , and evaluated average steady state transmissivity of the packed-off section containing the target structure.

Borehole ID	P_o (bar)	Q_{Po} (mL/min)	P1 (bar)	Q_{P1} (mL/min)	P2 (bar)	Q_{P2} (mL/min)	Section length (m)	Transmissivity (m^2/s)
KA1596A01	6.5	0.9	8	0	11	0	0.76	0
KA1596A02	1.75	0.5	5	3.7	7	6.5	1.99	$1.35 \cdot 10^{-9}$
KA1596A03	0	0.04	5	1.9			1.97	$4.3 \cdot 10^{-10}$
KA1596A04	0	0	5	63.5			2.82	$1.55 \cdot 10^{-8}$
KA2169A01	0.4	66	2.4	86			1.54	$4.57 \cdot 10^{-8}$
KA2169A02	3.5	88	5.5	216			1.54	$1.15 \cdot 10^{-7}$
KA2169A03	6	178	8	23			0.6	$9.35 \cdot 10^{-9}$
KA2423A01	19.5	2	21.5	2	23.5	0	1.36	$1.03 \cdot 10^{-9}$
KA2423A03	8.4	64	10.4	16	12.4	21	0.95	$6.2 \cdot 10^{-9}$
KA2548A01	15.9	6	17.9	0	19.9	1.8	3.29	$5.69 \cdot 10^{-10}$
KA2549A01	15.9	106	17.9	11	19.9	21.5	2.16	$6.27 \cdot 10^{-9}$

4 Epoxy resin injection

4.1 General strategy

When selecting suitable injection boreholes a number of factors and conditions need to be taken into account. These include the measured inflow to the borehole section, the groundwater pressure in the section, the resulting yield relative to applied excess pressure and the relative position of the borehole to the tunnel wall. The latter aspect implying that the farther away the borehole is from the tunnel wall the effects of stress redistribution (the effects of excavation damage assumed negligible at the distances in question away from the tunnel wall). A distinction is here made between the irreversible "damage" which is experiences in the immediate vicinity of the underground opening and the "disturbance", affecting state variables (stress field, hydraulic head distribution), which are considered insignificant and reversible (Bäckblom 2008). Still, it is generally expected that these effects are generally lower in conjunction with larger deformation zones compared to sections of normally fractured rock.

4.2 Selection of epoxy injection boreholes

4.2.1 Inflow

A too low groundwater flow (low transmissivity) implies problems to inject sufficient volumes of epoxy resin to invade the available porosity. At the same time a too high inflow implies the risk of washing away the isopropanol used to wet the fracture surfaces, cf. Section 4.4, hence hindering injection of epoxy.

The interval $0.001 < Q < 1$ [l/min] was considered as a suitable constraint for the current application. A general aim has been to employ as wide a spread in inflow (transmissivity) as possible within the indicated interval in the current application.

4.2.2 Assessment of injectability using hydraulic tests

The hydraulic tests carried out by means of water injection at selected excess head, cf. Section 3.6, showed that epoxy injection should be possible in seven boreholes only, distributed over the four sites. One site, however, at chainage 2/545, was deemed inadequate for the purpose of the project, but was still retained for an initial test of the developed work procedure.

4.2.3 Groundwater pressure

A general guide is to employ an overpressure of c. 5 bar during injection of epoxy. Restrictions related to the injection equipment imply problems in the event the injection pressure is in the interval 40–50 bar. The measured pressures need to be stable and reliable. If the groundwater flow is low the pressure registration is associated with uncertainty since a small leakage may entail a large change in pressure.

Constraints related to groundwater pressure were:

- Suitable ambient groundwater pressure $P < 30$ bar.
- Stable pressure registrations.
- The associated groundwater flow should not be "extremely" low.

4.2.4 Other aspects

In the case where more than one borehole of a set was found to be suitable, the borehole located farthest from the tunnel wall (least disturbance induced by stress redistribution) should be selected.

4.3 Review of epoxy resin and additives

A number of parameters have to be factored in when assessing the usefulness of a resin to be employed at *in situ* conditions at Äspö HRL.

1. Preservation of flow path geometry and internal structure: Suitability of the resin with respect to preserving *in situ* conditions *sensus stricto*. Effects of contrasting physical and chemical properties.
2. Injectability: The resin's viscosity must be low enough so that it can be easily injected into the fault rock zone (too high pressures would possibly disturb and erode the fault gouge).
3. Optimal resin in terms of physical properties (e.g. viscosity, gel time, stability, interaction with wet surfaces, etc).
4. The structural quality and strength of impregnated samples (assessed macroscopically using sawn samples and microscopically using thin sections).
5. Previous *in situ* experience, site-specific and international.

Another aspect not covered here is the interaction of resins with sorbing radionuclides.

A clear ambition from the onset has been to employ an epoxy resin rather than an acrylic resin. The argumentation for this is twofold; an acrylic resin requires an *in situ* heat source to initiate polymerisation of the acrylic resin, which introduces a series of practical problems. Furthermore, it is much easier to adapt an epoxy resin, e.g. by altering its composition, to a particular condition and need. Hence, the laboratory program assessing resins, described in Chapter 2, was entirely devoted to assessment of two epoxy resins. One of these was a two component epoxy resin, EpoTek 301 (www.epotek.com), which also was used with good results in the TRUE-1 Pilot Resin Experiment (Birgersson 2000a, b, Hakami and Gale 1999). This resin resembles the resin used by Nagra in conjunction with the EP prpoject (Alexander et al. 2003), see below.

The main alternative for the current application was to use EpoTek 301 for the injections both in fault rock zones and subsequently in Feature A (the latter located at the TRUE-1 site, cf. Winberg et al. (2000)). The viscosity of EpoTek 301 is about 100 times higher compared to water and the resin starts to cure a few hours after start of injection. Other resins employed by Nagra at the Grimsel test site have also been reviewed. The following resins used at Äspö and Grimsel were considered:

- Äspö HRL, the Pilot Resin Experiment. Epoxy resin, EpoTek 301. Viscosity about 0.1 Pa·s (0.1 Pa·s = 100 cps) (www.epotek.com).
- Grimsel laboratory, the Excavation Project, EP. Epoxy resin, Sika INJ 26. Viscosity about 0.1 Pa·s (Alexander et al. 2003).
- Grimsel laboratory, the Connected Porosity, CP, project. Acrylic resin, Sika NHC-9. Viscosity about 0.03 Pa·s at 5 ºC, < 0.01 Pa·s at 20 ºC (Möri et al. 2003).

The Excavation Project (EP) at Grimsel (Alexander et al. 2003) focused on flow path characterisation and included injection of an epoxy resin into a high porosity fault breccia with fault gouge. The investigated structure probably resembles the foreseen fault rock zones at Äspö from a mineralogical and chemical standpoint, although the latter may be less transmissive that the one investigated at Grimsel.

A one-component acrylic resin was used in the Connected Porosity Project (CP) (Möri et al. 2003) to characterise matrix porosity. The polymerisation of the resin starts when the temperature is raised above 40 ºC. The heat source used by Nagra reached a temperature of about 160°C. The maximum temperature at the rock wall in the borehole was about 80°C.

Nagra has developed and tested several resins. A general finding is that it is easier to use an epoxy resin at a new site (in consideration of differences in water chemistry and mineralogy). An acrylic resin requires more development, primarily regarding its overall chemical composition. Notable is that the two resins were developed for different reasons, one to access flow paths (epoxy), the other to access rock matrix porosity (acrylic resin). They both have their limitations in their impregnability and in their practical usability.

Furthermore, the viscosity and the curing time (or “pot time”) of an epoxy resin can be controlled well, for example by changing the composition of the resin. For a given resin the temperature and mixing ratio will also influence the viscosity and pot time.

The successful use of Epotek 301 in an Äspö HRL environment was shown by the injections made in conjunction with the TRUE-1 Pilot resin experiment (Winberg et al. 2000, Gale and Hakami 1999, Birgersson et al. 2000a, b), including penetration into hairline fractures with mean apertures in the order of 285 μm.

Resolve

Given the characteristics of the fault zones planned to be injected and the successful use of EpoTek 301 resin in the TRUE-1 Pilot resin Experiment, it was decided to proceed with the latter epoxy. Details on the methodology applied (including procurement and use of additives) in the Fault Rock Zones Characterisation project is given in Section 4.4.

4.4 Injection equipment and procedures

The injection system employed in the TRUE-1 Pilot resin injection experiment was based on a continuous in-line mixing of resin and hardener. It was possible to continuously mix and inject resin for time periods up to about 10 h. The injected volumes ranged from a few 100´s of millilitres up to more than 1,000 ml.

The current application, which can be viewed as a further development of that used in the TRUE-1 Pilot Resin Experiment, utilised equipment, cf. Figure 4-1, consisting of a 12 L vessel for the wetting agent (isopropanol), a manual rotating pump (used to push epoxy back in the injection line after draining to enable measurement of pressure and drainage), a gas tube with regulator, a customised 0.8 L pressure vessel conected together using three-way valves. The aim is to propagate and fill the fault rock zone with epoxy radially from the borehole section such that a 300mm overcoring is deemed meaningful. Assuming that the zone is 20 mm thick, has a porosity of 20%, and 0.5×0.5 m square of the zone is to be injected. This requires a minimum of 1 L epoxy to be injected in each borehole section. The amount of isopropanol should be larger, in the order of 3-10 L per borehole section. The injection pressure should not exceed the ambient pressure with more than 5 bars to avoid disturbance of the internal structure of the zone. Injection times should at the maximum be some 5–10 h.

The procedure was as follows :

A) Injection of isopropanol. This agent exchanges the water in the fractures which will enable and facilitate injection of the epoxy in the zone. The injection pressure should ideally be 2–3 bars above the ambient pressure, and 5 bars at the maximum. All other holes in structures closed in. Registration of injection flow, injection pressure and breakthrough of isopropanol in the tunnel. Criteria for termination were a) 10 L of isopropanol injected, c) at 15 h from start, provided at least 3 L has been injected.

B) Transition from isopropanol to epoxy. Injection of isopropanol by closing the two-way valve (A) below the isopropanol tank. The epoxy vessel is connected using the uppermost three-way valve (B). The pressure is regulated to c. 2–3 bars above ambient pressure using the gas regulator. The lower three-way valve (C) is switched to to the epoxy vessel. The outlet valve (D) is switched carefully to the drain to exchange isopropanol for epoxy. During this action the pressure in the borehole section may reduce, but should not be below ambient pressure. When 0.1 L of epoxy has exited through the drain, the valve is turned to to the crank pump upon which the pressure in the borehole increases to the pre-set regulated pressure and injection of epoxy commences. In order to monitor the pressure in the borehole during the hardening process, Isopropanol is gently pushed/pumped reversed through the outlet valve (D) into the outlet hose using the crank pump.

C) Injection of Epoxy (mixed with 14 g//L of the fluorescent dye Epodye to facilitate easy visual detection of invaded pore spaces in subsequent analysis) is at first made at a pressure that exceeded ambient pressure with 2–3 bars. Given that 1 L of epoxy is to be injected and injection is expected to continue 5–10 h at the most, the injection flow should be at least 0.3 L/h. If the initial flow is too low this can be remediated by increasing the pressure, to 5 bars above ambient pressure at the most. Alternative strategies to deal with too low injection flow rates were devised. All other holes in the structure were closed in. Registration of injection flow, injection pressure and breakthrough of isopropanol in the tunnel. Criteria for termination were too low injection flow rate, usually after some 10-20 hours.

A potential problem arising from heat emission from a rapid hardening of the epoxy was counter-measured by keeping the epoxy vessel in a container filled with 12°C cooling water during the injection procedure. It was noted that the hardening time for the epoxy was 5–6 hours at 12–13°C (For comparison the temperature in the tunnel vary from 13–20°C over a typical year, while the temperatures in the rock are c. 13–14°).

Each of the injected pilot holes was equipped with a mechanical packer system, cf. Section 3.4, which included a massive 74 mm diameter plastic dummy in the packed-off part of the borehole in order to minimise epoxy consumption, and a pipe through the dummy such that the hole can be filled with resin from the bottom (cf. Figure 3-10). An inner rod is fixed to the packer by means of a threaded coupling. Another, outer rod slides along the inner rod, being pressed by means of a nut on the threaded exposed end of the inner rod against the packer, thus expanding the rubber coils of the packer, cf. Figure 3-10.

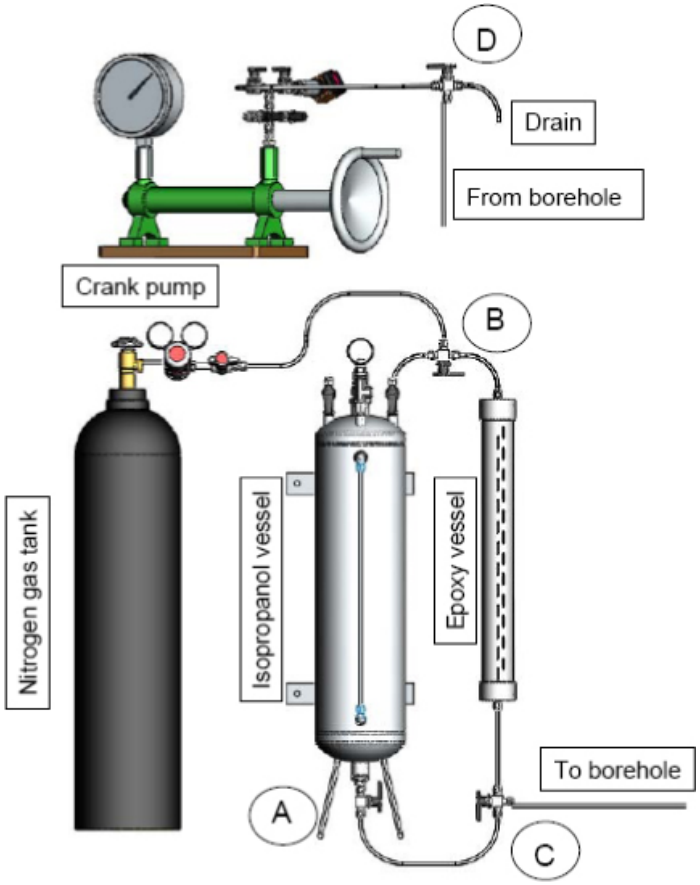

Figure 4-1. *Schematic illustration of the epoxy resin equipment used in the current application. From left to right: Gas tank with regulator, Pressure vessel for isopropanol (V=12L), customised pressure vessel (V=0.8L) for epoxy resin. The functional use of the indicated valves is discussed in the text.*

4.5 Results

The volumes of isopropanol and epoxy, the maximum pressures reached and the durations of the two *in situ* injection phases in the respective boreholes are accounted for in Table 4-1.

Epoxy was successfully injected in all boreholes apart from KA2548A01 and KA2423A01, the latter two with corresponding low injected volumes of isopropanol. Notable are the highly successful resin takes in KA2169A01 (V=1.05 L) and KA2423A03 (V=0.56 L), see also Table 3-3. With a few exceptions, most of the epoxy injections lasted in the order of some 20 hours, which was in the upper end of projected injection times, cf. Table 4-1.

Table 4-1. Compilation of measured pressures, volumes of isopropanol and epoxy injected and the associated time frames of injection.

		Isopropanol			Epoxy		
Borehole	**Ambient pressure Po (bar)**	**Volume (L)**	**Duration (hrs)**	**P_{max} (bar)**	**Volume (L)**	**Duration (hrs)**	**P_{max} (bar)**
KA1596A02	2.8	2.55	16	5.9	0.12	11.2	9.6
KA1596A04	0.16	11.97	22.5	3.2	0.14	23	12
KA2169A01	0.8	8.58	1.5	2.8	1.05	21	4.9
KA2169A02	2.8	10.91	1.1	4.8	0.44	22	10
KA2169A03	6.9	3.56	22.2	11.1	0.26	>24	16.1
KA2548A01	16.7	0.3	>5	24.6	0	NA	NA
KA2549A01	16.5	3.15	16	18.7	0.69	22	20.1
KA2423A03	8.5	2.67	16	10.6	0.56	22	13.6
KA2423A01	19.6	0.04	1	26.7	0	NA	NA

5 Overcoring and sample preparations

5.1 General

Before overcoring the epoxy must be allowed to fully harden. In this case the curing time was conservative with more than five months between the resin injection and the overcoring.

The overcoring involves drilling of 300 mm boreholes, guided by the existing pilot 76 mm exploration holes previously used for the epoxy resin injection, and produces drill cores (over cores) 277 mm in diameter. The retrieved cores form the basis for the subsequent study of the nature and characteristics of the connected pore space. The overcoring activities were applied to the following resin-injected drill holes: KA1596A02, KA1596A04, KA2169A01, KA2169A02, KA2169A03, KA2423A03, and KA2549A01. Borehole-specific data are provided in Table 5-1.

The activities were carried out in accordance with a pre-defined procedure, cf. Section 5.2 for a condensed account, which in some cases required modifications/adaptations for the individual boreholes in accordance with local conditions met during the over-coring process.

Table 5-1. Borehole-specific data for the seven injection holes which have subsequently been overcored (in metres).

Hole ID	Pilot length	Target Zone position	Packer position	Injected length	Resin take [litres]	Specif.ic resin take [l/m]	Over-cored length	Length of target core
KA1596A02	5.62	4.32–5.00	3.45–3.63	1.99	0.1214	0.06	6.15	4.3–6.15
KA1596A04	4.1	2.05–3.05	1.10–1.28	2.82	0.1387	0.05	3.2	1.9–3.2
KA2169A01	3.62	2.30–2.65	1.90–2.08	1.54	1.054	0.68	3.6	1.9–2.6
KA2169A02	4.32	2.70–3.35	2.60–2.78	1.54	0.44	0.29	4.4	No core
KA2169A03	4.28	3.70–4.20	3.50–3.68	0.6	0.26	0.43	4.4	3.55–4.4
KA2423A03	2.93	2.20–2.65	1.80–1.98	0.95	0.5635	0.59	3.1	1.9–3.1
KA2549A01	3.69	1.67–2.24	1.35–1.53	2.16	0.690	0.32	2.4	1.3–2.4

5.2 Technical procedure

Overcore drilling was, when applicable, carried out in accordance with a developed protocol. Below follows a description of a typical work sequence, slightly abbreviated and modified.

1) Removal of outer piping and hoses attached to the outer end of the mechanical packer (and possible removal of the mechanical packer itself).
2) Removal of the 76 mm massive PET (dummy) cylinder and 6 mm injection pipe, by means of drilling using full face drill bit, until 0.1 m before the target zone (cf. location of target zone in Table 5-1). In the event the packer equipment and/or the plastic dummy assembly start to rotate, it will be removed.
3) Overcoring down to c. 0.10 m before the target zone with a single 300 mm core barrel of 0.75 m length (Figure 5-1). The resulting core diameter is 277 mm (by comparison the cores from the 76 mm pilot boreholes have a diameter of 52 mm). Each round of cored section (uptake) varied in length, generally being 0.65 to 0.75 m long.
4) In many cases, the core will break due to an existing natural fracture, but when required, core breaks were induced by means of a curved, flat “steel flask” in the annular slot between the core and the borehole wall, expanded by means of hydraulic oil, applied some 0.4 m from the bottom of each drill round. The *in situ* core was acting as a lever to break (itself) at its base inside the drill hole (Figure 5-2 and Figure 5-3).

5) Drilling of each 0.75 m round was followed by careful recovery of the core by means of a specific core recovery tool (Figure 5-4).
6) The target zone recovery coring section was defined as 0.1 m before the target zone to 0.5 m beyond, the latter to avoid excessive and detrimental stress on the target zone during application of the core breaking tool. The target zone recovery was enabled using a single core barrel of 2.25 m length, aiming to recover the remaining core, including the target zone, in one single piece (Figure 5-1). Breakage, if required and recovery was aimed to be carried out using the same method as for the shorter drill rounds.
7) Core orientation, labelling and sawing into manageable pieces.
8) Due to the large core diameter, giving a weight of 150–170 kg per metre of core, handling of the core had to be done with a tractor equipped with a crane (Figure 5-5).

Figure 5-1. *300 mm core barrels with space for 0.76 m and 2.25 m core length, respectively. Scale bar on top of leftmost barrel is 2 m.*

Figure 5-2. *Tools for core breakage.*

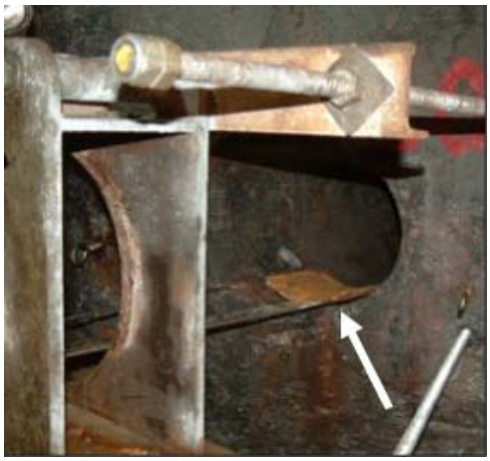

Figure 5-3. *Insertion of tool for core breakage.*

Figure 5-4. *Core recovery tool.*

Figure 5-5. *Core lifting.*

Figure 5-6. *Core logging table with rotating cylindrical supports.*

5.3 Documentation of retrieved overcores

Details regarding the application and local adaptation of the overcoring procedure presented in Section 5.2 to the conditions met at the seven overcored boreholes is provided by Mærsk Hansen and Staub (2004). Four cores, KA2169A01, KA2169A03, KA2423A03, and KA2549A01 were recovered with complete, or almost complete, success. Fractures in or near the target zones were found to be filled with epoxy and the cores were intact (KA2169A01, KA2169A03, and KA2423A03) or almost intact (KA2549A01). These cores, including the target structure/-s, were mapped in detail by covering the cylindrical envelope surface of the core with transparent plastic film. Identified cataclastic structures, fractures, quartz fillings and mylonitic foliation were mapped with ink on the film. Likewise, noted epoxy infillings were marked. By this procedure, a 1:1 scale drawing of the entire cylindrical envelope surface of the target zone and the adjacent wall rock was obtained. The drawings are shown at reduced scale in Maersk Hansen and Staub (2004), cf. Appendix 1 therein.

In addition, the entire core from each hole was logged at 1:10 scale, with respect to fracture position, fracture orientation, fracture wall alteration, fracture mineral fill and/or coating and epoxy filling. Details on the logging and the drawings are presented in Maersk Hansen and Staub (2004), cf. Appendix 2 therein.

The cores were also routinely photographed using a digital camera. Epoxy grouted zones were, in addition photographed under UV light (wavelength spectrum of approximately 315–400 nm) enabling enhanced visualisation/identification of resin-filled pore spaces.

In the following, brief accounts are given of information obtained in the 76 mm pilot boreholes and the corresponding 300 mm boreholes, and associated cores.

5.3.1 KA2549A01 overcore

Pilot: The original target zone was not identified by pilot drilling as a zone. Individual fractures occurred, but could not be made to fit with two subsequent intercepts in boreholes KA2549A02 and KA2549A03 at this site (Maersk Hansen et al. 2003).

However, another zone, almost perpendicular to the original target zone appeared in the pilot core as four fractures crossing at approximately 2 metres, two with an angle of approximately 10° to the core axis and two of approximately 30°. Subsequent BIPS imaging in the borehole only detected three of them (probably due to poor visibility in the water-filled borehole) and established their geometries to 78°/47°, 69°/44° and 64°/56°, respectively, being in accordance with both core logs and tunnel mapping. The zone was interpreted as being made up of 4 individual fractures. A fourth pilot hole, KA2548A01 was drilled in order to pass 1 metre beyond this zone, but did not intercept it.

Overcoring: In the overcored KA2549A01, at the target zone at c. 2 metres depth, (Figure 5-7), two epoxy-impregnated fractures were observed with an orientation of 268°/62°. The dip was measured *in situ* by aiming with the inclinometer at the core stub in the hole, before overcoring, and the angle was subsequently used for core orientation. The two fractures diverge into four fractures, with orientations of 292°/50° (one such divergence can be seen in Figure 5-8). A few fractures at L=1.5–1.7 metres, with an orientation of 136°/85° were also impregnated with epoxy, and also some minor randomly oriented fractures were well impreganted with epoxy (Figure 5-9).

Interim conclusions:. The large diameter core gives a more detailed picture of the structure, showing a system of sub-parallel fractures which diverge and merge, rather than being the interpreted four individual subparallel fractures. The lack of intercept in KA2548A01 can be explained by a shift in geometry between KA2548A01 and the other holes, or alternatively that the structure peters out in this area.

Figure 5-7. *KA2549A01. Recoverd core with target zone close to metal core bit, and outline (red) of area shown enlarged in Figure 5-8.*

Figure 5-8. *KA2549A01. Target zone, with fracture diverging towards the right, impregnated with epoxy, and approximate outline of Figure 5-9 indicated by white frame at extreme right.*

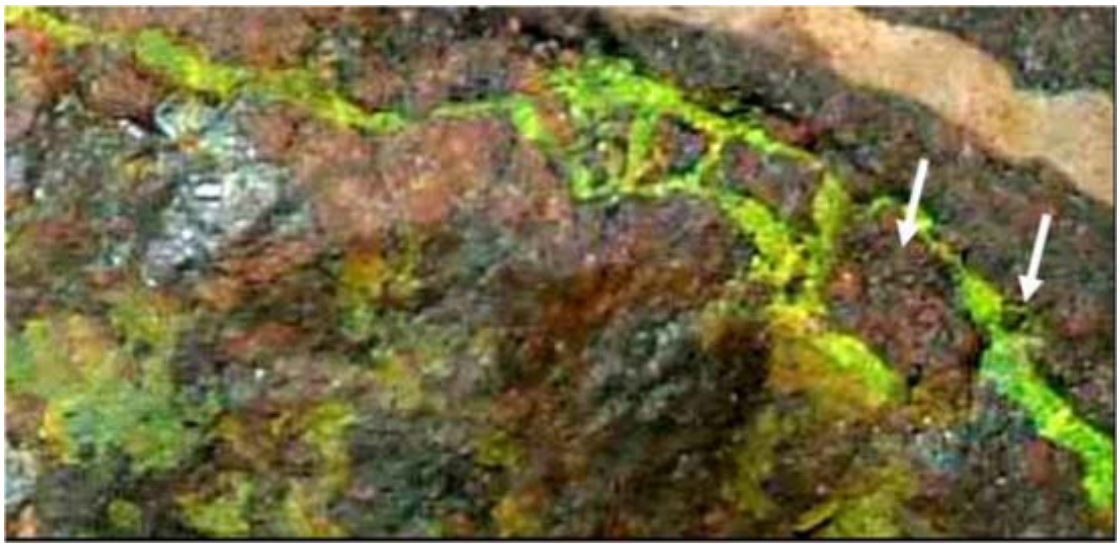

Figure 5-9. *KA2549A01. Epoxy fill detail, c.f. Figure 5-8 for relative position. Arrows mark cm-sized and millimetre-sized pieces and fragments, respectively, encircled by epoxy.*

5.3.2 KA2169A01 overcore

Pilot: The target structure at L=2.5 metres is a fracture with a width of 2–3 mm filled with breccia, appearing to be potentially water conducting, and with an angle of 40° to the core axis. BIPS logging indicated an orientation of 164°/37° for the structure. Nearby, another two fractures oriented 169°/87° and 165°/85° occur at L=2.1 and 2.2 metres, respectively.

Overcoring: Overcoring showed that the target fracture is connected to adjacent subparallel fractures **(**Figure 5-10**)**. There is no visible epoxy in the zone, but three fractures at L=2.1–2.35 metres are filled with epoxy, two oriented 340°/70° and one 130°/78°, with a sub-system of splays (Figure 5-11). No connection with the target zone is visible in the core, but fracture orientations indicate that they will intersect or merge.

Interim conclusions: The target structure consists of a few sub-parallel converging master fractures. They contain clay minerals which may have obstructed epoxy intrusion. Three fractures striking NW-SE, two 340°/70° and one 130/78 as well as adjacent minor splay fractures (Figure 5-12) have been impreganted well with epoxy.

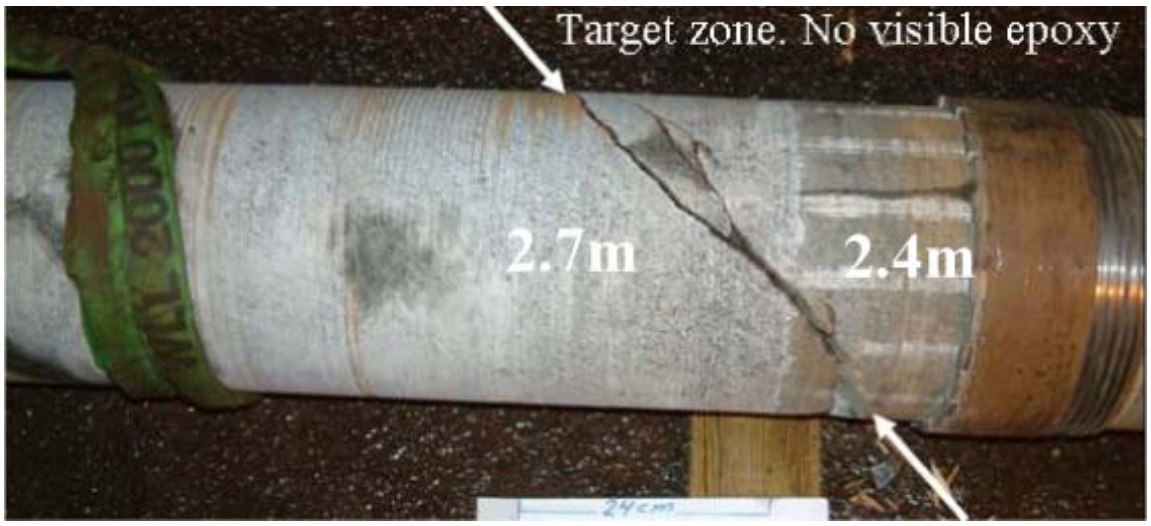

Figure 5-10. *KA2169A01. Recovered core with target zone at L=2.5 metres, with no visible epoxy. Hidden under the drill bit (at far right) are epoxy-filled fractures at L=2.10–2.35 metres (cf. Figure 5-11).*

Figure 5-11. *KA2169A01. Recovered core segment with epoxy-filled diagonal fractures at L=2.15–2.35 metres (center-right). Photograph under ordinary light.*

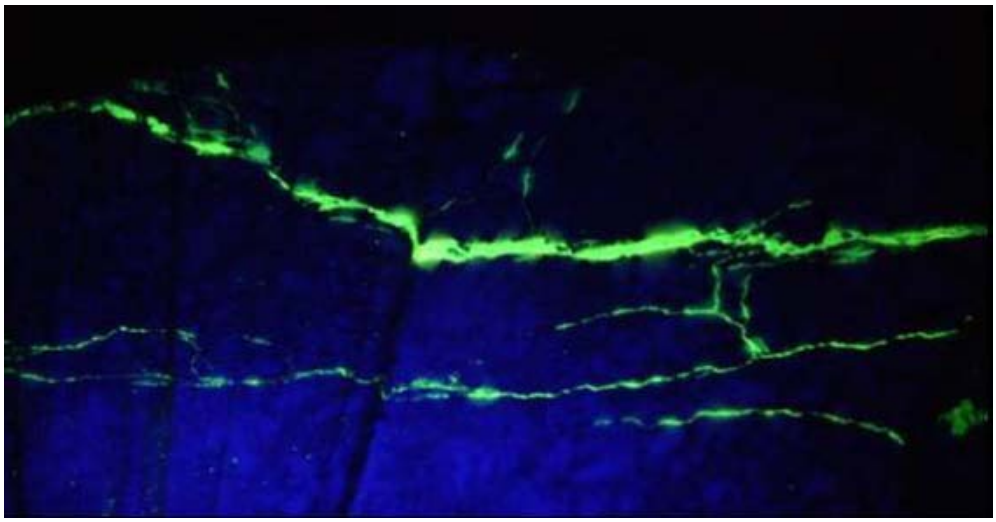

Figure 5-12. *KA2169A01. Epoxy-filled fractures on a surface cut across the core at L=2.20 metres at UV light. Approximate 1:1 scale (Apologies for poor quality in photograph).*

5.3.3 KA2169A02 overcore

Pilot: The pilot drill core identified a 0.05 m thick structure with fault crush at L=3.00 metres, with a 30° angle to the core axis. The BIPS log indicates an orientation of 308°/89°, which is in accordance with the angle relative to the core axis and the zone's tunnel appearance.

Overcoring: The core was damaged during drilling. Only debris, with patches of epoxy, was recovered from the target zone. No directional data could be measured (Figure 5-13).

Interim conclusions: Clayey infilling may have obstructed epoxy intrusion and may also have resulted in bad cohesion of the fault gouge and breccia material.

5.3.4 KA2169A03 overcore

Pilot: The pilot core showed a 2 cm thick structure with fault crush at c. 4.0 metres, with a 30° angle to the core axis. The BIPS log indicated an orientation of 310°/80°, in accordance with tunnel and core data.

Overcoring: The target structure appeared as an up to 5 cm wide zone with mylonitic foliation, (foliation caused by shearing, common in fault zones) with an orientation of 300–315°/80°, and with sub-parallel, converging and diverging epoxy-filled master faults, with orientations of 300–315°/80°, and also epoxy-impregnated cavities and minor splay fractures (Figure 5-14 and Figure 5-15).

Interim conclusions: The structure appeared in the over core as projected and has a structure similar to that observed in the pilot borehole. The overcore is filled well with epoxy (cf. epoxy take in Table 5-1) both in NW-SE striking master faults and in splays (Figure 5-15), preserving the rock material, and resulting in excellent core recovery.

Figure 5-13. *KA2169A02. Epoxy patches on fracture surfaces of recovered core segments.*

Figure 5-14. *KA2169A03. Recovered core with target zone at L=3.90 metres, with many indications of epoxy (yellow streaks along the diagonally oriented fracture in the centre of the photograph). An enlargement of the area at the L=4.00 metre mark is shown in Figure 5-15.*

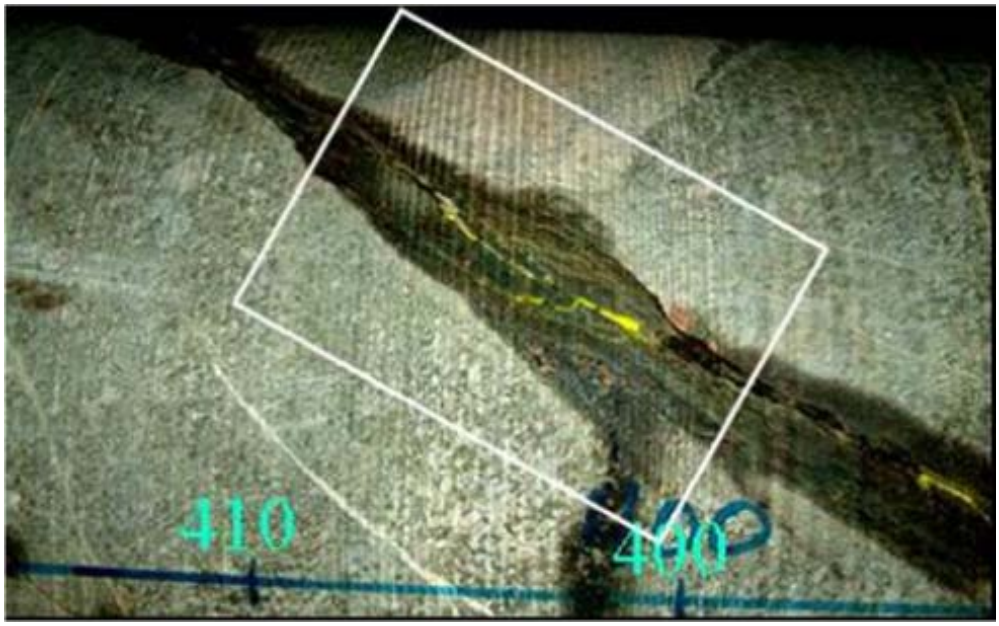

Figure 5-15. *KA2169A03, L=3.90 metres. Above: Epoxy grouted structure flanked by mylonitic foliation.*

5.3.5 KA2423A03 overcore

Pilot: The pilot borehole showed three 0.02 m thick zones with fault crush at c. 2.4 metres, with a 40° angle to the core axis. The BIPS log indicates an orientation of 165–170°/75°, which is in accordance with tunnel and pilot core data.

Overcoring: An up to 0.1 m wide zone was identified with mylonitic foliation with a geometry of 150–160°/80–85°, approximately 50° to the core axis. This zone contains converging and diverging epoxy-filled master faults with orientations of 150–160°/80–85° but also abundant epoxy-filled cavities and splay fractures. Also sealed fractures can be observed (Figure 5-16).

Interim conclusions: The structure appeared as projected and had characteristics similar to those observed in the pilot borehole (Mærsk Hansen et al. 2003). It is filled well with epoxy, both in master fractures and splays, preserving the rock material and resulting in excellent core recovery. Apart from that, the nature and orientation of this zone is very much akin to the structures experimented upon in the TRUE-1 Project (Feature A), cf. Winberg et al. (2000) and the TRUE Block Scale Continuation (Structure #20), cf. Andersson et al. (2002a).

To enable a comparison between different types of characterisation images the BIPS image from KA2423A03 is shown in Figure 5-17. This location corresponds to that of the main fractured zone selected for further study.

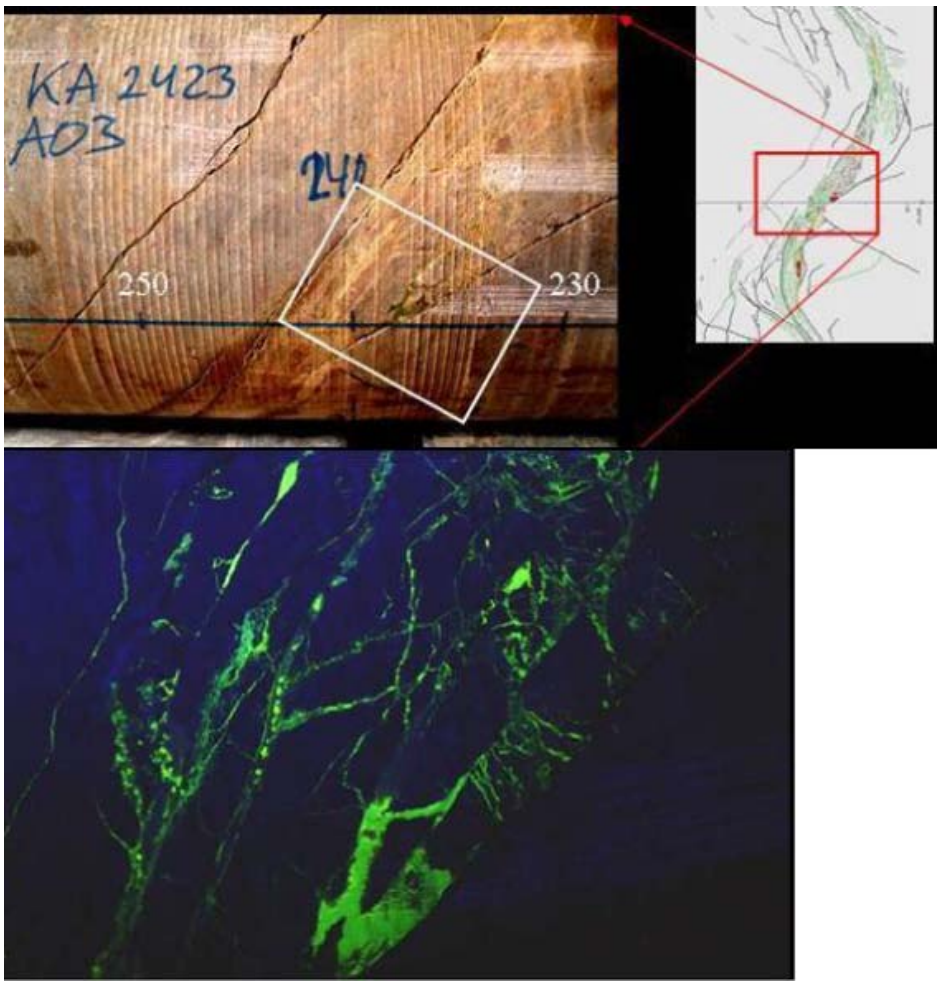

Figure 5-16. *KA2423A03, Recovered core with target zone at 2.4 metres, 50° to core axis, and with mylonitic foliation along the zone, and with epoxy (dark green in middle of rectangle indicating outline of UV picture below). The pore spaces appear to be well connected. NB. The cm-wide spaces in the lower part of the blow-up are interpreted to be a result of the angle of the cutting plane relative to the geometry of the pore.*

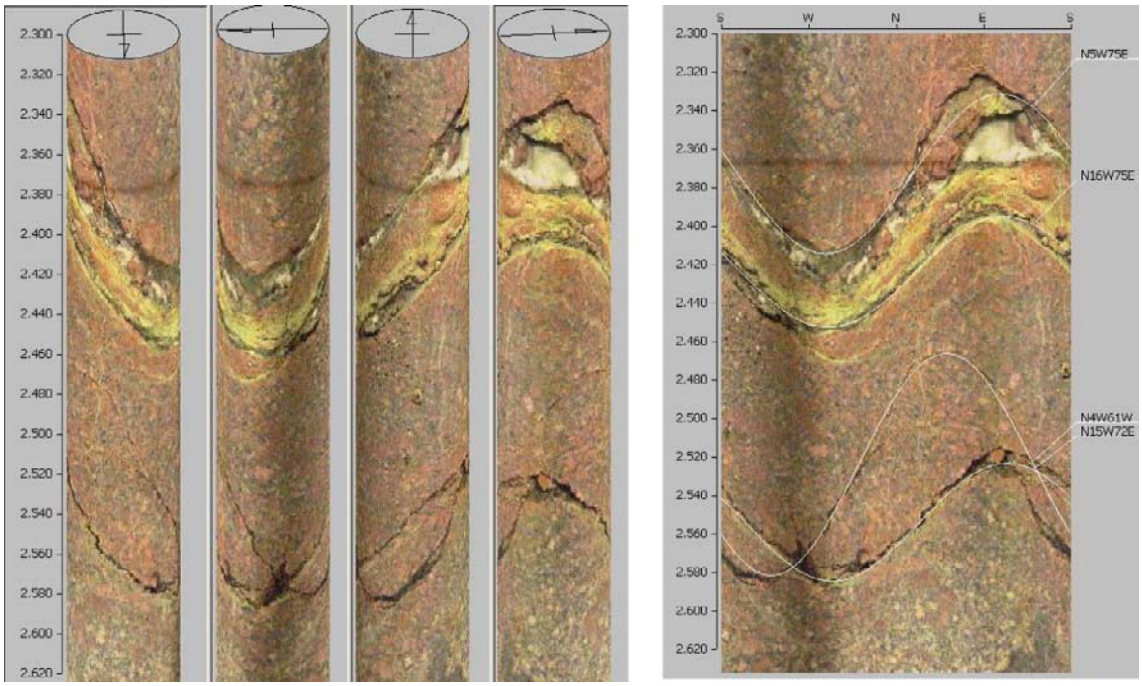

Figure 5-17. *BIPS image, the upper fracture zone is the location of the main structure imaged in Figure 5-16.*

5.3.6 KA1596A02 overcore

Pilot: The pilot core showed a 0.25 m thick zone with fault gouge (rather chloritic phyllonite) at c. 4.7 metres with an angle to the core axis of 40°. The BIPS log showed associated fractures with orientations of 54°/70°, 45°/78°, 37°/83°, and 23°/86°, which are in accord with tunnel and core data.

Overcoring: The core at the position of the target zone was severely damaged by drilling and only loose debris, presumably from the zone, was recovered. Some epoxy had intruded into the fault gouge, but only up to a few cm away from pilot borehole perimeter, and hence only sporadic epoxy was observed on the surface of the overcore. However, epoxy is abundant in fractures at L=3.7–3.9 metres with an orientation of 145/80°, i.e. approximately perpendicular to the zone and approximately parallel with the principal horizontal stress orientation.

Interim conclusions: The structure appears as expected and shows a structure similar to that observed in the pilot borehole. Clayey infillings has obstructed epoxy impregnation of the fault gouge, but, as in the case of KA2169A01 and KA2169A03, epoxy is abundant in steep fractures oriented in the NW quadrant. The difficulty to inject epoxy is in line with the results of the hydraulic tests that preceded the epoxy injection, cf. Section 3.4.

Figure 5-18. *KA1596A02. Recovered core with target zone at c. 4.6 metres. Apologies for poor quality in photograph.*

5.3.7 KA1596A04

Pilot: The pilot core indicated three 0.05 m thick zones with fault gouge at approximately L=2.3–2.8 metres, with a 30° angle to the core axis. The BIPS log indicated orientations of 49–52°/60–80°, which are in accord with core and tunnel data.

Overcoring: The core at the position of the target zone was severely damaged when removed from the core barrel, but loose debris could to some extent be identified with respect to position in core. Epoxy was abundant in 130/80–85° fractures at L=2.1 metres and 2.7 metres and in one 0°/63° fracture at L=1.9 metres (Figure 5-19). Some epoxy had also intruded into the fault gouge, but only up to a few centimetres from pilot borehole perimeter, and no epoxy was observed on the surface of the overcore (Figure 5-20). Some pieces of intact fault gouge were also recovered and secured in sealed air-tight plastic bags and sent to the laboratory for further testing of porosity and other petrophysical parameters, cf. Section 6.1.

Interim conclusions: The structure appeared as projected and has a structure similar to that observed in the pilot drill hole. Clay fill has obstructed epoxy impregnation of the fault gouge but, as in the case of KA2169A01, KA2169A02, and KA2169A03, epoxy is abundant in steep fractures oriented in the NW quadrant, but also in one fracture oriented 0°/63°.

Figure 5-19. *KA1596A04. Recovered core with epoxy at L=1.9 metres with face of epoxy impregnated fracture (0°/63°) at L=1.9 metres.*

Figure 5-20. *KA1596A04. Zone with fault gouge, partially impregnated with epoxy at L=1.9–3.0 metres. No epoxy seen on cylindrical surface of the overcore. Centimetre- sized breccia pieces seen in the lower part of the picture (centre).*

5.4 General results

Epoxy is abundant in steeply dipping fractures with a strike of 130–170° at all four sites 1596 – Model D, 2163 – Model C, 2430 – Model B, and 2545 – Model A (cf. Section 5.3). Both single fractures and breccias appear to be epoxy-filled. At 1596 very little epoxy has intruded in the NE striking target structure with clayey fault gouge (clay minerals, dominating the <2 μm fraction) in chloritic phyllonite (a mica or chlorite-rich rock type formed by shear), and the epoxy does not show the surface of the 277 mm core. At 2545, the target structure striking E-W is filled well with epoxy. Epoxy intrusion appears to have been efficient, and epoxy has intruded into very narrow spacings, barely visible to the human eye (down to c. 50 μm, cf. Hakami and Wang (2005)).

Given the general results and the established kinship between the structure in KA2423A03 and the structures investigated as part of TRUE-1 and TRUE Block Scale, cf. Section 5.3.5, emphasis in the remainder of analysis work, mainly pore space analysis using image analysis, was placed on results from borehole KA2423A03. Chemical analysis work, however, also included material from additional boreholes.

5.5 Basic sectioning of overcores

Following the basic mapping and documentation described in the preceding section, the cohesive cores were sectioned in manageable lengths and were subsequently cut in half-pipes along the centre line of the cores. Relevant parts of one of the half pipes were sent off for further sectioning and image analysis whereas the second half-pipe was retained as an archive sample at Äspö HRL. In the continued analysis focus is placed on the core from KA2423A03.

The box including samples from borehole KA2423A03 (pieces B1-B4) are detailed in Table 5-2, see also Figure 5-17, Figure 5-21 and Figure 5-22 for geometrical reference. Sample B1 has one open fracture whereas samples B2 and B3 exhibit complex fracture networks in conjunction with the fault intersection, and B4 has no fracture. How the samples from this core were cut is illustrated in Figure 5-23. The samples B2 and B3 were selected for use in the subsequent image analysis.

Table 5-2. Description of samples collected in borehole KA2423A03.

Sample No.	Fractures	Epoxy occurrence	Comments
B1	Yes, one open	No, only at borehole wall	
B2	Yes, complex	Yes	
B3	Yes	Yes, both in single fracture and fractured zone	Neighbouring sample to B2. Broken in the contact between intact rock and fractured zone.
B4	None	No	One cut perpendicular and the other with angle c. 45 degrees relative to the zone.

Figure 5-21. *The core was cut along the core axis into two halves. Only one half (upper half) was used in the current study. This image shows samples B1, B2, B3 and B4 from borehole KA2423A03. The left side of the core is positioned closest to the tunnel (borehole collar).*

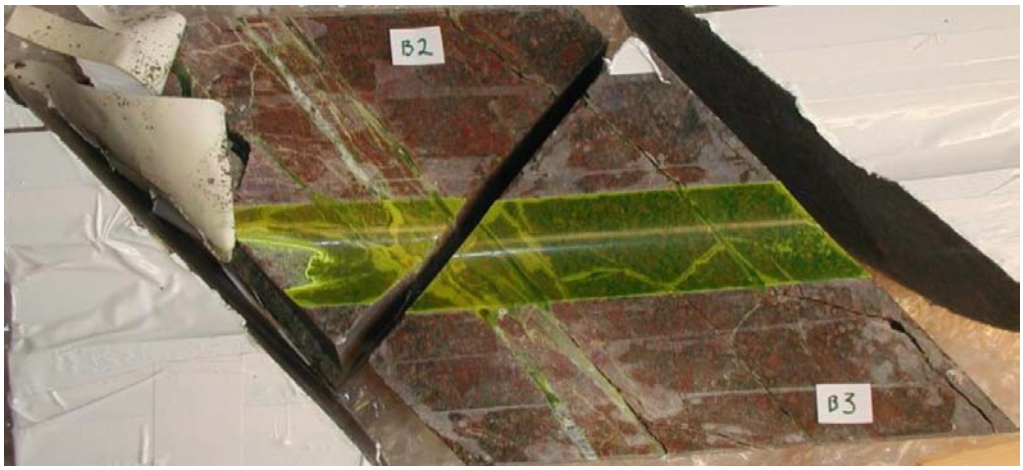

Figure 5-22. *This figure is similar to Figure 5-21, but the samples (B2 and B3 from borehole KA2423A03) are rotated such that the cut surfaces are seen. The trace of the 76 mm injection hole may be noted in the centre of the photograph (light green epoxy). (Vertical up direction is normal to the image, directed inwards.)*

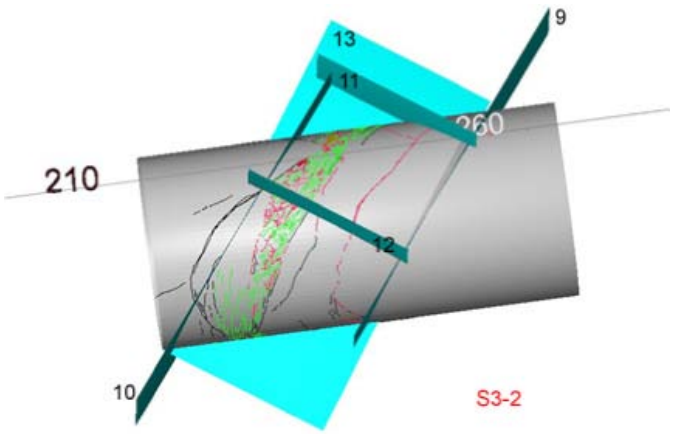

Figure 5-23. *The drill core surface of KA2423A03 was mapped and this image shows a perspective view of the 3D-reconstruction of the core used for the planning of cutting. The cutting planes were chosen such that the sample would include the whole fractured zone being the target of this study. The orientation of the fault is approximately 155/83 (strike dip) (Maersk-Hansen and Staub 2004).*

6 Petrophysical and chemical analyses

In the following chapter, petrophysical, mineralogical and geochemical analyses of recovered core materials are presented. The petrophysical work was employed as a back-up applied to a selected core from 1/596 (KA1596A04) at which the resin injection failed, but were large amounts of fault gouge material were collected. Hence, the only remaining possibility was to use standard procedure petrophysics to obtain a quantification of porosity. The geochemical work comprises XRD on thin sections and ICP applied to select core materials from the 76 mm characterisation boreholes.

The objectives of work presented here were to:

- Provide quantification of selected petrophysical properties (Porosity, BET surfaces and particle size distribution of samples of the fault gouge core material from borehole KA1596A04 (Section 6.1).
- Provide mineralogical and geochemical description of the geological material from the investigated target structures at 1/600, 2/163 and 2/430 m (Section 6.2).

6.1 Petrophysical measurements of porosity and BET surfaces

6.1.1 General

The analysis work performed concerns examination of several physical properties of 9 clayey samples collected from the highly friable core from KA1596A04, cf. Section 3.2.1. The samples analysed are described in Section 5.1.2 and the measurement techniques and methodologies are briefly described in Section 5.1.3. The established properties are presented in Sections 5.1.4 and 5.1.5, respectively. The sample preparations and measurements were conducted by the Technical Research Institute of Sweden (SP).

6.1.2 Sample description

The sampling was done in immediate conjunction with the overcoring drilling process of borehole KA1596A04 at L=1/596m. The selected samples were immediately placed in air-tight plastic bags and were put in water to minimise loss of moisture and any chemical alteration due to the handling and transport. The materials of the nine samples (A1 through A9) are all made up of hard clayish pieces with embedded visible rock fragments and sampled at three discrete depths in the borehole. Some of the samples were visibly wet when obtained at the laboratory (A1, A2, A3 and A9) while the others were dry, see Figure 6-1.

Figure 6-1. *Photographs of fault gouge samples (wet state) from the overcore of borehole KA1596A04. Samples denoted A1–A3 (L=2.4m), A4–A6 (L=2.8m), cf. Table 6-1.*

6.1.3 Properties measured and procedures employed

Volume measurements

The AccuPyc method (SP-method 1338) involves measurement of the amount of displaced gas. The pressures observed upon filling the sample chamber and then discharging it into a second empty chamber allows computation of the volume of the solid phase volume. Gas molecules rapidly fill the tiniest pores of the sample; only the truly solid phase of the sample displaces the gas.

Each sample was immersed in a beaker with water from the Äspö Hard Rock Laboratory and the difference in volume (in millilitres) directly after immersion was noted.

Original water content of the sample

The establishment of water content was carried out according to SP-method 3772. The sample was dried at 40°C and under vacuum until steady state was reached. The result was calculated as the difference between the original "wet" weight and the final dry weight.

BET surfaces

The BET analysis using TriStar 3000 (ISO 9277) provides high-quality surface area and porosimetry measurements on solid materials using the gas adsorption technique.

In order to perform the analysis, the sample must be crushed to sizes smaller than 10 mm. 3–7 g of the crushed material (randomly selected) was used for each analysis. The material was dried at 40°C and subsequently ventilated by nitrogen gas.

Particle size distribution

The dried material was sieved to different particle sizes (according to the SS-02 71 23 protocol). The relation between the total weight of the sample and sieved fractions provides the particle size distribution. Sedimentation analysis and wet sieving was not performed due to the very small amount of sample material available.

Table 6-1. Compilation of weights, volumes and estimates of porosity (by volume) for the analysed samples from KA1596A04 at depths varying between 2.4 and 2.9 m from the tunne, cf. Figure 6-1l. Volume derived by the AccuPyc method is based on five repeated measurements.

Sample	March 10 2004	+5 days	+5 days			Volume	Porosity (%)	
	Total weight incl beaker (grammes)	Weight after Drying (grammes)	Weight of water	Volume (AccuPyk) (cm^3)	Volume st dev	Archimedes (cm^3)	(vol water/vol sample) Gas	Archimedes
A1 (L=2.4m)	71.98	68.93	3.05	23.45	0.08	25.0	12.99	12.19
A2 (L=2.4m)	91.18	88.15	3.03	29.08	0.09	30.0	10.42	10.09
A3 (L=2.4m)	72.47	70.36	2.11	24.13	0.11	27.0	8.74	7.81
A4 (L=2.8m)	23.49	21.37	2.12	6.13	0.04	7.0	34.63	30.33
A5 (L=2.8m)	118.08	116.15	1.94	40.26	0.03	49.0	4.81	3.96
A6 (L=2.8m)	24.03	22.27	1.76	6.52	0.05	9.0	26.97	19.53
A7 (L=2.9m)	36.18	34.59	1.59	11.30	0.03	11.0	14.10	14.48
A8 (L=2.9m)	51.96	50.98	0.98	16.84	0.06	17.0	5.83	5.78
A9 (L=2.9m)	253.43	248.78	4.65	88.27	0.17	92.0	5.27	5.05
Mean:					0.07		13.75	12.14

6.1.4 Volumes, weights and estimates of porosity

The volumes of the samples established both by the gas method (AccuPyc) and by employing Archimedes principle are indicated in Table 6-1. Similarly, the weights of the wet samples and the dried samples are provided (both entries including the weight of the sample beakers). The weight of water in the samples, as assessed by a drying process over a period of 5 days, is given in Table 6-1. Estimates of porosities expressed as volume of water divided by volume of the sample were calculated by assuming that the density of water is equivalent to 1,000 kg/m^3, the results are given Table 6-1.

6.1.5 BET-surfaces

The resulting BET surfaces for the analysed nine samples are provided in Table 6-2. The values of BET surface ranges from 0.6 to 8.9 m^2/g. No correlation between the BET area and the volume of the sample can be noted.

Table 6-2. BET surface of samples from KA1596A04. Borehole lengths at which the samples were collected are given in parentheses, cf. Figure 6-1. Mean value of five repeated measurements of each sample.

Sample	BET m^2/g	Stdev m^2/g
A1 (L=2.4m)	3.50	0.03
A2 (L=2.4m)	2.78	0.02
A3 (L=2.4m)	5.52	0.05
A4 (L=2.8m)	8.88	0.48
A5 (L=2.8m)	0.59	0.001
A6 (L=2.8m)	2.01	0.12
A7 (L=2.9m)	5.73	0.05
A8 (L=2.9m)	4.34	0.23
A9 (L=2.9m)	8.33	0.08

6.1.6 Particle size

The particle size distributions established on the basis of sieving of three samples along the core of KA1595A04 are shown in Figure 6-2. Obvious from the resulting distributions is the total lack of correlation between particle size distribution and the location of the sample away from the tunnel wall. Notable is also the relatively large difference between the three samples.

6.2 Mineralogy and geochemistry

The four structures selected considered for injection of epoxy resin in fault rock are located at chainages 1,600 m, 2,163 m, 2,430 m and 2,545 m in the Äspö tunnel, see detailed account of the characterisation work in Section 3.2, specifically Table 3-1. This section provides an account of the mineralogical and geochemical analyses of fault rock materials from the target structures located at three of the listed sites. Given that it was early recognised that Structure 2545, showed a more complex geometry than the other structures, and therefore was considered unsuitable for injection experiments, no mineralogical sampling was carried out on geological material from this structure.

Table 6-3 shows details on the samples collected for mineralogical identification and geochemical analyses. The analyses comprise XRD (X-ray diffractometry) for mineral identification with emphasis on clay minerals, microscopy of thin sections from wall rock and fragments in the structure for description of mineral/crystal arrangements and ICP analyses (Ion Coupled Plasma spectrometry) for quantification of chemical composition. The sampled and analysed materials can grossly divided in cm-sized pieces and mm-sized fragments from roughly from 20 mm down to 2 mm. However, it is noted that there are coarser fragments present ain the zone as well.

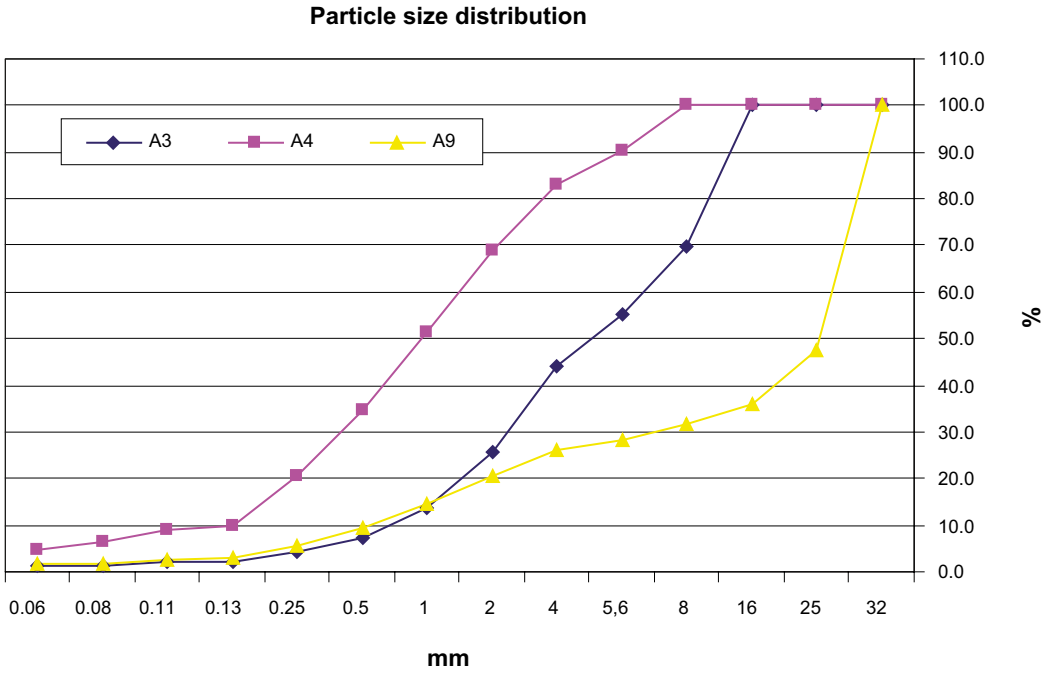

Figure 6-2. *Particle size distribution related to samples A3 (L=2.4 m), A4 (L=2.8 m) and A9 (L=2.9 m) from the KA1596A04 overcore.*

Table 6-3. Samples from the resin experiment boreholes selected for mineralogical identification and laboratory analyses.

Structure	Borehole intercept	Analyses made
1596	KA1596A01 L=5.40–5.65 m	Cm-sized piece of fault rock and 1–2 mm fragments for thin sections <0.125 mm fraction for XRD and ICP analyses.
2169	KA2169A02 L=2.70–2.85 m	Cm-sized piece of fault rock and 1–2 mm fragments for thin sections <0.125 mm fraction for XRD and ICP analyses.
2423	KA2423A03 L= 2.36–2.53 m	Cm-sized piece of fault rock and 1–2 mm fragments for thin sections <0.125 mm fraction for XRD and ICP analyses.

6.2.1 Structure 1596

This is the investigated structure with the largest thickness (in the order of 0.4 to 0.5 m). It consists of material extremely enriched in chlorite/clay minerals (macroscopically interpreted as phyllite) distributed on both sides of a quartz-rich pegmatite (1–2 dm wide). The zone has largely the same appearance in all four boreholes intercepting the structure but there are variations in the details; for example in borehole KA1596A04 a chlorite/clay rich 5 cm thick splay is found 0.5 m from the main structure and the quartz-pegmatite varies in thickness between the four borehole intercepts with the structure. Furthermore, results of sieving of three samples from KA1596A04, in the same structure, are provided in Section 6.1.6. The relatively differences in grain size distribution between the three samples from KA1596A04, cf. Figure 6-2, indicate an inhomogeneous character of the zone on the decimetre scale.

XRD

From macroscopical observations (and also supported by XRD analysis) of sieved material from this zone it is seen that also the larger pieces (0.5 to 2 mm) are very rich in chlorite/clay minerals although quartz and K-feldspar are also observed. XRD identification of the clay minerals shows that corrensite dominates the sample. Corrensite is swelling mixed layer clay with alternating layers of chlorite and smectite/vermiculite. The sample from KA1596A01 show layers that are not well ordered indicating a possible transformation state of the clay mineral at this location.

Microscopy

The samples of fault rock consist of very quartz-rich and highly altered rock with high amount of re-crystallized quartz. Red-stained parts of the thin section are due to minute hematite crystals included in the pores of secondary feldspars (albite) replacing primary plagioclase. Thin mylonites seen in the upper part of the thin section (Figure 6-3) are associated with epidote, high chlorite content and with quartz being increasingly fine-grained. Some mylonite bands contain hematite crystals and are dark brown in colour. The mylonite is cut discordantly by several calcite-filled fractures with widths of up to 1 mm (areas coloured white in Figure 6-3). These calcite-filled fractures run across the entire thin section.

The smaller fragments (1–2 mm) consist of the same type of material but with slightly higher amounts of mylonite and hematite-stained chlorite and with lower amounts of quartz.

Chemical composition

The chemical composition of the <0.125 mm fraction is given in Table 6-4. The large portions of Al_2O_3 (15.4 wt%), Fe_2O_3 (12.8 wt%) and MgO (14.6 wt%) are in line with the high content of chlorite and corrensite in the fault gouge material found in this structure. The analysed components sum up to 89 wt% which supports a high content of H_2O and other volatiles, which, apart from microscopy and chemical analyses, provides support for the high chlorite content in the sample.

Figure 6-3. *KA1596A01. Mylonite rich in epidote, quartz and chlorite cut by a calcite-filled fracture (white on the right hand side of image). Note that the mylonite becomes more fine-grained towards the upper part of the image (the dark layer in the upper part of the image is chlorite-rich). Photomicrograph with crossed polars.*

Table 6-4. Chemical composition of samples (< 0.125 mm size fraction).

Element	Unit	Sample		
		KA 1596A01	KA 2169A02	KA 2423A03
SiO2	weight %	38.1	41.8	21.2
Al2O3	weight %	15.4	14.7	5.73
CaO	weight %	3.33	10.3	39.8
Fe2O3	weight %	12.8	10.2	3.43
K2O	weight %	3.65	1.83	2.93
MgO	weight %	14.6	7.12	2.76
MnO	weight %	0.31	0.18	0.11
Na2O	weight %	0.25	2.84	0.34
P2O5	weight %	0.22	0.45	0.05
TiO2	weight %	0.85	1.25	0.15
Sum	weight %	89.5	90.7	76.5
Ba	ppm	460	612	450
Be	ppm	7.88	2	1.58
Co	ppm	46.5	18.8	7.17
Cr	ppm	960	233	13.7
Cs	ppm	2.14	<0.1	<0.1
Cu	ppm	47	148	67
Ga	ppm	47.6	61.6	<1
Hf	ppm	3.86	7.8	19.1
Mo	ppm	<2	<2	<2
Nb	ppm	9.49	12.9	7.33
Ni	ppm	416	129	<10
Rb	ppm	154	59	51.2
S	ppm	323	1,280	3,580
Sc	ppm	20.1	14.9	3.45
Sn	ppm	11.1	8.87	1.56
Sr	ppm	296	1,440	362
Ta	ppm	1.23	0.67	4.98
Th	ppm	9.78	3.2	6.58
U	ppm	4.25	3.14	0.55
V	ppm	158	159	84.1
W	ppm	6.5	150	179
Y	ppm	15.5	26.4	78.3
Zn	ppm	443	438	122
Zr	ppm	124	340	49.1
La	ppm	26.3	67.8	25.9
Ce	ppm	53.6	140	52.5
Pr	ppm	<1	7.96	<1
Nd	ppm	20.8	65.9	18.5
Sm	ppm	2.83	7.14	0.93
Eu	ppm	0.38	1.02	<0.05
Gd	ppm	<0.4	2.55	<0.4
Tb	ppm	<0.1	<0.1	<0.1
Dy	ppm	1.97	3.09	4.49
Ho	ppm	0.40	0.52	0.86
Er	ppm	<0.1	<0.1	<0.1
Tm	ppm	<0.1	<0.1	<0.1
Yb	ppm	<0.2	0.64	1.43
Lu	ppm	0.10	0.06	0.18

6.2.2 Structure 2169

The NW trending structure intersected by the boreholes KA2169A01, -A02, -A03 and -A04 at this location is hosted in quartz monzodiorite and runs parallel with a set of thin epidote- sealed fractures (or very thin mylonites). The zone contains fault crush as well as fault gouge at least in boreholes KA2169A02 and -A03 and to some extent in KA2169A01. The largest thickness is found in borehole KA2169A02 (c. 15 cm of crush and fault gouge) whereas in borehole KA2169A04 its appearance is more of a single fracture. From the sampling of the zone in borehole KA2169A02 the following "grain size distribution" was obtained, cf. Table 6-5. The total weight of this sample was 456g.

Table 6-5. Sieved mass fractions from sample collected in Structure 2169.

Fraction (mm)	Sieved mass (g)	Percent
> 2	434	95.2
1–2	8	1.8
0.5–1	7	1.5
0.25–0.5	2	0.4
0.125–0.25	1	
<0.125	5 (of which 79% belongs to the clay fraction < 2 μm)	1.1

XRD

The XRD analysis of the fraction > 2 μm together with macroscopical observations show that the coarser fractions are dominated by quartz, plagioclase, calcite, K-feldspar, illite, epidote and chlorite. A few grains containing idiomorphic calcite crystals in the order of 50–100 μm indicated growth of these crystals in open pore space. In similarity with the analysed sample from Structure 1596, the XRD identification of the clay mineral fraction (<2 μm) shows a dominance of the swelling clay corrensite.

Microscopy

In the pieces of fault rock (crushed part of the zone), primary Fe-Mg-silicates are almost completely altered to prehnite and epidote (and some chlorite). The secondary epidote and prehnite crystals are frequently euhedral. Clusters of prehnite-epidote crystals (up to 2 mm in size) are found in between grains of primary quartz and feldspars (Figure 6-4).

The fragments (1-2 mm) consist of the same altered minerals as in the pieces described above. The fragments contain larger amounts of calcite (~5–10 vol.%) and epidote-rich mylonite (~10–15 vol.%) supporting the basic interpretation that the structure is an old semi-ductile structure that has subsequently been reactivated during the brittle regime. Because earlier deformed rock (epidote rich mylonite) is found in the fragments in the zone, supports the fact that the structure is an old semi-ductile structure, subsequently reactivated during the brittle regime.

Chemical composition

The analysis of the chemical composition in the >0.125 mm fraction (Table 6-4) shows that Al_2O_3 (14.7 wt%), CaO (10.3 wt%), Fe_2O_3 (10.2 wt%) and MgO (7.1 wt%) in addition to SiO_2 (41.8%) make up the sample. This is in accordance with the observed high amounts of epidote and prehnite (both being Ca-Al silicates), but also of chlorite and corrensite. The relatively high strontium content 1,440 ppm can be explained by the presence of epidote. The total sum of analysed oxides amounts to 90.7 wt% which means that about 9 wt% constitutes volatiles like H_2O or carbonates.

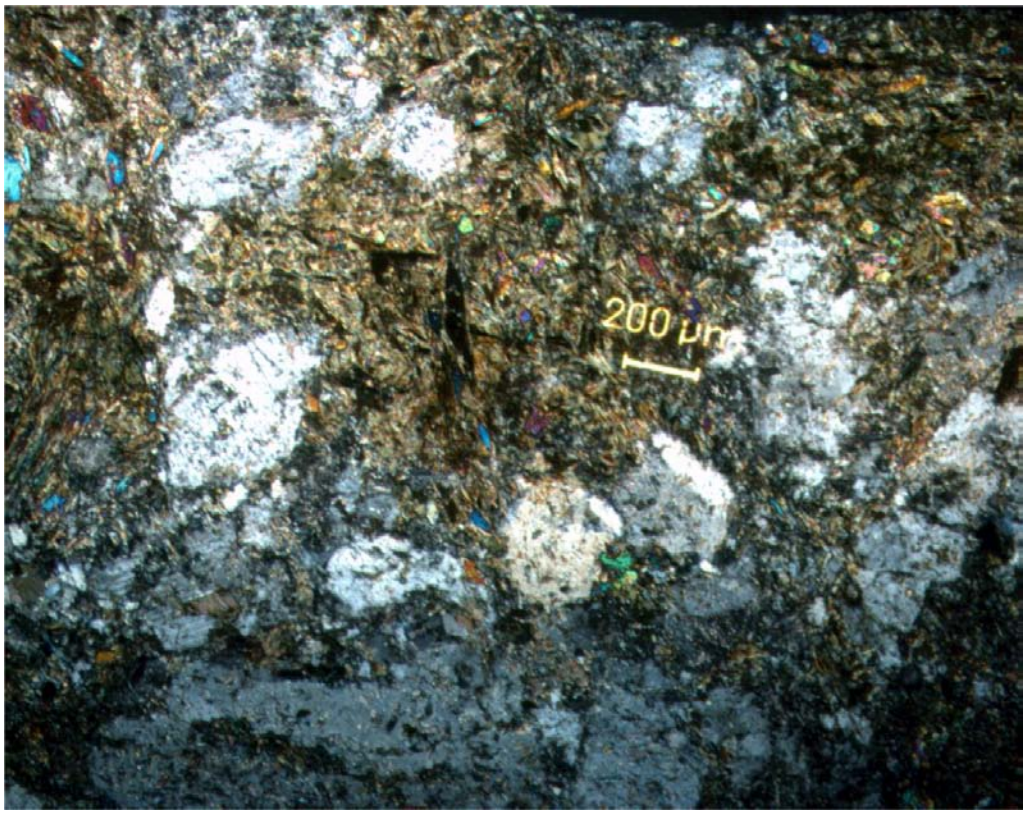

Figure 6-4. *KA2169A02 – Cluster of epidote- and prehnite crystals encircled by primary crystals of K-feldspar and quartz (grey). Photomicrograph with crossed polars.*

6.2.3 Structure 2423

This is a reactivated epidote-rich mylonite hosted in red-stained and hydrothermally altered granite/granodiorite. The zone varies in thickness from 0.04 m (KA2423A04) to 0.1 m (KA2423A01). All four borehole intercepts are characterised by open pore space and fault crush. Sieving of the sample from the zone intercept in KA2423A03 shows the following grain size distribution, cf. Table 6-6. The total weight of the sample was c. 52 g. The 1–2 mm fraction was characterised by grains of altered granite and mylonite and possibly some clay-cemented grains. Grains of quartz, fluorite and sulphides, precipitated as a result of hydrothermal circulation, are frequent. The observed idiomorphic crystal growth indicates open pore spaces in the order of at least 100 μm.

Table 6-6. Sieved mass fractions from sample collected in Structure 2423.

Size fraction (mm)	Sieved mass (g)	Percent
> 2	39	75.0
1–2	4	7.7
0.5–1	3	5.8
0.25–0.5	2	3.8
0.125–0.25	2	3.8
< 0.125	1.5 (of which 82% belongs to the clay fraction (<2 μm)	2.9

XRD

The fraction >0.125 mm was dominated by calcite, quartz and some fluorite, whereas the clay mineral fraction (<2 μm) is dominated by chlorite but also contains swelling clays of less ordered type, including components of chlorite, smectite/vermiculite and illite.

Microscopy

The fault rock pieces consist of highly altered granitic rock with mylonitic/cataclasitic parts. Larger fragments of quartz and K-feldspar are abundant within the mylonite, which itself consist of fine-grained epidote, quartz and chlorite (Figure 6-5). Fractures filled with prehnite, calcite, adularia and fluorite cut through cataclasite and mylonite (*Figure 6-6*). The youngest fracture minerals seen in the thin sections are adularia and calcite (Figure 6-7).

The fragments (1–2 mm) consist of the same minerals and rock types as the larger pieces e.g. mylonite and cataclasite (Figure 6-8). Differences are that the fragments (1–2 mm) are richer in calcite (c. 30% compared to <10% in the fault rock pieces) and fluorite (large cubic crystals, cf. Figure 6-9).

Chemical composition

The analysis of the chemical composition in the >0.125 mm fraction (Table 6-4) showed that CaO (39.8 wt%), SiO_2 (21.2%), Al_2O_3 (5.73 wt%), Fe_2O_3 (3.43 wt%), K_2O (2.93 wt%) and MgO (2.76 wt%) make up most of the sample. In addition there is a loss of c. 24 wt% (H_2O and carbonates) which together with the high calcium content are in accord with the large portion of calcite in this sample. The sulphur content (attributed to the presence of pyrite) is relatively high (3,580 ppm) compared with KA2169A02 (1,280 ppm) and KA1596 (only 323 ppm).

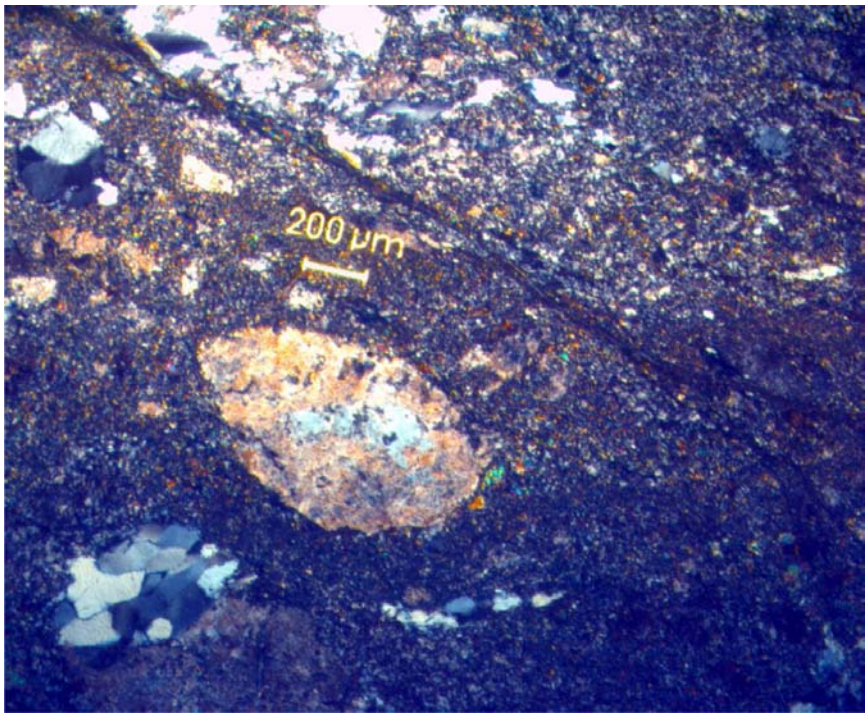

Figure 6-5. *KA2423A03 – Mylonite rich in epidote, quartz and chlorite with fragments of K-feldspar and quartz. Photo micrograph with crossed polars.*

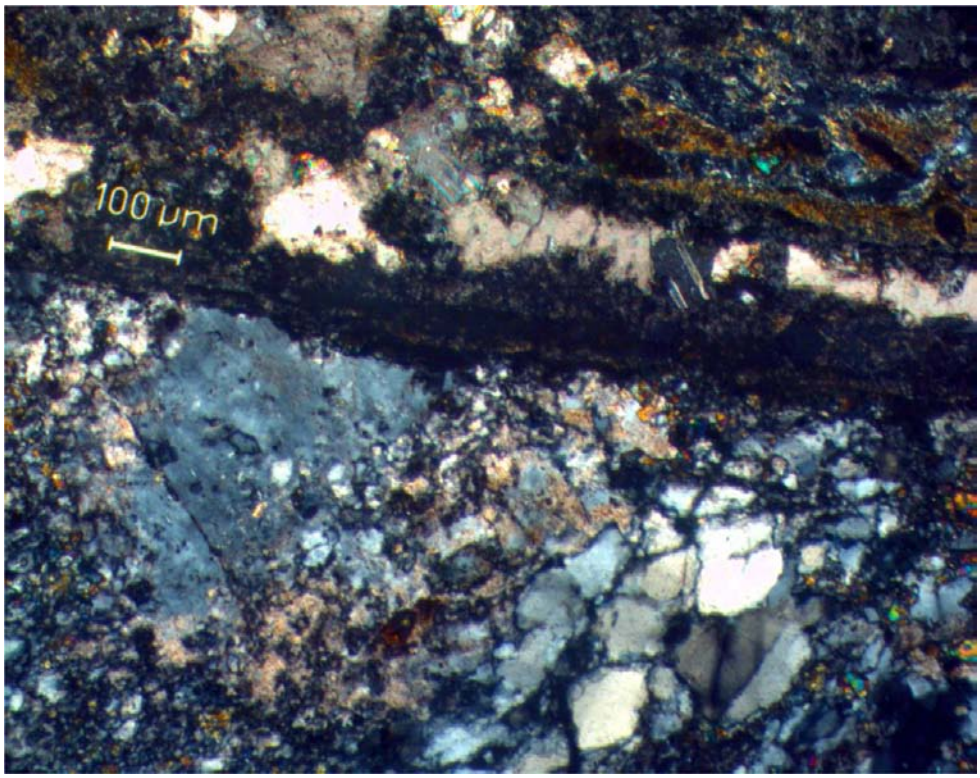

Figure 6-6. *KA2423A03 – Fracture (upper part of the image running "subhorizontally" from left to right in the image) filled with prehnite, calcite, adularia and fluorite cut through cataclasite and mylonite. Photo micrograph with crossed polars.*

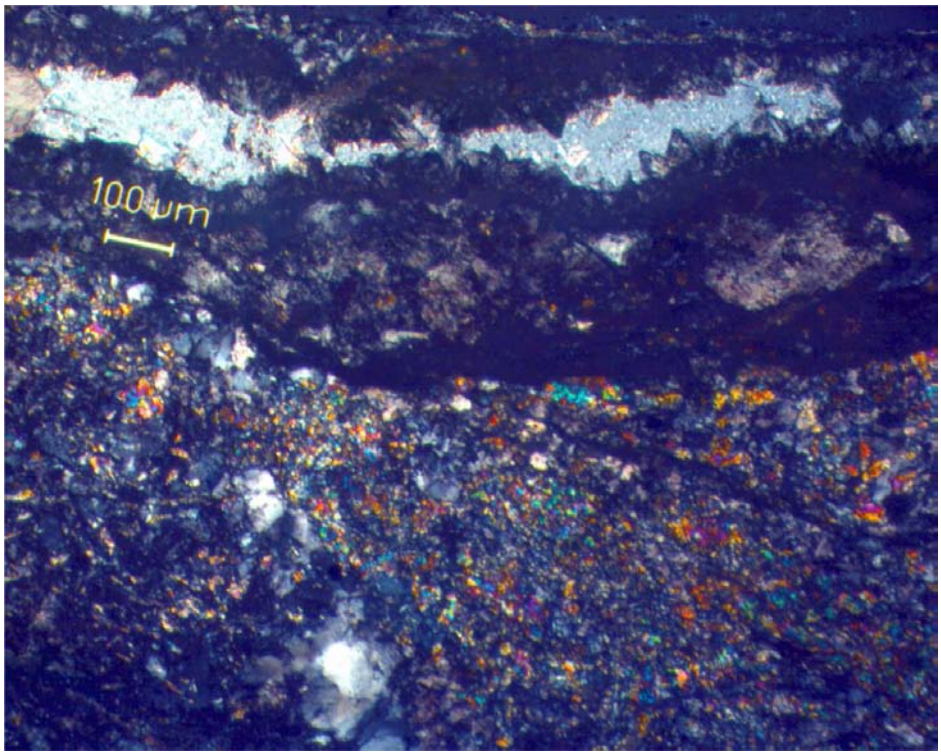

Figure 6-7. *KA2423A03 – Fracture (upper part of the image running "subhorizontally" from left to right in the image) filled with adularia (euhedral crystals) and calcite (centre of the fracture). Photo micrograph with crossed polars.*

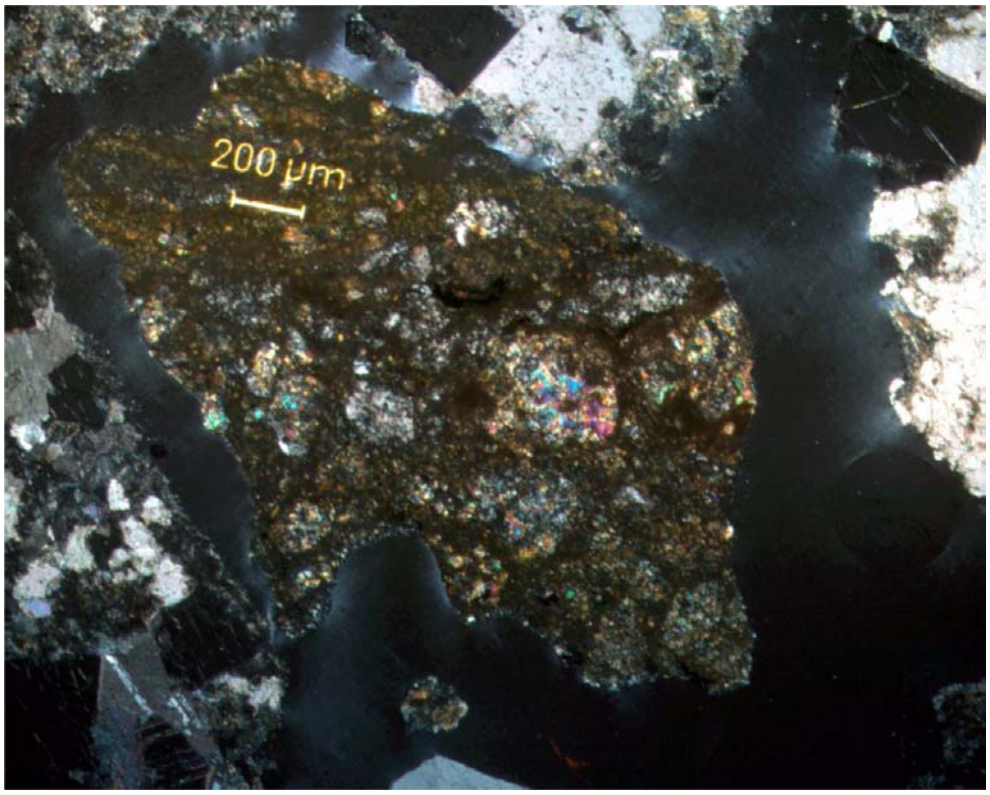

Figure 6-8. *KA2423A03– Fragment of crushed rock containing cataclasite, rich in e.g. epidote. Photo micrograph with crossed polars.*

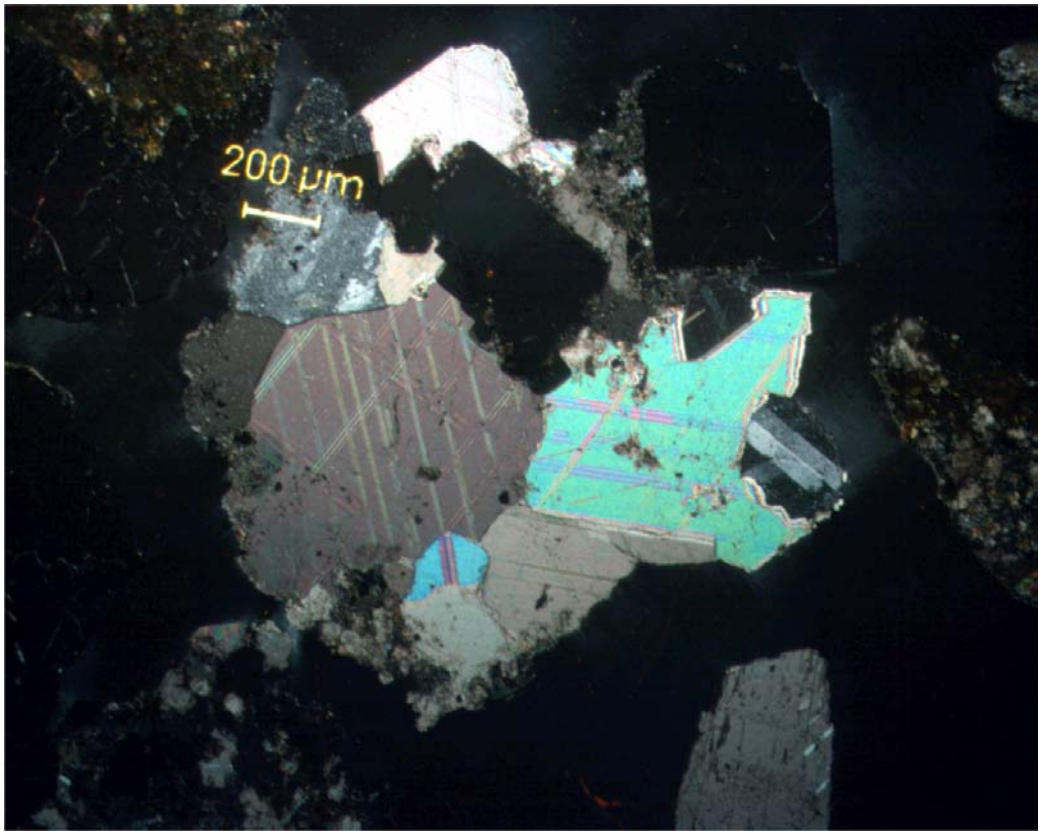

Figure 6-9. *KA2423A03 – Fragment of crushed rock containing calcite and fluorite (black, cubic crystals). Photo micrograph with crossed polars.*

6.2.4 Discussion

The results from the chemical and mineralogical analyses of KA2423A03 support the fact that this is (in similarity with the other two structures studied) a ductile/semi-ductile structure that has later been reactivated and, especially in the case of Structure 2423, later subjected to hydrothermal circulation that have resulted in mineralisations of epidote, calcite, fluorite and pyrite. Idiomorphic crystals are common indicating readily available pore space in many parts of this structure. Also later alteration has formed clay minerals like the disordered swelling clay mineral of mixed-layer type, which has been identified in the fine fraction from this structure.

If comparing the three structures studied in detail in the Fault rock characterisation project, it can be concluded in brief;

- The common characteristics are that these structures were formed early in the geological history (during ductile to semi-ductile conditions) and they were later reactivated during brittle conditions. Differences are that;
- Structure 1596 coincides with a mafic lens or dike with pegmatitic material. This has resulted in a very diversified material present in the zone, with on the one hand material very rich in chlorite/corrensite (from the mafic rock) and on the other hand very quartz-rich coarser material (from the pegmatite),
- Structure 2169 and Structure 2423 are more common to features hosted in granitoids, showing altered fragments including chlorite, quartz, K-feldspar, epidote and altered plagioclase. Hydrothermal solutions have later precipitated calcite, fluorite and pyrite grains. Volumetrically, this is much more prominent in Structure 2423 than in Structure 2169. It is also evident that the voids are more common in KA2423, although distributed very inhomogenously.
- Basically all of the studied structures have mylonitic precursors, and show later brittle reactivation during hydrothermal conditions (prehnite-pumpellyite facies and chlorite facies can be assumed), which have resulted in the present system of water conducting fractures. The differences between the structures are related to size of the structure at the point of intersection. The Feature A at the TRUE-1 site is more of a single (or double) fracture. Structure #20 of the TRUE Block Scale rock volume and structure 2423 are more similar (showing more fault breccia, pieces and fragments) with the possible difference that structure 2423 appears to be more rich in hydrothermal minerals like calcite, fluorite and epidote, although these minerals are relatively frequent in Structure #20 as well.
- When comparing the investigated fault rock structures with other experiences from the Äspö tunnel, and also with results of the site investigations in Laxemar-Simpevarp, it can be concluded that the fault rock structures investigated here are structures typical for the area, and especially Structures 2169 and 2423 show characteristics that are commonly seen in minor deformation zones in the Laxemar-Simpevarp area. The characteristics of Structure 1596 are a little bit less common, considering it is in part very rich in chlorite and clay, but similar characteristics have also been seen in nearby Simpevarp.

A straight forward comparison between the structures at Äspö HRL and those seen in the Forsmark area is more difficult, but similarities include the common ductile/semi-ductile precursors with subsequent hydrothermal circulation causing calcite precipitation and formation of Ca-Al silicates (e.g. epidote and prehnite). The general impression is that with the exclusion of the larger deformation zones in Forsmark, the structures are less rich in clay minerals compared with those seen in Äspö and in the Laxemar/Simpevarp area.

7 Image analyses of resin-invaded pores

The aim of the image analysis was to provide qualitative and quantitative measures related top the pore spaces of fault rock zones and to explore the possibilities to provide indirect quantification of porosity from image analysis.

A detailed account of the theory and application of fracture image acquisition, image pre-processing, fracture delineation and tracing, fracture network analysis (number, location, orientation, size, shape, connectivity etc.) is provided by Hakami and Wang (2005). In the following sections an account is given of the application of the image analysis to the generated 2D slices from the target structure of borehole KA2423A03.

7.1 Fracture zone slices

The sample preparation and image acquisition for the fractured zone encountered in borehole KA2423A03 is described by Hakami and Wang (2005), cf. Section 2.1 and 2.2 therein/. Figure 7-1 shows a cut through the retrived core and the further sectioning into two samples B2 and B3. The cuts of sample B2 are parallel to the plane of the image. The thickness of a slice is about 18mm. The B3 cut number one is the leftmost cut and the surface on the left side of this cut to is referred to as 3B-1a and the surface on the right side is 3B-1b, etc. Only the a-sides of the cuts have been subject of study.

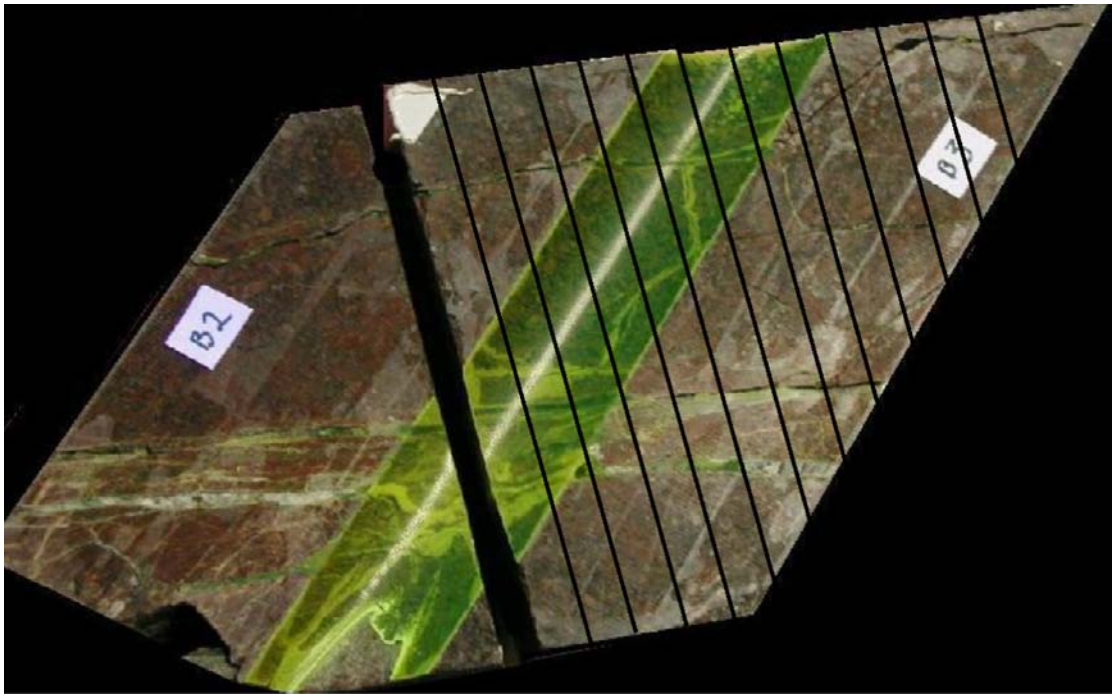

Figure 7-1. *Samples B2 and B3 from KA2423A03 were cut in two orthogonal directions. The cuts of sample B2 are parallel to the plane of the image. The thickness of a slice is about 18mm. The B3 cut number one is the leftmost cut and the surface on the left side of this cut to is referred to as 3B-1a and the surface on the right side is 3B-1b, etc.*

Figure 7-2 (a and b), shows the overview images of the 12 B3 slices at UV illumination. These images provide the overview and shape of the whole drill core sample slices (The images that were actually used for the image analysis where not these ones but images at the intermediate scale, i.e. taken a little closer to the samples including only the epoxy network part.) In the lower part of the images one can notice the thin epoxy layer that surrounded the dummy in the pilot borehole used for the injection. Note that the intersection of the core of the fractured zone is such that only the first four slices fully cover the fractured zone. Therefore, in the following, this is considered when interpreting and comparing the results. All images could, however, be considered as a possible pattern of a fractured zone image in general, some consisting only of a few fractures and others being more complex. It may be noted that the main core of the fractured zone is covered well by the first four surfaces and partly by slice #5 to #8 but in the slices #9 to #12 only some of the fractures on the side of the fractured zone are covered. This must of course be considered when analysing the results of image analysis.

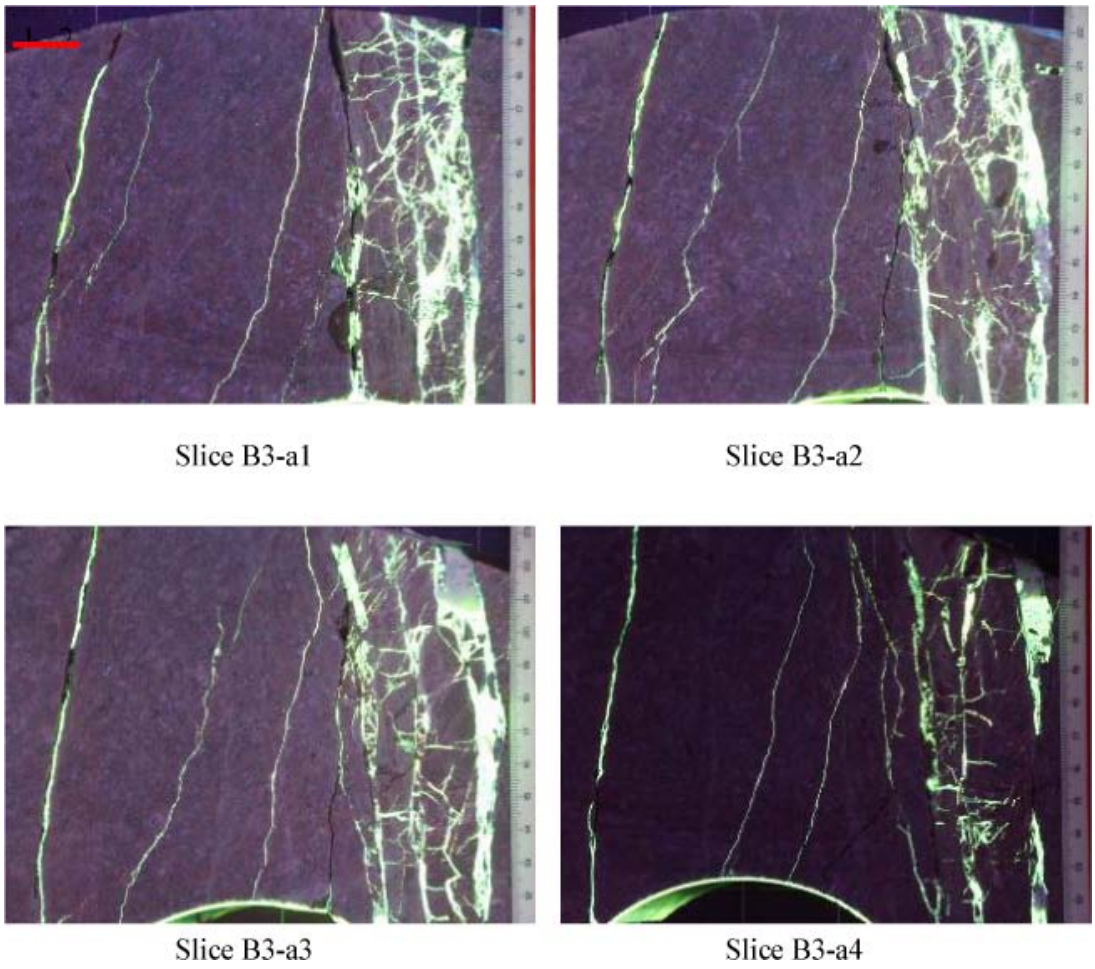

Figure 7-2a. *B3–B13 slice images (first four on this page and the following eight on next page) at UV illumination. These images provide the overview and shape of the whole drill core sample slices (The images that were actually used for the image analysis where not these ones but images at the intermediate scale, i.e. taken a little closer to the samples including only the epoxy network part.) In the lower part of the images one can notice the thin epoxy layer that surrounded the dummy in the pilot borehole used for the injection. Note that the intersection of the core of the fractured zone is such that only the first four slices fully cover the fractured zone. Therefore, in the following, this is considered when interpreting and comparing the results. All images could, however, be considered as a possible pattern of a fractured zone image in general, some consisting only of a few fractures and others being more complex.*

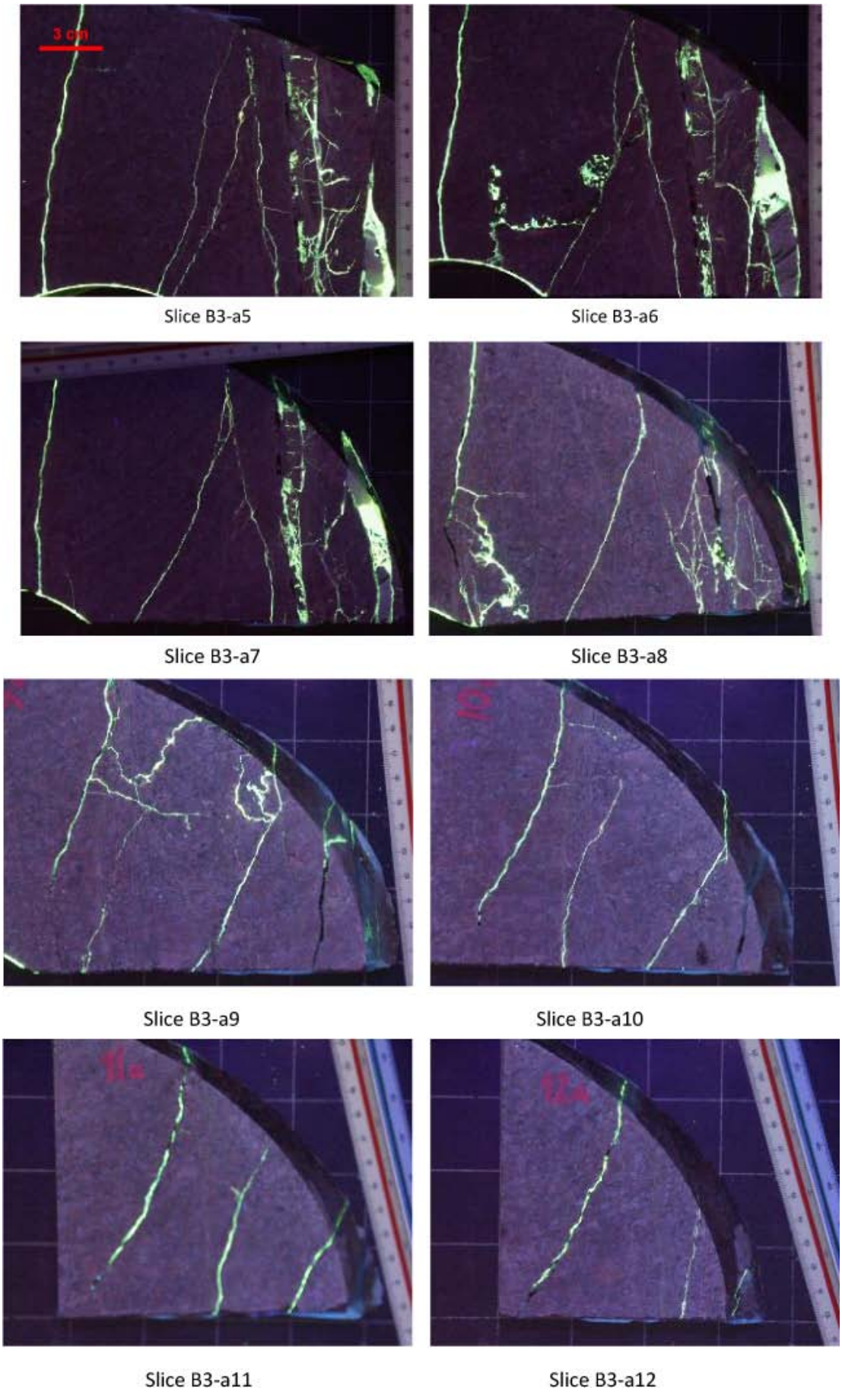

Figure 7-2b. *See caption on preceding page.*

Figure 7-3, shows the seven UV overview images of B2 sample slices. These images provide overview and shape of the whole drill core sample slices. The images that were actually used for the image analysis are not these ones shown, but images at the intermediate scale, i.e. taken a little closer to the samples including only the epoxy network part. The overall colour of images may have some variation, which was caused by either slight differences in the UV lighting (or disturbances from extra lighting) or differences in the epoxy fluorescence strength on the rock surface. However, these minor variations are not judged to affect our results significantly and the overall quality of the images used for analysis was judged sufficient for this study, including elements of methodology development.

Images were taken at three different scales (Hakami and Wang 2005), one for overview of the whole sample (*Overview slice resolution*), which may be used for three-dimensional construction and analysis, and an intermediate scale (*Main fracture zone resolution*) used for the main fracture network analysis. These images are taken slightly closer to the sample such that only the epoxy filled fractures are covered. Finally, some more close-up images (*Complicated fracture network resolution*) have been taken to enable more detailed studies of some parts of the fracture surfaces.

7.2 Image processing of slices

For each slice image, the UV colour image is converted to a grey scale image, using the green part of the colour image. Then some image enhancement was applied followed by binarisation. After the thresholding[1] the image was further processed by using smoothing, dilation and thinning operations and even some manual changes in the images were introduced at some locations (Hakami and Wang 2005). This was performed with the aim of obtaining a binary image suitable for the net image, i.e. to enhance the connections along fractures and highlight the inherent structural pattern of the fracture network at the scale studied. However, these operations will not produce a suitable image for displaying the structure inside the major fractured zone, since infilling material disappears in the image and the pore volume becomes exaggerated. The original binary image after thresholding should also be the optimal image for assessing some type of overall (apparent) porosity of a given image of a slice.

As representative examples, images from B2-a1 are displayed. Figure 7-4 shows the image at ordinary (daylight) lighting, and Figure 7-5 shows the corresponding image of B2-a1 at ultraviolet (UV) lighting. The fractured zone consists of three larger (or thicker) fractures which are connected by a number of smaller and thinner fractures. Inside the large fractures, some parts contain infilling minerals and some parts are epoxy-filled pores, some being enhanced by the geometry of the cut relative to the geometry of the pores/fractures.

To the left in the image in Figure 7-4 there is a large epoxy-filled area. This is not representing the true pore space in the undisturbed fractured zone because this slice is the first slice very close to the pilot drill hole such that what is seen is the epoxy layer filling up the annular space between the dummy and the borehole wall. This fact is compensated for in the analysis of this image by reducing the white area with 400 mm^2 (estimated based on visual inspection directly on the rock samples itself).

The binary image after pure thresholding, cf. Hakami and Wang (2005), is shown in Figure 7-6 and the binary image obtained after some further processing to enhance the fracture network structure is shown in Figure 7-7.

[1] During the **thresholding** process, individual pixels in an image are marked as "object" pixels if their value is greater than some threshold value (assuming an object to be brighter than the background) and as "background" pixels otherwise. This convention is known as threshold above. By presenting the values above the thresholed in one colour (say white) and the background as black, a **binary image** has been created (**binarisation**).

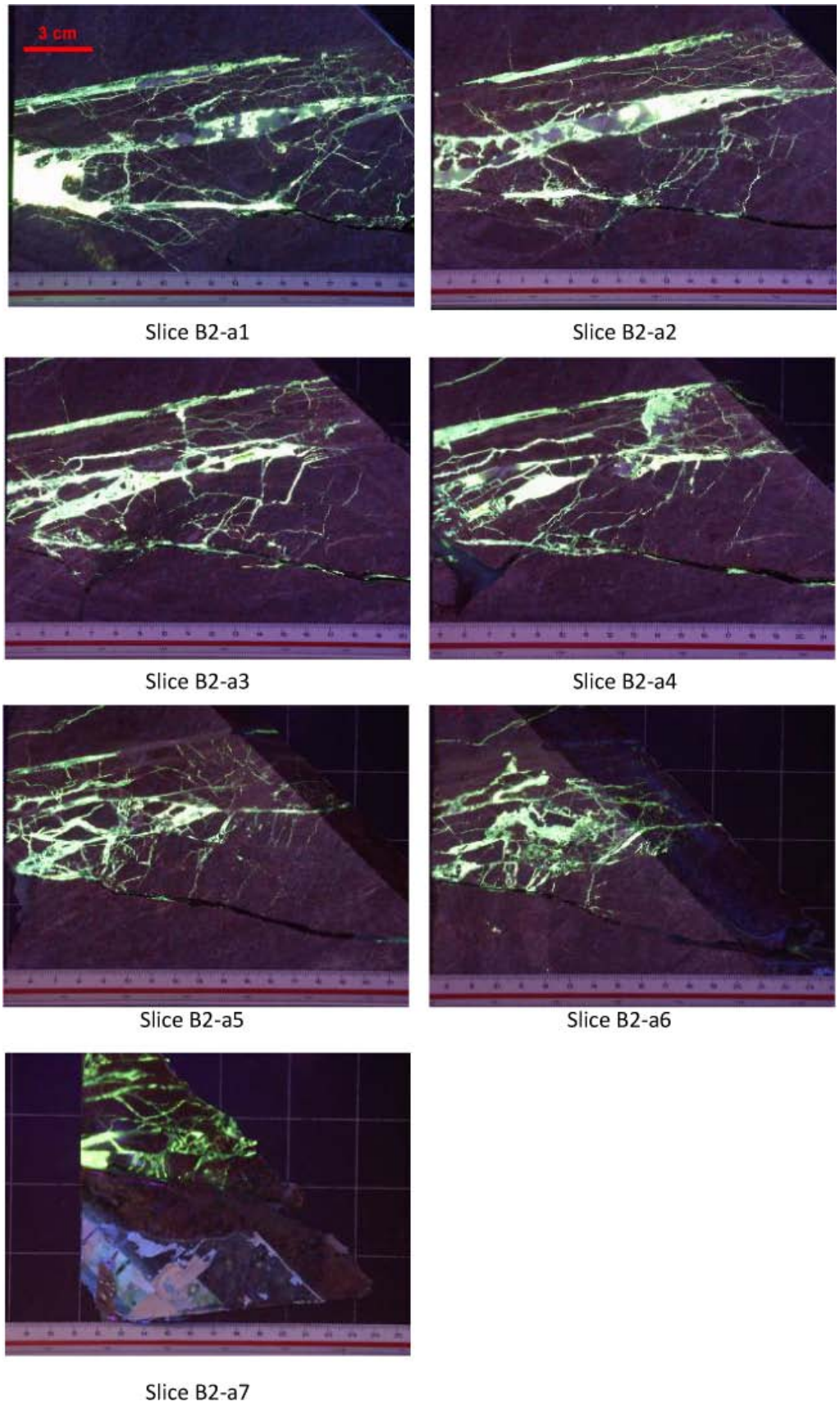

Figure 7-3. *Sample B2, seven slices, a-sides of cuts at UV illumination. These images provide overview and shape of the whole drill core sample slices. (The images that were actually used for the image analysis where not these ones but images at the intermediate scale, i.e. taken a little closer to the samples including only the epoxy network part.)*

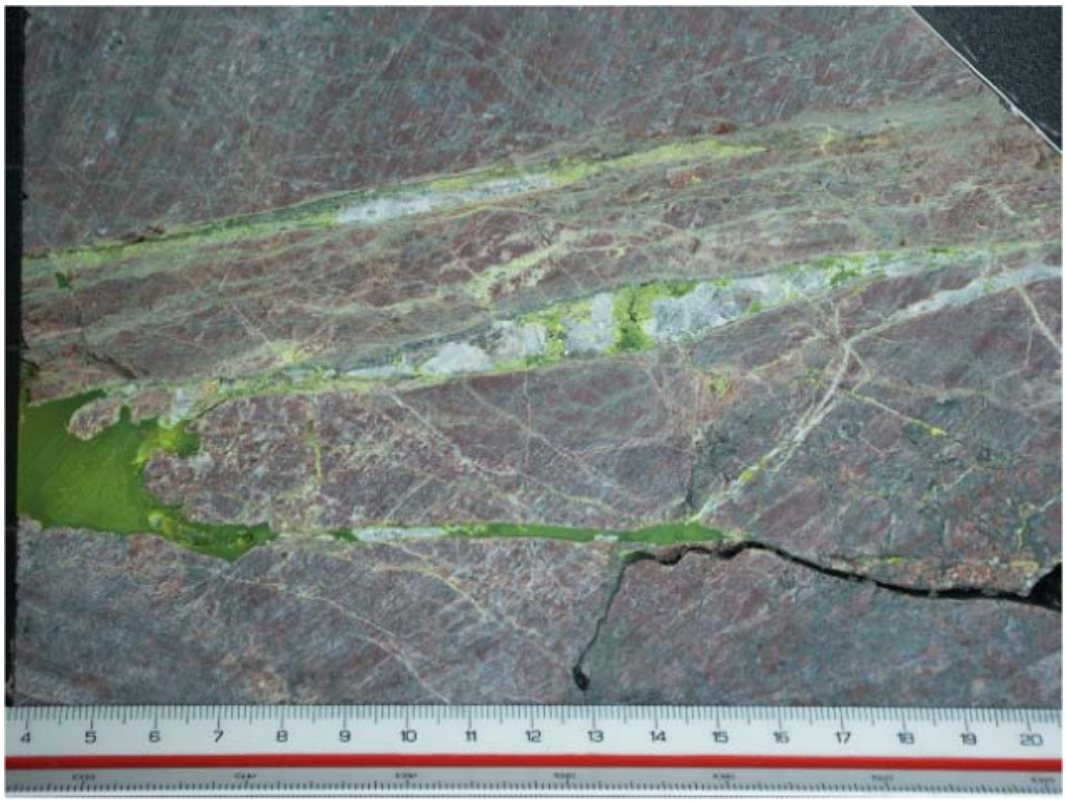

Figure 7-4. *B2-a1 image at ordinary light; the scale factor is 0.062 mm/pixel, image size 2,560×1,920 pixels = frame size 169 mm × 127 mm.*

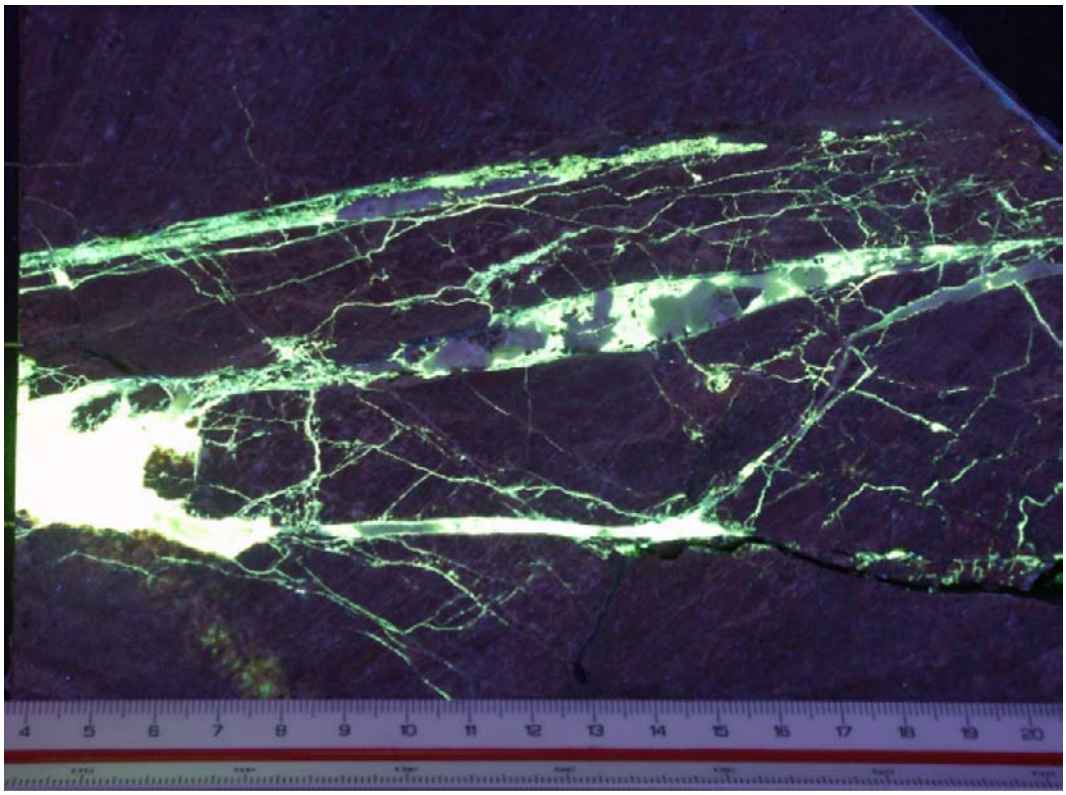

Figure 7-5. *B2-a1: the UV image corresponding to the image in Figure 7-4.*

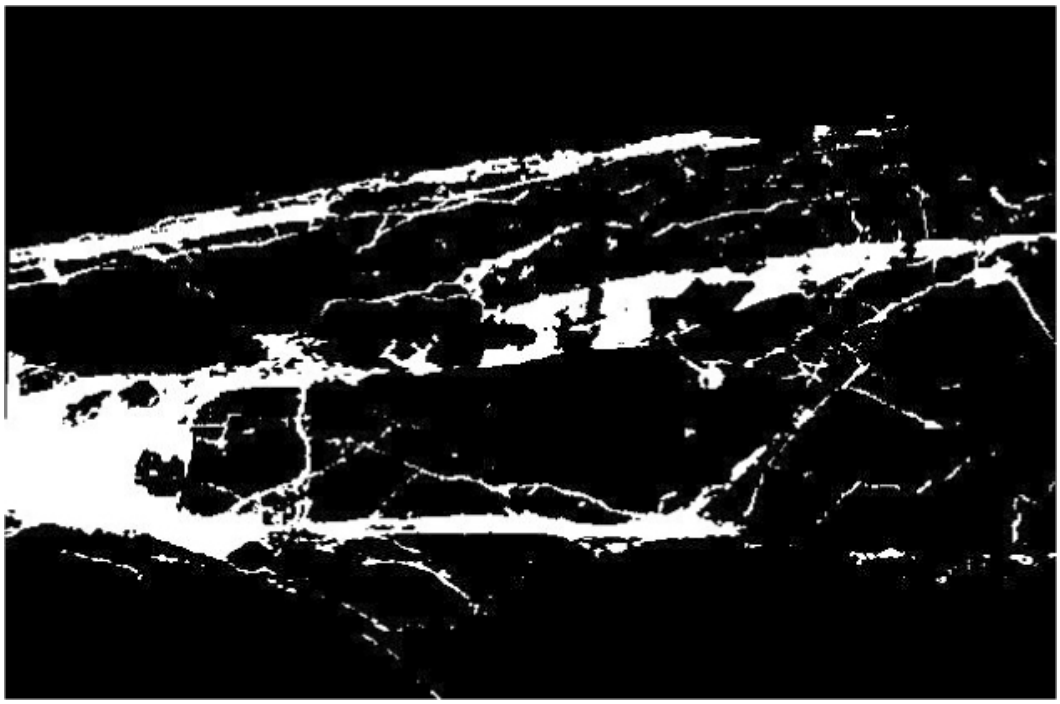

Figure 7-6. *B2-a1; Binary image after the image Figure 6-5 has been converted to grey scale (image based on the green image after applying a light smoothing and finally an automatic (between class variance) BCV thresholding (Sonka et al. 1995)). This image is also shrunk compared to the original image and the image size is now 640×480 pixels. The scale factor is 0.264 mm/pixel.*

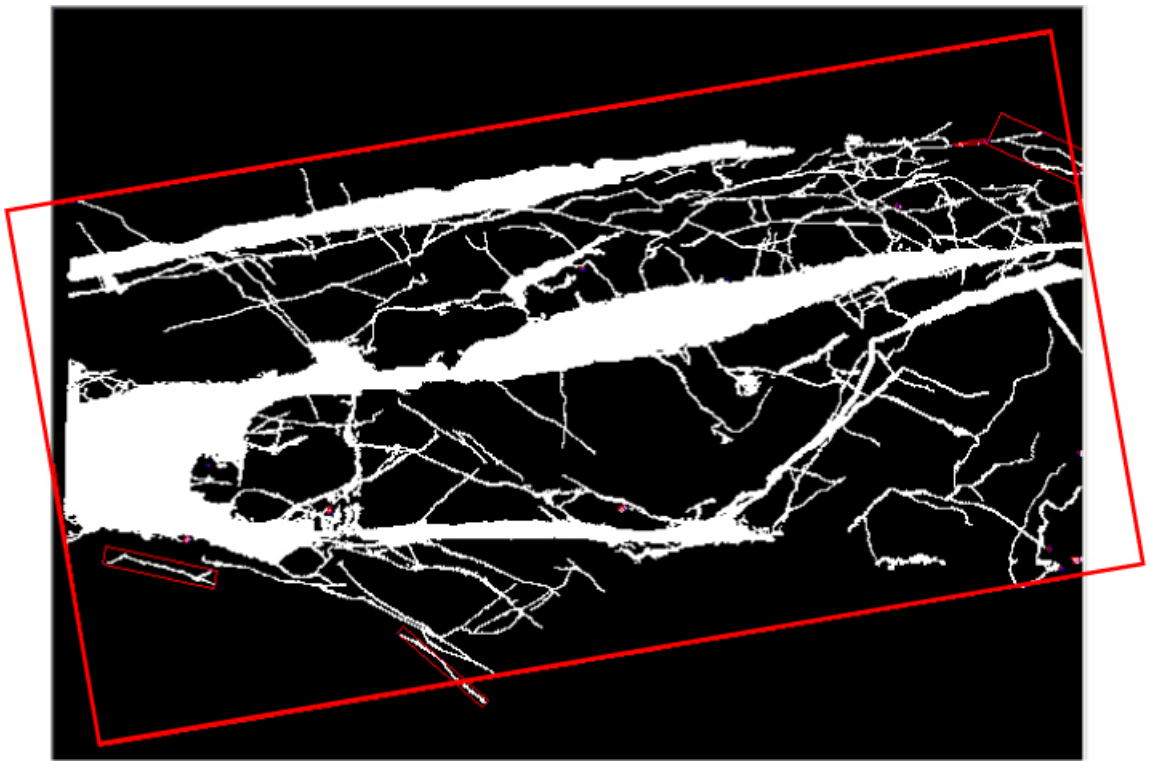

Figure 7-7. *B2-a1; "binary image"; the image is, after automatic thresholding, further processed to get the resulting connected fracture network (one large object). This image is used as the starting point for the network analysis. The fractured zone is circumscribed by a minimum size rectangle, a so-called Ferret Box (the largest red box in this case) that is determined from a combination of the network centre and its second moments and boundaries.*

In order to estimate some kind of indirect measure of porosity for the whole fracture zone slice it is required to determine the area that could be regarded as being the area of the fractured zone. This task could seem straightforward but is by no means trivial. The fractured zone in Figure 7-7 is circumscribed by a minimum size rectangle, a so-called Ferret Box (the largest red box in this case) that is determined from a combination of the network centre and its second moments and boundaries. From the example given in Figure 7-7 it is difficult to say if the outer part of the zone should simply be at the wall of the upper major fracture, or at the termination of the small connecting fractures, as the red box indicates. The zone could be taken to extend outside the image where some additional sub-parallel fractures are found. Obviously, if the porosity is calculated as the simple percentage of pores (epoxy-filled in our case) then the porosity will be mainly dependent on how the "area" (Ferret box) of the fractured zone is determined. Furthermore, as demonstrated by Hakami and Wang (2005), the estimate of the indirect measure of porosity is also governed by the resolution of the image. For this reason this parameter, which should be labelled as an "apparent porosity", should be used with care.

The red box in Figure 7-7 is calculated as the smallest rectangular object that circumscribes the largest object of the binary image. The binary image can provide information such as porosity, size and shape, and orientation of fractures, but no information on the connectivity, space density, and complexity of a fracture network. As described by Hakami and Wang (2005) skeletons of the fracture network need to be produced first. There are many skeleton algorithms described in the literature; most of them produce the detailed information of skeletons of objects. In this case, a network includes a lot of fractures, some of them are thick (but including loose particles, and with rough boundaries) and some of them are thin. To make skeletons for these kinds of networks, it was preferred to mainly consider the principal skeletons, and not the auxiliary skeletons caused by the boundary roughness and particles, because the auxiliary skeletons may cause an overestimation of fracture density. In parallel to testing out different algorithms, a morphological algorithm was employed for identifying the principal skeletons, that is non-sensitive to the boundary roughness and particles (see Figure 7-8). The image can then be used for calculating the fracture space density and average thickness. The problem is that these skeletons are not completely connected to each other (being simply segments), in which case, the particles (encircled connected objects formed by skeleton parts, e.g. an individual mineral aggregate) and junctions (where fractures intersect) cannot be detected. In order to detect junctions and particles, another skeleton algorithm was used (sometimes called thinning algorithm) that makes skeletons continuous (see Figure 7-9 and Figure 7-10). To distinguish it from the first skeleton algorithm (morphological skeleton algorithm), the latter is denoted the Thinning algorithm in what follows. After detection of junction points, these points were subtracted from the network and a fracture "branch image" identifying and forming geometrically the individual parts of the skeleton. An example is shown in Figure 7-11 (the sample image is taken from a B3 slice).

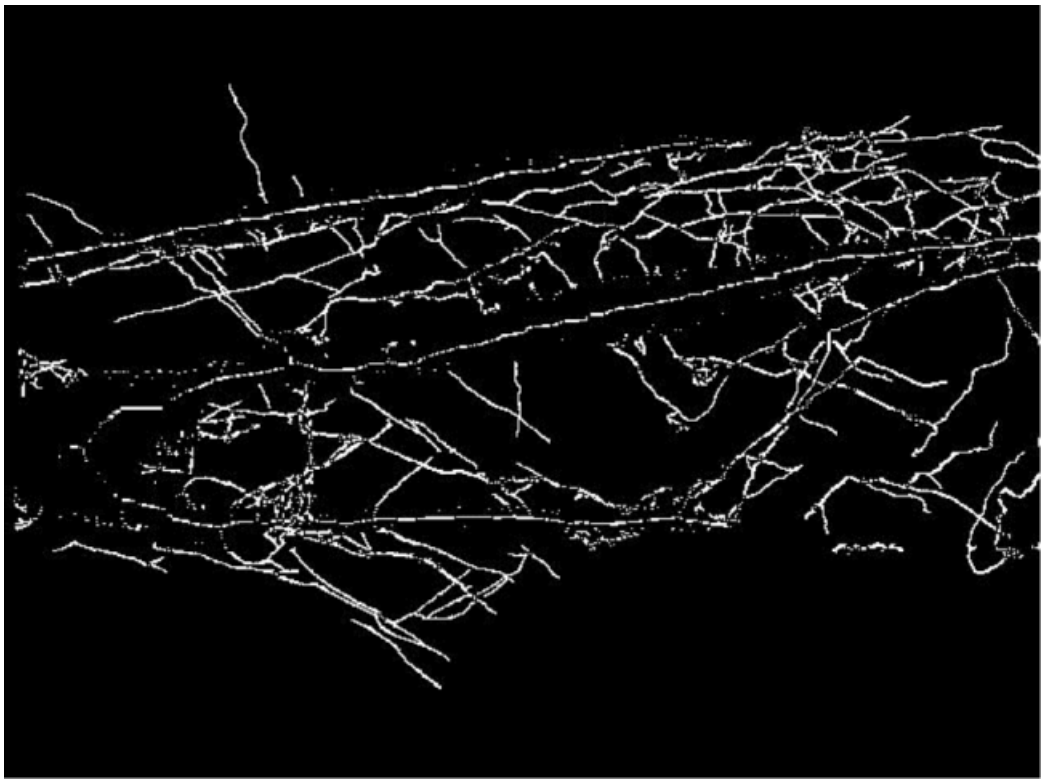

Figure 7-8. *B2-a1 Skeleton image: Morphological operations used on the binary image to abstract the skeletons of fractures.*

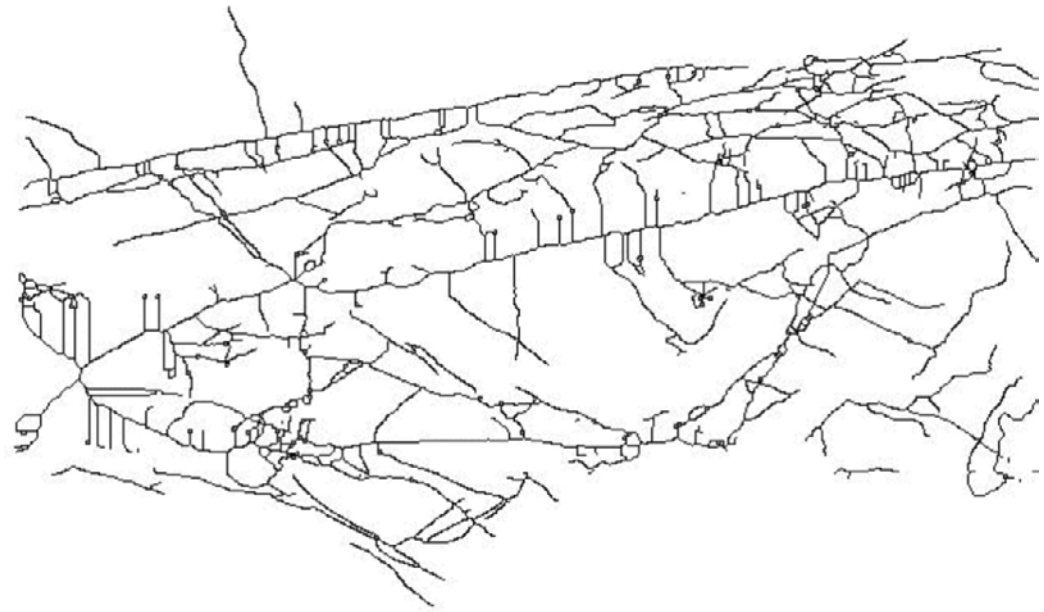

Figure 7-9. *B2-a1 Network image (Thinning image). From this network, one may estimate the connectivity and complexity of the network. It is used for calculating the number of junctions and to study fracture branches.*

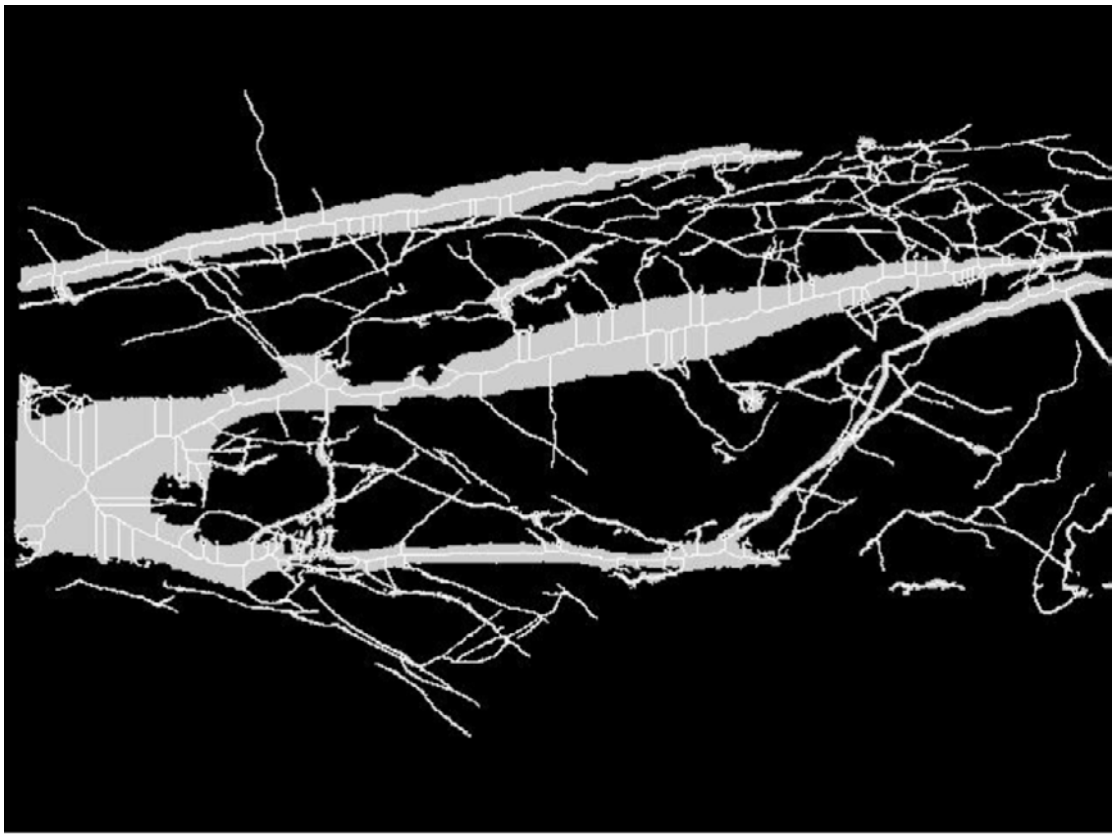

Figure 7-10. *B2-a1 Network image overlay on the binary image. Here, the grey colour represents the detected fractures, and the white colour represents the skeletons.*

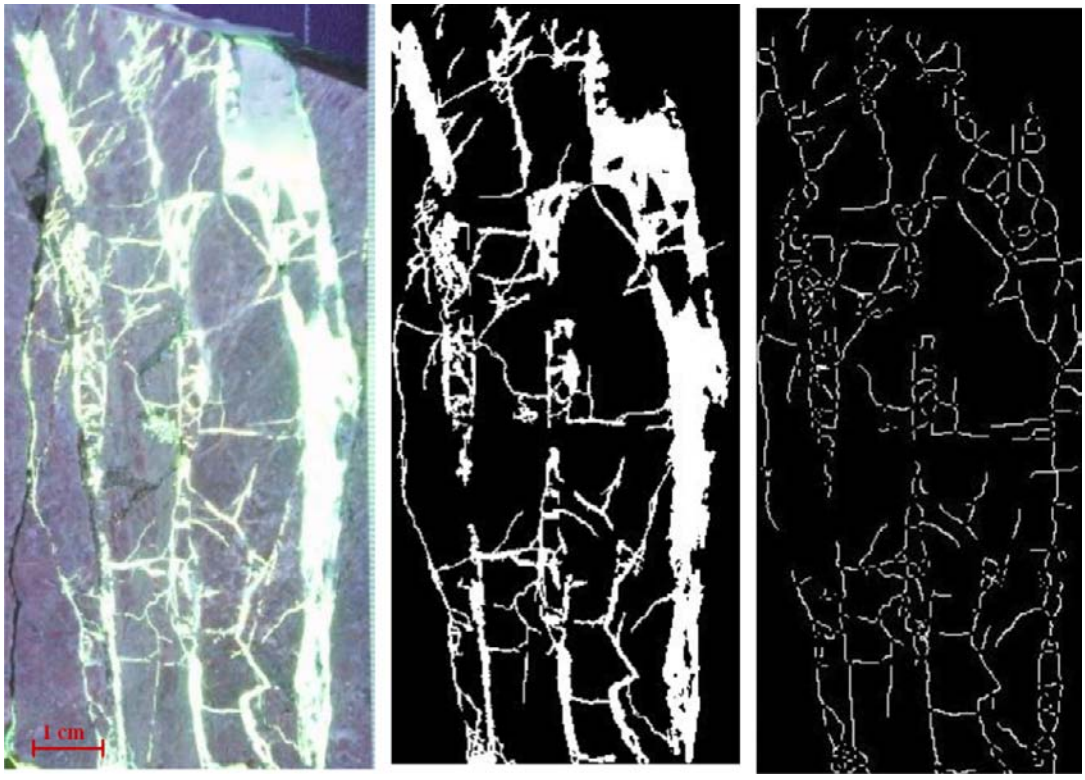

Figure 7-11. *B3-a3 image processing results. (a) original image, (b) binary image, and (c) branch image.*

7.3 Two dimensional fracture network property analysis

For each of the seven UV images from the B2 slices the following base data were measured: Ferret lengths (L) and widths (W, width is the direction across the zone), the epoxy filled area (A_e), the skeleton (net) area (A_n) (area bounded by the skeleton), the number of particles (P) and the number of junctions (J). The results are listed in Table 7-1.

To present different characteristics of the fracture network observed in the B2 slices, the basic data in Table 7-1 were used to calculate a number of characteristic parameters described in the following.

Figure 7-12 presents the variation in fractured zone size (L×W) and shows that the area of the zone decreases from slice #1 to #7, caused mainly by a decreasing section of the zone captured in the images (clearly seen from sample photos in Figure 7-3). This parameter, as such, thus does not describe any interesting change in the zone character, but it may still be important in the evaluation of other results. It is relevant as a "check" parameter and the original image should be consulted to find the explanation if any strange variation is noted. In this particular case the decrease in zone coverage may explain some of the trends seen in other parameters.

Figure 7-13 shows that the estimated *apparent porosity* of the fracture network (A_e/(L×W)) is fairly stable and the average value is 18.6%. From slice #1 to #7 the apparent porosity varies between 15–23%. As indicated previously, the parameter apparent porosity as defined here is difficult in the sense that the value becomes sensitive to the way the "fracture zone area" is defined and the resolution of the image. Hakami and Wang (2005), cf. Chapter 5 therein, showed that when the resolution of image was increased three times, the estimated porosity increased (for 8 analysed image frames) by between 8 and 72 (relative) % units.

Table 7-1. B2 slices – basic data and parameters inferred from the image analysis.

Slice[1]	L [mm]	W [mm]	Epoxy area, A_e [mm^2]	Net area, A_n [mm^2]	Particles, P	Junctions, J
1	173	87	1,863	1,074	163	138
2	173	88	2,257	982	95	95
3	150	86	1,912	824	92	124
4	150	86	2,148	835	137	98
5	131	82	1,867	684	96	93
6	124	76	2,179	660	82	50
7	84	57	1,267	253	65	128

[1] This is actually the a-side of a certain cut of the sample (the b-side of the cut was not analysed).

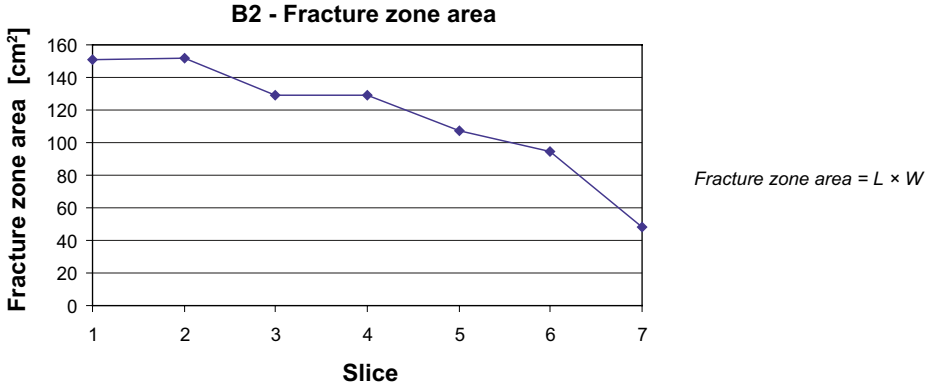

Figure 7-12. *B2 – variation in fracture zone (Ferret Box) area.*

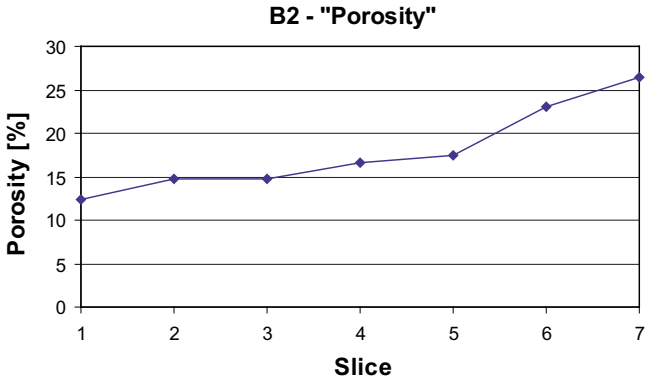

$$\text{"Porosity"} = \frac{A_e}{L \times W}$$

Figure 7-13. *B2 – variation in apparent porosity (%) of analysed slices.*

Figure 7-14 presents junction density which is a characteristic that was determined for the fracture network. It is calculated as the total number of junctions divided by the length. A more complicated network has more fracture junctions. The highest values for junction density are obtained for slices #3 and #5; their fracture pattern is more complicated than the fracture network in the other slices, as may be qualitatively noticed also directly in the images in Figure 7-3.

The same analysis has been performed for the sample B3 slices. In B3 the first four slices have similar Ferret Box orientations. Since Ferret Boxes for slices #1 to #4 involve the same fractured zone, the slices #5 through #8 slices only include a part of the fracture network, and the remaining slices are outside the same fractured zone. The detailed measurement results are listed in Table 7-2.

In Figure 7-15, it may be noted that the fracture zone size is stable from slices #1 to #4, and the remaining slices have a larger zone size. The apparent porosity for the analysed slices (Figure 7-16) decreases dramatically from slice #1 to #12.

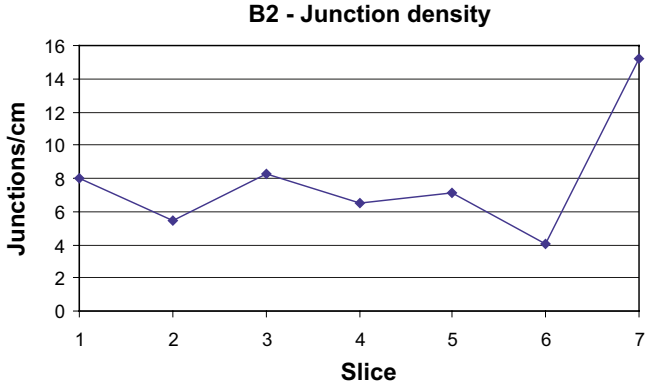

$$\text{Junction density} = 10 \times \frac{J}{L}$$

Figure 7-14. *B2 – variation of junction density (cm^{-1}).*

Table 7-2. B3 slices – Basic data and parameters inferred from the image analysis.

Slice[1]	L [mm]	W [mm]	Epoxy area, A_e [mm^2]	Net area, A_n [mm^2]	Particles, P	Junctions, J
1	125	49	1,559	528	140	265
2	127	57	1,547	490	118	235
3	128	57	1,613	547	124	244
4	126	51	1,120	429	116	222
5	130	123	1,232	541	89	154
6	136	119	1,082	568	77	166
7	116	116	705	423	74	131
8	109	102	471	303	32	104
9	120	120	527	280	4	33
10	99	97	230	162	9	17
11	107	87	143	118	0	5
12	99	86	121	100	5	13

[1] This is actually the a-side of a certain cut of the sample (the b-side of the cut was not analysed).

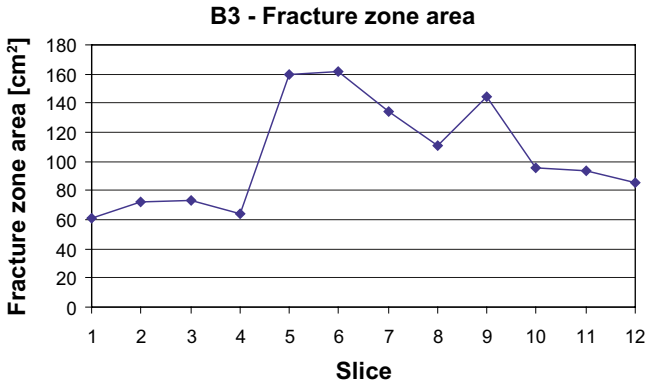

$$\text{Fracture zone area} = L \times W$$

Figure 7-15. *B3 – variation in fracture zone (Ferret Box) area.*

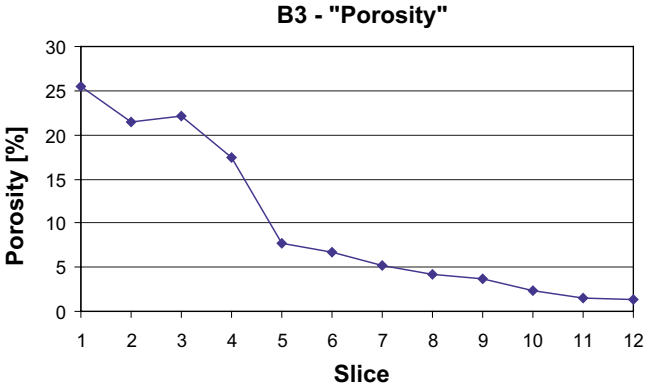

$$\text{"Porosity"} = 100 \times \frac{A}{L \times W}$$

Figure 7-16. *B3 – variation in apparent porosity (%) of analysed slices.*

When comparing the results from samples B2 and B3 some similarities and differences are notable. The Ferret box width is in the same order for both samples, which is to be expected since the samples are located close to each other and the width should not be dependent on the orientation. The estimated value of apparent porosity is also similar for the B2 and B3 samples (if we consider B3 slices #1 to #8 only). Values of apparent porosity obtained here for analysed samples of geological material from KA2423A03 are not directly comparable with the measured porosity values reported in Table 6-1. Notonly are they obtained with different methods but they also relate to two different localities and also represent geological material of different nature, see Chapter 5 and Section 6.2. Despite these restrictions, it is notable that the values of porosity are of the same order.

A clear difference is seen is in the junction density which is around 7 cm^{-1} in B2 (Figure 7-14), about 19 cm^{-1} for B3 (slices #1 to #4) and around 11 cm^{-1} in B3 (slices #5 to #8), cf. Figure 7-17. This is important given that one of the selected parameters does pick up the difference in shape character that is not easy to observe visually from the overview images in Figure 7-2a (B3) and Figure 7-3 (B2). The shapes of the "blocks" of the network are more square-shaped in B3 and relatively smoother compared with the more lens-shaped blocks seen in B2. The interpretation is that most of the shear movement has been more (sub-) parallel to the planes of the B2 images than to the B3 planes.
A dominant direction in shear movement will induce anisotropy in the fracture pattern. The orientation of shear is sinistral, when looking at the a-side of the B2 slices and this corresponds to a sinistral shear displacement of the subvertical fault zone studied.

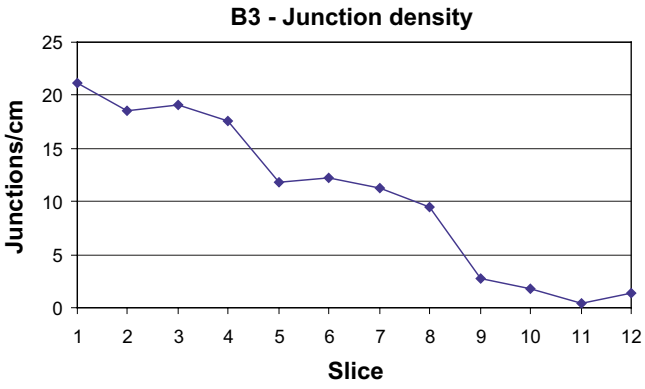

$$Junction\ density = 10 \times \frac{J}{L}$$

Figure 7-17. *B3 – variation in junction density (cm^{-1}).*

7.4 Conclusions

The image analysis may be divided into three principal parts. The first part is the methodology developed for sample collection and image acquisition of fault rock pore space. The second part includes the methodology development for the image processing and analysis, and the third part is the characterisation of the studied fault rock using the image data. The conclusions for these parts are summarised below.

7.4.1 Sample collection and image acquisition

The developed method, including impregnation of the fault rock *in situ*, has worked out satisfactorily, providing the necessary reinforcement of the friable material relative to sampling disturbances and providing enhanced visibility of the geometry of the pore space. An important factor in the latter context is the amount of fluorescence added to the epoxy, which should be high. This, in combination controlled illumination, using fixed lamp positions, and a stable surrounding (dark room) facilitates the image acquisition. Stable image acquisition conditions provide a stable image quality and, as a result, a faster image analysis.

7.4.2 Image processing and analysis

Image analysis has been shown to be a useful and versatile tool when identifying geometrical patterns and for providing a basis for quantitative parameters that describe the geometrical properties of the pore space of a fault zone fracture network, or a single fracture in crystalline bedrock.

Decision on what image processing steps and image analysis to be undertaken in a specific case should be made based on the general character of the pore space, the image quality and, most importantly, the objectives of the specific study. In order to make the image analysis, as a first step it is necessary to construct binary (only black or white) images from the original greyscale (or colour) images.

Attempts have been made to determine some fault zone apparent porosity (porosity here expressed as the ratio between the sums of epoxy-filled white areas divided by a “total area”). However, porosity has proven to be a difficult parameter since it is difficult to define unambiguously, such that the parameter can be made precise and relevant also for comparison of different zones and use in modelling. The porosity of a fault zone is expected to vary considerably normal to the fault plane, while being somewhat more constant (continuous) along the zone. Furthermore, the lower bound of an impregnated pore (size) to be included in the quantification would also be dependent on the epoxy impregnation and the image scale (resolution).Close-up images would consequently tend give a higher value on porosity (as discussed in Section 7.3).

7.4.3 Character of studied fault structure

The minor fault studied was sampled from the wall of the Äspö hard rock laboratory access tunnel with a 300 mm diameter borehole (KA2423A03). Half of the core was used for the study and cut into slices in two perpendicular directions. Through direct visual studies of ordinary images of the fault cross section, the conceptual understanding of how such structures are geologically built up was improved. Through the image analysis of the UV-light images the pore volume, as infilled with fluorescent epoxy, could be quantitatively characterised.

The fault zone structure is complex, consisting of on average five to six sub-parallel fractures connected to each other. The character of the fractures in the network differs. The major fracture plane is the plane where most of the shear movement has occurred, most probably at several shearing episodes, separated in time. This fracture has a large variation in aperture. At some points the aperture is cm-wide and at other points the fracture is entirely filled with calcite and other fracture filling minerals. Another characteristic of the main fault is sections with porous infilling, i.e. infilling consisting of small assemblies of infilling minerals and fragments of the host rock (denoted fault gouge). Fore the most part, this porous material was impregnated with the epoxy, indicating that there is certain porosity/permeability also in these sections.

The general character of the fault zone appears to be constant at the scale of the studied fault zone sample (about 20 cm long). However, the detailed geometry is not so simple that it enables a direct connection between sections with 2 cm interdistance, across the thickness of the sample slices, other than for the major fractures of the fault zone.

The width of the studied fault zone is about 6 cm ("width" here being the maximum distance perpendicular to the plane of the interconnected epoxy filled fracture network in the sample). An attempt to define an apparent porosity parameter was made, but it is shown that this parameter is sensitive to its underlying definition and is therefore not recommended as a characterising parameter.

The anisotropy of the fracture network is observed by the differences in network junctions on planes from sample B2 compared to B3. B2 and B3 are neighbouring parts of the zone which are cut into slices in different directions. The number of junctions per cm section across the fault rock plane is in the order of 7 cm^{-1} for B2 and 19 cm^{-1} for B3. This is explained by the fact that the fracture network pattern will be determined by the directions of movements on the fault. In planes sub-parallel to the movement (B2) the pattern is less complicated, with fewer junctions and with more smooth lens-shaped particles.

The methodology developed in this study is judged to be suitable also for application to the conductive structure (Feature A) at the TRUE-1 site, which has been the subject to an extensive series of tracer tests, cf. e.g. Winberg et al. (2000).

8 Revisit of conceptual models

Conceptual models of fractures and fault rock zones have been developed for Äspö conditions as part of the FCC programme (Mazurek et al. 1996, Bossart et al. 2001) and within the TRUE programme (Winberg et al. 2000, Andersson et al. 2002a, 2007, Dershowitz et al. 2003). The laboratory programme (related to retention properties) preceding TRUE-1 (Winberg et al. 2000) was focused on the intact rocks of Äspö and largely ignored the fracture rim zone (Byegård et al. 1998). The results of the intercomparison between blind model predictions of the outcome of the TRUE-1 *in situ* tracer experiments using radioactive sorbing tracers showed clear evidences of a higher retention in the rim zone (fault rock zones) compared with that of intact rock. Alternative hypotheses were put forward including higher retention (diffusion/sorption) in the fracture rim zone (including altered wall rock of increased porosity and possible contributions of fine grained fault gouge) (Cvetkovic et al. 2000), effects of high porosity fault gouge alone (Jakob et al. 2003) or increased accessible flow-wetted surface (Neretnieks 2002). While triple-tube coring had not been employed, no hard evidence to support the existence of non-cohesive fault gouge existed, although indirect but clear evidences had been found in terms of traces of clay on the fracture surfaces of Feature A (Winberg et al. 2000). Complementary laboratory investigations employing PMMA impregnations applied to Feature A specific materials, clearly evidenced an elevated porosity in the close vicinity of the fracture surface (Byegård et al. 2001). Extended *in situ* hydraulic and tracer tests conducted in the vicinity of Feature A (Andersson et al. 2002b) reinforced the earlier interpretation of Feature A as being a well isolated hydraulic feature, thus introducing doubt that the flow-wetted surface had been underestimated. An integrated evaluation of the TRUE-1 tests is presented by Widestrand et al. (2007) and Cvetkovic et al. (2007).

Work conducted as part of TRUE Block Scale continuation addressed by modelling the possible effects of heterogeneity in the properties of the fracture rim zone affecting retention. This applied both to longitudinal (Poteri 2003) and transverse (Cvetkovic and Cheng 2002, 2010). An integrated presentation of the TRUE Block Scale and TRUE Block Scale Continuation tests is presented by Cvetkovic et al. (2010) and Cvetkovic and Frampton (2010).

Prior to, and parallel with, the conceptualisation work at the TRUE-1 site Mazurek et al. conducted a global inventory of water conducting features in the Äspö HRL access tunnel through characterisation and classification aiming at investigation concepts, conceptual models and geological parameterisation for modelling geosphere solute transport (Mazurek et al. 1996). The results of this work, which included at compilation of a total of 88 fractures, showed that all water-conducting features larger than the tunnel diameter (c. 5 m) are faults consisting of interconnected systems of shear fractures (master faults) and tension fractures (splay fractures). Based on the arrangement of master faults and splay fractures, five types of conductive features were distinguished. It was noted that no other systematic discriminator (e.g. hydraulic parameter or mineralogy) could be identified, and probably can not be defined. The fracture types can vary and blend into each other along the extent of a given feature, a characteristic also noted in the characterisation of the conductive structures in the TRUE Block Scale rock volume (Andersson et al. 2002a). Moreover, Mazurek et al. (1996) provide conceptual models covering both larger-scale characteristics and mm-cm scale structure of the flowing elements of the conductive structures. The work by Mazurek and co-workers also included resin impregnations of rock core specimens (diameter =200 mm) in the laboratory which were used to sustain the conceptualisation on a decimetre scale, which largely corresponds to the scale of the samples used for epoxy resin impregnation in the current study. Overall, the supporting epoxy resin imagery shown in Mazurek et al. (1996), cf. e.g. Figure 8-8 therein, show similar characteristics as that noted in the KA2423A imagery in the current study, at the corresponding scale. This work was followed by further work focused on the TRUE-1 site, including geological-hydrogeological conceptualisation of the site and Feature A (being focus for tracer experiments) (Bossart et al. 2001).

The introduction of triple tube core drilling in conjunction with the TRUE Block Scale project (Andersson et al. 2002a, Winberg et al. 2003) furnished for significant improvement of the conceptual microstructural models of typical conductive fractures at the Äspö HRL. The description of the rim zone microstructure model was improved with a higher resolution of the brecciated materials within zones, where the fine-grained non-cohesive fault gouge was complemented by cm-sized fault

breccia pieces and mm-sized fault breccia fragments. The microstructural model was also quantified in terms of geometry (typical thicknesses) and typical values of porosity, but also of diffusivity (or rather formation factor) and K_d of the rim zone and fault gouge, the latter calculated from CEC, selectivity coefficients, mineralogy and the ambient water composition (Andersson et al. 2002a, Dershowitz et al. 2003). The derived K_d values have subsequently been verified experimentally in the laboratory (Byegård and Tullborg 2012). However, still remaining without quantification was the *in situ* porosity of the fault gouge materials which largely had been attributed porosities in the order of 10–20%, mainly based on earlier inferences by Mazurek et al. (1996).

The current work presents estimates of apparent porosity based on image analysis of binary coded epoxy injected fault rock. The measure based on image analysis provides a measure of the "fraction of area filled with epoxy". This resin-based porosity is bound to be less than the "true" *in situ* porosity. This while epoxy has not penetrated all potentially open pores, primarily due to incomplete connectivity in the fracture networks at the applicable scales, but also due to shortcomings in resin behaviour during resin injection. Furthermore, the epoxy-filled pores need to be sufficiently large to be seen by the camera. It should also be emphasised that the image-based apparent porosity does not provide a pure porosity estimate of fault gouge alone, but rather provide an integrated measure of the bulk (connected) flow porosity over the photographed width of the studied conductive feature (NB. In principle it should be possible to reduce the box to cover only the fault gouge). The determined porosity ranges from 11–70%. The porosity detemined in this way is determined by 1) the distribution of pore sizes in the averaging area/volume, 2) the penetration capacity of the epoxy in the available pores, 3) the size of the averaging area/volume, 4), and the resolution of the photographic image. As shown by Hakami and Wang (2005), a threefold increase in resolution from 0.021 mm/pixel to 0.066 mm/pixel entails increases in porosity between 8 and 72 (relative) percent. Given that the porosity determination is strongly dependent on image resolution, renders the method employed as being non-robust. In order to make the quantification of porosity using image analysis practically useful there exists a need for some type of normalisation against an independent standardised porosity determination.

Revisiting the five classes of structural arrangement of conductive structures introduced by Mazurek et al. (1996), the imagery of the zone at chainage 2/423 m (as obtained from borehole KA2423A03) compare with Types 3 (fault zone with two master faults with connecting splays) with superimposed elements of Type 2 (2 or more parallel master faults, with splays, but lacking connection, or being poorly connected to the main fault). Given that epoxy is observed in fractures parallel to the main fault without being visibly connected in the section, suggest connections in the third dimension which cannot be traced in the 2D slice in a direct manner.

The produced imagery for the most part provides support for the current conceptualisation and associated microstructural models as devised by the TRUE Block Scale Project. The collected information and the imagery on multiple parallel rock slabs, all geodetically constrained, offer an opportunity to (at least in theory) for reconstruction of highly detailed models of the 3D network of interconnected pores on a decimetre to metre scale. However, such an endeavour is not of high priority since numerical model representations rather tend to strive towards a reduction of the complexity of conceptual models of natural systems. However, the imagery collected from Section 2/423 m, given the geometrical and structural kinship between this structure and the TRUE target structures (Feature A, Structure #20 and Structure #19) provide support for and further sustain the conceptualisation and microstructural models developed and applied within the TRUE project.

9 Discussion and conclusions

9.1 General

The basic objective of the Fault Rock Zones Characterisation programme was to provide deeper insight into the internal structure of conductive structures at Äspö HRL, similar to the ones investigated deeper into the rock at the TRUE-1 and TRUE Block Scale sites. In the latter cases the investigated structures lack outcrop in the tunnel. The rationale of the current study has been to identify conductive structures, akin to e.g. Feature A (TRUE-1) and Structure #20 (TRUE Block Scale), that are readily exposed and accessible in the Äspö HRL access tunnel.

Various means to impregnate the conductive structures for subsequent study of the pore structure were reviewed. The intention being that the developed/applied technology for epoxy-based characterisation developed should subsequently be applied to Feature A at the TRUE-1 site.

9.2 Identification of conductive structures

The basis for the identification of structures suitable for investigation was the inventory of conductive fractures and faults in the Äspö access tunnel made by Mazurek et al. (1996), supplemented by field inspection in the tunnel. Eventually four structures at four different locations outcropping in the tunnel were selected for further study; at 1/596m, 2/163m, 2/423 m and 2/545m, respectively. The conductive structures identified during the tunnel mapping were reviewed and incorporated in 3D CAD models (Stigsson et al. 2003). The four selected localities was mapped in detail and described geologically on the basis of available boreholes and tunnel walls, cf. Chapter 2 and Maersk-Hansen et al. (2003).

9.3 Drilling and geological characterisation

At all four sites, the respective target structure/feature was straddled with four short near-parallel 72 mm triple-tube cored holes, intersecting the individual target structures at variable depth from the tunnel wall. The boreholes were logged with the BIPS borehole TV imaging system.

9.4 Geological and mineralogical characteristics

The results from the chemical and mineralogical analyses of material from KA2423A03 support the fact that this is (in similarity with the other two structures studied) a ductile/semi-ductile structure that has later been reactivated and, especially in the case of Structure 2423, been later subjected to hydrothermal circulation resulting in formation of epidote, calcite, fluorite and pyrite. Idiomorphic crystals are common indicating readily available pore space in many parts of this structure. Subsequent alteration has formed clay minerals such as the disordered swelling clay mineral of mixed-layer type which has been identified in the fine fraction from this structure.

A comparison of the investigated fault rock structures with past experience from Äspö tunnel, and also from the site investigations in Laxemar-Simpevarp, shows that the fault rock structures investigated here are typical to the area. Typically, Structures 2169 and 2423 show characteristics that are commonly seen in minor deformation zones in the Laxemar-Simpevarp area. The characteristics of Structure 1596 are less common, considering it is rich in chlorite and clay, but similar characteristics have also been seen in nearby Simpevarp.

9.5 Packer installations

Based on the earlier performed flow and pressure registrations and the geoscientific characterisation, nine of the 16 boreholes were equipped with a mechanical packer sealing off the target section (including the target fault zone), the latter also equipped with dummy material reducing the annular volume of the section to a minimum. The connections to the upper part of the packer (standpipe and circulation hoses) were designed to be easily dismounted before commencing the overcoring activities.

9.6 Hydraulic properties and groundwater flow

The open boreholes were logged for (total) water flow and equipped with lids and pressure gauges. Water injection tests were subsequently made at different excess pressures to assess transmissivity and injectability to resin. The results showed transmissivites ranging from $1{\cdot}10E^{-10}$ m^2/s to $1.2{\cdot}10^{-7}$ m^2/s. It was deemed futile to attempt resin injection in sections showing transmissivities below $6{\cdot}10^{-10}$ m^2/s. Consequently, boreholes KAS1596A01 and KAS1596A03 were left without instrumentation.

9.7 Selection of resin and epoxy resin injections

A range of different epoxy and acrylic resins were reviewed at the onset of the current study, which also included discussions of the Grimsel experiences with representatives of Nagra, Switzerland. Eventually, the epoxy EpoTek 301 was selected. Although showing similar characteristics as the epoxy resins employed by Nagra, the EpoTek 301 was chosen on the basis of its merits experienced during the TRUE-1 Pilot Resin Experiment (Birgersson et al. 2000a).

The noted zero resin yields of KA2423A01 and KA2548A01 resulted in seven of the originally nine injected boreholes taking measurable amounts of resin. Although the performed water injections indeed indicated injectability, the zero resin yield came with low surprise given the transmissivites of the two boreholes, $1{\cdot}10^{-9}$ and $6{\cdot}10^{-10}$ m^2/s, respectively.

9.8 Overcoring, core mapping and sectioning of overcores

Given the results of the resin injection, only seven boreholes were eventually overcored. As described in Chapter 4, a methodology was developed which was subject to continuous adaptation to the conditions met in the individual boreholes being overcored. The critical element in retrieving the cores was the establishment of a clean break at the desired length coordinate. A strive was to make use of naturally occurring fractures for the breaks to the extent possible. In the case a break was to be made in a non-fractured part of the core, force was applied to the core with a customised hydraulically inflatable steel flask. Both types of core breaks were inhibited to some extent by the fact that the dummy body in the section was solid. Any new application should employ a pre-sectioned or pre-weakened dummy body along the borehole to enable added flexibility in locating the breaks.

The overcores were put on a rotating bed on which they were photographed and mapped. The use of a transparent plastic foil to map the target sections worked out well, and produced reference images to which detailed photographs could be referenced, cf. Section 4.3 and Maersk-Hansen and Staub (2004).

On the basis of the core mapping, detailed RVS images were constructed of the cores on which were superimposed sequential sectioning plans. Primary cuts orthogonal and parallel to the core axis were made in a nearby quarry. Subsequent cuts were made using a diamond saw. Reference rulers were attached to the core allowing for 3D referencing.

9.9 Image analysis of resin impregnated rock samples and their quantification

The image analysis carried out has focused on the resin impregnated rock associated with the structure in KA2423A03 and has involved a variety of developments to improve the quality of the photographs (type of camera, magnification/resolution, lightning conditions and angles of illumination, shielding off of unwanted extra lighting). Images were also collected using microscope and a CCD camera and were found useful for analysis of single fractures (reaching resolutions in the order of 0.003 mm/pixel).

An account is given of 2D image analysis of the generated slices including transformation of the imagery to grey scale (binary image), thresholding, skeleton imaging and superposition of analysis window (Ferret-box) for assessment of network properties. The latter includes quantification of various characteristics of the network such as the area covered by epoxy, the area made up by the skeleton, e.g. the number of By plotting a given entity vs. sequential slices, an indication of the variability/complexity in network properties is obtained.

9.10 Porosity

An indirect estimate of porosity from image analysis is obtained as the sum of epoxy-filled area in the Ferret-box divided by the total area of the box. This implies that the apparent porosity measure is a "bulk" value, which most likely is lower that the "true" *in situ* porosity. The porosity values obtained range from c. 11–70%, depending on the distribution of pores, epoxy penetration, averaging area/volume and the resolution of the imagery. Porosity obtained by conventional techniques has been obtained for (non-epoxy impregnated) fault gouge material from 1/596m (zone NE-2) indicating average porosity between 12–14%-vol, cf. Section 6.1. Comparative calibrations between image-based and conventional porosity determinations are not possible while undisturbed and non-impregnated (by epoxy) samples are required for such comparisons. The latter situation is inherent while it is very difficult to sample these types of structures with conventional core drilling

In conclusion, given the dependence on image resolution the image-based apparent porosities may at best be regarded as ball-park relative measures of porosity of complete fault zones. The method employed does not allow firm quantification of fault gouge porosity for the samples analysed in this study. However, the values of apparent porosity for fault gouge obtained in this study comply with the lower end of the interval suggested by Mazurek et al. (1996).

In the case of sedimentary rocks, Prêt et al. (2004) report results from PMMA injections in carbonate fault zone with a clay rich heterogeneous fault gouge made up of clast of host rock surrounded buy a clay matrix. Image analysis based quantification of the porosity of the fault gouge indicates a porosity of the clay matrix ranging between 10 and 15%, compared to the 2.7 to 8% porosity of the clasts.

Recently, tests with PMMA impregnation on rock cores from Grimsel have been reported (Kelokaski et al. 2006), indicating matrix porosities in the 0.52–0.73%, which were in parity with mercury intrususion porosimetry values of 0.53–0.83%. The main challenge in bringing the PMMA technique *in situ* is the need for drying of the rock involved as MMA cannot replace water. Preliminary results from *in situ* application of PMMA in intact tunnel wall rock at Grimsel suggest porosities in the order of 0.4%, being some 20–30% lower than the corresponding PMMA values on core material (Siitari-Kauppi M, personal communication). This porosity is in the order of that presented by Möri et al. (2003) in the CP experiment at Grimsel and this is about 1/3 of the porosity measured on drill cores in the laboratory, assumed subject to de-stressing. This provides added support for the use of *in situ* resin impregnation to assess porosity.

9.11 Revisitation of conceptual models

The information obtained from the current study, both descriptive geometrical information, and quantitative information is not in conflict with the decametre conceptual microstructural models, applicable to Äspö HRL conditions, devised by Mazurek et al. (1996), Andersson et al. (2002a) and Dershowitz et al. (2003). The information provides opportunity for introducing additional detail in the microstructural model. In fact, there is information and potential for reconstructing microstructural models (fracture network models) in 3D. The latter has not been pursued as part of this study. It is also questionable whether additional detail in conceptual models for numerical calculations is desirable, or even relevant. Furthermore, the ambition to produce firm and unambiguous quantification of the porosity of fault gouge has not worked out. The reason in part being attributed to the underlying resolution of the imagery.

However, foremost the produced imagery provides additional supporting information which may be used to properly inform and sustain current conceptual models of fault rock zones at a lesser level of detail. The results also provide support for the use of *in situ* resin impregnation for assessing relevant values on *in situ* porosity.

10 References

SKB's (Svensk Kärnbränslehantering AB) publications can be found at www.skb.se/publications.

Alexander W R, Ota K, Frieg B, 2003. Grimsel Test Site – Investigation Phase IV (1994–1996): The Nagra-JNC in situ study of safety relevant radionuclide retardation in fractured crystalline rock – II: The RRP project methodology development, field and laboratory tests. Nagra Technical Report 00-06, National Cooperative for the Disposal of Radioactive Waste, Switzerland.

Andersson P, Byegård J, Dershowitz B, Doe T, Hermanson J, Meier P, Tullborg E-L, Winberg A (ed), 2002a. Final report of the TRUE Block Scale project. 1. Characterisation and model development. SKB TR-02-13, Svensk Kärnbränslehantering AB.

Andersson P, Wass E, Gröhn S, Holmqvist M, 2002b. Äspö Hard Rock Laboratory. TRUE-1 Continuation project. Complementary investigations at the TRUE-1 site – crosshole interference, dilution and tracer tests, CX-1 – CX-5. SKB IPR-02-47, Svensk Kärnbränslehantering AB.

Andersson P, Byegård J, Billaux D, Cvetkovic V, Dershowitz W, Doe T, Hermanson J, Poteri A, Tullborg E-L, Winberg A (ed), 2007. TRUE Block Scale Continuation project. Final report. SKB TR-06-42, Svensk Kärnbränslehantering AB.

Birgersson L, Gale J, Hakami E, 2000a. Äspö Hard Rock Laboratory. First True Stage, Pilot Resin experiment. Summary report. SKB IPR-00-04, Svensk Kärnbränslehantering AB.

Birgersson L, Gale J, Hakami E, 2000b. Äspö Hard Rock Laboratory. First True Stage, Pilot Resin experiment. Background information. SKB IPR-00-05, Svensk Kärnbränslehantering AB.

Bossart P, Mazurek M, Hellmuth K-H, Schneebeli M, Siitari-Kauppi M, 1991. Grimsel Test Site: Structural geology and water flow-paths in the Migration shear-zone. Nagra Technical Report 91-12, National Cooperative for the Disposal of Radioactive Waste, Switzerland.

Bossart P, Hermanson J, Mazurek M, 2001. Äspö Hard Rock Laboratory. Analysis of fracture networks based on the integration of structural and hydrogeological observations on different scales. SKB TR-01-21, Svensk Kärnbränslehantering AB.

Byegård J, Tullborg E-L, 2012. Äspö Hard Rock Laboratory. TRUE-1 Continuation project. Sorption experiments and leaching studies using fault gouge and rim zone material from the Äspö Hard Rock Laboratory. SKB P-11-20, Svensk Kärnbränslehantering AB (in prep).

Byegård J, Johansson H, Skålberg M, Tullborg E-L, 1998. The interaction of sorbing and non-sorbing tracers with different Äspö rock types. Sorption and diffusion experiments in the laboratory scale. SKB TR-98-18, Svensk Kärnbränslehantering AB.

Byegård J, Widestrand H, Skålberg M, Tullborg E-L, Siitari-Kauppi M 2001. First TRUE Stage. Complementary investigations of diffusivity, porosity and sorptivity of Feature A-site specific geologic material. SKB ICR-01-04, Svensk Kärnbränslehantering AB.

Bäckblom G, 2008. Excavation damage and disturbance in crystalline rock – results from experiments and analyses. SKB TR-08-08, Svensk Kärnbränslehantering AB.

Cvetkovic V, 2010. Significance of fracture rim zone heterogeneity for tracer transport in crystalline rock. Water Resources Research 46, W03504. doi:10.1029/2009WR007755

Cvetkovic V, Cheng H, 2002. Äspö Hard Rock Laboratory. TRUE Block Scale project. Evaluation of block scale tracer retention understanding experiments at Äspö HRL. SKB IPR-02-33, Svensk Kärnbränslehantering AB.

Cvetkovic V, Frampton A, 2010. Transport and retention from single to multiple fractures in crystalline rock at Äspo (Sweden): 2. Fracture network simulations and generic retention model. Water Resources Research 46, W05506. doi:10.1029/2009WR008030

Cvetkovic V, Cheng H, Selroos J-O, 2000. Evaluation of tracer retention understanding experiments (first stage) at Äspö. SKB ICR-00-01, Svensk Kärnbränslehantering AB.

Cvetkovic V, Cheng H, Widestrand H, Byegård J, Winberg A, Andersson P, 2007. Sorbing tracer experiments in a crystalline rock fracture at Äspö (Sweden): 2. Transport model and effective parameter estimation. Water Resources Research 43, W11421. doi:10.1029/2006WR005278

Cvetkovic V, Cheng H, Byegard J, Winberg A, Tullborg E-L, Widestrand H, 2010. Transport and retention from single to multiple fractures in crystalline rock at Äspo (Sweden): 1. Evaluation of tracer test results and sensitivity analysis. Water Resources Research 46, W05505. doi:10.1029/2009WR008013

Dershowitz B, Winberg A, Hermanson J, Byegård J, Tullborg E-L, Andersson P, Mazurek M, 2003. Äspö Hard Rock Laboratory. Äspö Task Force on modelling of groundwater flow and transport of solutes. Task 6C. A semi-synthetic model of block scale conductive structures at the Äspö HRL. SKB IPR-03-13, Svensk Kärnbränslehantering AB.

Frieg B, Alexander W R, Dollinger H, Bühler C, Haag P, Möri A, Ota K, 1998. In situ resin impregnation for investigating radionuclide retardation in fractured repository host rocks. Journal of Contaminant Hydrology 35, 115–130.

Hakami E, Gale J, 1999. Äspö Hard Rock Laboratory. First TRUE Stage pilot resin experiment. Pore space analysis. SKB IPR-99-14, Svensk Kärnbränslehantering AB.

Hakami E, Wang W, 2005. Äspö Hard Rock Laboratory. TRUE-1 Continuation project. Fault rock zones characterisation. Characterisation and quantification of resin-impregnated fault rock pore space using image analysis. SKB IPR-05-40, Svensk Kärnbränslehantering AB.

Hellmuth K-H, Lukkarinen S, Siitari-Kauppi M, 1994. Rock matrix studies with carbon-14-polymethylmethacrylate (PMMA); method development and applications. Isotopenpraxis Isotopes in Environmental and Health Studies 30, 47–60.

Jakob A, Mazurek M, Heer W, 2003. Solute transport in crystalline rocks at Äspö – II: Blind predictions, inverse modelling and lessons learnt from test STT1. Journal of Contaminant Hydrology 61, 175–190.

Kelokaski M, Oila E, Siitari-Kauppi M, 2001. Äspö Hard Rock Laboratory. TRUE Block Scale project. Investigation of porosity and microfracturing in granitic fracture wall rock and fault breccia specimens using the PMMA technique. SKB IPR-01-27, Svensk Kärnbränslehantering AB.

Kelokaski M, Siitari-Kauppi M, Sardini P, Möri A, Hellmuth K-H, 2006. Characterisation of pore space geometry by ^{14}C-PMMA impregnation – development work for in situ studies. Journal of Geochemical Exploration 90, 45–52.

Mazurek M, Bossart P, Eliasson T, 1996. Classification and characterization of water-conducting features at Äspö: Results of investigations on the outcrop scale. SKB ICR-97-01, Svensk Kärnbränslehantering AB.

Mærsk Hansen L, Staub I, 2004. Äspö Hard Rock Laboratory. TRUE-1 Continuation project. Fault rock zones characterisation. Overcoring (300 mm) of impregnated fault rock zones at chainages 2/430, 2/545, 2/163 and 1/1600. SKB IPR-04-10, Svensk Kärnbränslehantering AB.

Mærsk Hansen L, Hermanson J, Staub I, Tullborg E-L, 2003. Äspö Hard Rock Laboratory. TRUE-1 Continuation project. Fault rock zones characterisation. Preliminary structural-geological description of target structures based on borehole data and tunnel mapping. SKB IPR-03-50, Svensk Kärnbränslehantering AB.

Möri A, Mazurek M, Adler M, Schild M, Siegesmund S, Vollbrecht A, Ota K, Ando T, Alexander W R, Smith P A, Haag P, Bühler C, 2003. Grimsel Test Site – Investigation Phase IV (1994–1996): The Nagra-JNC in situ study of safety relevant radionuclide retardation in fractured crystalline rock. IV: The in situ study of matrix porosity in the vicinity of a water conducting fracture. Nagra Technical Report 00-08, National Cooperative for the Disposal of Radioactive Waste, Switzerland.

Neretnieks I, 2002. A stochastic multi-channel model for solute transport – analysis of tracer tests in fractured rock. Journal of Contaminant Hydrology 55, 175–211.

Poteri A, 2003. Äspö Hard Rock Laboratory. TRUE Block Scale Continuation project. Retention processes discrimination for various assumptions of fracture heterogeneity. SKB IPR-03-42, Svensk Kärnbränslehantering AB.

Poteri A, Billaux D, Dershowitz B, Gómez-Hernández J J, Cvetkovic V, Hautojärvi A, Holton D, Medina A, Winberg A (ed), 2002. Final report of the TRUE Block Scale project. 3. Modelling of flow and transport. SKB TR-02-15, Svensk Kärnbränslehantering AB.

Prêt D, Sardini P, Beaufort D, Zellagui R, Sammartino S, 2004. Porosity distribution in a clay gouge by image processing of ^{14}C-PolyMethylMethAcrylate (^{14}C-PMMA) autoradiographs: case study of the fault of St. Julien (Basin of Lodève, France). Applied Clay Science 27, 107–118.

Rhén I, Gustafsson G, Stanfors R, Wikberg P, 1997. Äspö HRL-Geoscientific evaluation 1997/5. Models based on site characterization 1986–1995. SKB TR 97-06, Svensk Kärnbränslehantering AB.

SKB, 2008. Site decription of Forsmark at completion of the site investigation phase. SDM-Site Forsmark. SKB TR-08-05, Svensk Kärnbränslehantering AB.

SKB, 2009. Site decription of Laxemar at completion of the site investigation phase. SDM-Site Laxemar. SKB TR-09-01, Svensk Kärnbränslehantering AB.

Sonka M, Hlavac V, Boyle R, 1995. Image processing, analysis and machine vision. London: Chapman & Hall.

Stigsson M, Hermanson J, Forssberg O, 2003. Äspö Hard Rock Laboratory. TRUE-1 Continuation project. Fault rock zones characterisation. Review of existing structural information and construction of local RVS models of four potential experimental sites. SKB IPR-03-49, Svensk Kärnbränslehantering AB.

Wahlgren C-H, Curtis P, Hermanson J, Forssberg O, Öhman J, Fox A, La Pointe P, Drake H, Triumf C-A, Mattsson H, Thunehed H, Juhlin C, 2008. Geology Laxemar. Site descriptive modelling, SDM-Site Laxemar. SKB-R-08-54, Svensk Kärnbränslehantering AB.

Widestrand H, Byegård J, Cvetkovic V, Tullborg E-L, Winberg A, Andersson P, Siitari-Kauppi M, 2007. Sorbing tracer experiments in a crystalline rock fracture at Äspö (Sweden): 1. Experimental setup and microscale characterization of retention properties. Water Resources Research 43, W10413. doi:10.1029/2006WR005277

Winberg A, Andersson P, Hermanson J, Byegård J, Cvetkovic V, Birgersson L, 2000. Äspö Hard Rock Laboratory. Final report of the first stage of the tracer retention understanding experiments. SKB TR-00-07, Svensk Kärnbränslehantering AB.

Winberg A, Andersson P, Byegård J, Poteri A, Cvetkovic V, Dershowitz W, Doe T, Hermanson J, Gómez-Hernández J J, Hautojärvi A, Billaux D, Tullborg E-L, Holton D, Meier P, Medina A, 2003. Final report of the TRUE Block Scale project. 4. Synthesis of flow, transport and retention in the block scale. SKB TR-02-16, Svensk Kärnbränslehantering AB.